

# Simulating infinite vortex lattices in superfluids: a novel scheme and its applications

Submitted in part fulfilment of the  
requirements for the degree of  
Doctor of Philosophy of Imperial College London  
and the  
Diploma of Imperial College London  
by

Luca Mingarelli

Imperial College London

January 2018









# Declaration of Originality

I certify that this thesis, and the research to which it refers, are the product of my own work, and that any ideas or quotations from the work of other people, published or otherwise, are fully acknowledged in accordance with the standard referencing practices of the discipline.

Luca Mingarelli,

January 2018

A handwritten signature in black ink that reads "Luca Mingarelli". The signature is written in a cursive style with a large, sweeping initial 'L'.



# Copyright

The copyright of this thesis rests with the author and is made available under a Creative Commons Attribution Non-Commercial No Derivatives licence. Researchers are free to copy, distribute or transmit the thesis on the condition that they attribute it, that they do not use it for commercial purposes and that they do not alter, transform or build upon it. For any reuse or redistribution, researchers must make clear to others the licence terms of this work.



*A mio padre*



# Acknowledgements

I would like to express my gratitude to my advisors, Ryan Barnett and Eric Keaveny, for all the support and guidance I have received throughout the past years. In times of struggle and confusion, all that is needed is to find open doors.

To everyone else knowing to have played a major role in my life, academic and non: thank you for your vicinity.





Thesis Advisor: Dr. Ryan Barnett

# Abstract

This thesis is mostly based on the research presented in [1, 2, 3]. We introduce a novel efficient framework to treat infinite periodic vortex lattices in rotating superfluids under a mean-field Gross-Pitaevskii description. In doing so, we introduce a generalisation of the Fourier transform which correctly diagonalises the kinetic energy terms while respecting the required twisted boundary conditions. We call this integral transform a *Magnetic Fourier transform*. Testing the method, we re-obtain known results in the lowest-Landau-level regime, and further extend to stronger interacting regimes.

We provide an extension of the above method to treat multicomponent systems, demonstrating that new degrees of freedom need to be introduced for each new component. We then employ this method to investigate the ground states of binary superfluid systems whose constituents have equal masses, thereby extending previous work carried out in the lowest-Landau-level limit to arbitrary interactions within Gross-Pitaevskii theory. In particular, we find that the interactions depauperate the phase diagram, with only the triangular lattice phase surviving in the limit of strong interactions. Withal we prove this applies regardless of the mass ratio of the constituents.

We further investigate binary superfluid systems with non unitary mass ratios, obtaining a range of novel and exotic vortex lattice configurations. Finally we derive a linear relation which accurately describes the phase boundaries in the strong interaction regime.



# Contents

<b>Introduction</b>	<b>15</b>
<b>1 Bose-Einstein Condensation, Superfluidity and Symmetries</b>	<b>31</b>
1.1 Bose-Einstein Condensation . . . . .	31
1.1.1 Non-interacting systems . . . . .	32
1.1.2 Interacting systems: the Gross-Pitaevskii equation . . .	35
1.1.3 Time-independent solutions and characteristic lengths .	38
1.2 Mixtures of condensates . . . . .	42
1.2.1 SU(2) symmetric point . . . . .	48
1.3 Quantum Fluid Dynamics of the Gross-Pitaevskii equation . .	50
1.4 Rotation of superfluids . . . . .	52
1.4.1 Density of vortices . . . . .	56
1.4.2 Properties of Single Vortices . . . . .	59
1.4.3 Existence of ground states and their nature under ro- tation . . . . .	63
1.5 Symmetries of the system . . . . .	67
1.5.1 Landau levels . . . . .	69
1.5.2 The Magnetic Translation Group and Twisted Bound- ary Conditions . . . . .	71

---

<b>2</b>	<b>Numerical Methods</b>	<b>79</b>
2.1	Imaginary Time propagation . . . . .	80
2.1.1	Imaginary time propagation for non-linear systems . . . . .	82
2.2	Methods for propagation in time . . . . .	86
2.2.1	Time propagation . . . . .	86
2.2.2	Split-step methods for linear Schrödinger equation . . . . .	89
2.2.3	Split-step methods for the non-linear Gross-Pitaevskii equation in real time . . . . .	90
2.2.4	Split-step method for the non-linear Gross-Pitaevskii equation in imaginary time . . . . .	94
2.3	Outlook . . . . .	97
<b>3</b>	<b>A Discrete Model for Infinite Vortex Lattices</b>	<b>99</b>
3.1	A non-linear Hofstadter model . . . . .	101
3.2	Twisted Boundary Conditions on the lattice . . . . .	105
3.2.1	1D lattice, Open Boundary Conditions . . . . .	105
3.2.2	2D lattice model with Twisted Boundary Conditions . . . . .	107
3.3	The Magnetic Fourier Transform . . . . .	111
3.4	The Discrete Model . . . . .	115
3.4.1	The Split-Step Magnetic Fourier Method . . . . .	118
3.4.2	Dynamical variation of the aspect ratio . . . . .	119
3.5	Numerical Tests . . . . .	122
3.6	Outlook . . . . .	127
<b>4</b>	<b>Mixtures of Attractive Superfluids</b>	<b>129</b>
4.1	Locking of vortices . . . . .	130
4.2	Vortex lattice configurations . . . . .	132
4.3	Multiply quantised vortices . . . . .	133
<b>5</b>	<b>Mixtures of Repulsive Superfluids: Equal Masses</b>	<b>135</b>
5.1	Reconsidering boundary conditions for multicomponent systems	136

5.2	Computational framework for multicomponent systems . . . .	140
5.2.1	The relation between model and physical parameters .	146
5.3	Components with equal masses: the phase transitions . . . . .	148
5.4	Components with equal masses: the phase diagram . . . . .	154
5.4.1	Linearity of the phase boundaries . . . . .	154
<b>6</b>	<b>Mixture of Repulsive Superfluids: the General Case</b>	<b>159</b>
6.1	General considerations regarding commensurability . . . . .	160
6.2	The mass ratio $m_2/m_1 = 2$ . . . . .	166
6.3	Higher mass ratios . . . . .	169
	<b>Conclusion</b>	<b>173</b>
<b>A</b>	<b>Significance of the phases <math>\tau_x</math> and <math>\tau_y</math></b>	<b>193</b>
<b>B</b>	<b>Linearity of the phase boundaries</b>	<b>197</b>



# List of Figures

0.1	Interest in the literature (as rate of occurrence of the topics) for <i>Bose-Einstein Condensation</i> and <i>Cold Atoms</i> in time [8].	16
0.2	Early imaging of stable vortex configurations in superfluid $^4\text{He}$ [39]. . . . .	19
0.3	In the method proposed by [42], the two traps $V_{ 1\rangle}$ and $V_{ 2\rangle}$ are rotated about each other at a frequency $\omega_r$ , while the transition between states $ 1\rangle$ and $ 2\rangle$ are driven at the effective frequency $\Omega_{\text{eff}} = \sqrt{\Omega^2 + \delta^2}$ . Here $\Omega$ is the Rabi frequency at which the population would oscillate between the two states if the detuning $\delta$ was absent. A singly quantised vortex can be obtained when $\omega_r \approx \Omega_{\text{eff}} \approx \delta$ . . . . .	20
0.4	The detuned off-resonance laser gives rise to a rotating gradient in the AC Stark shift, thus imprinting a $2\pi$ winding of the phase in the condensate [41]. . . . .	21
0.5	Tkachenko oscillations of the vortex lattice in Bose-Einstein condensate [55]. The black lines are sines fitted to the vortex lattice distortion. . . . .	23

---

0.6	Predicted ground state configurations for a mixture of two condensates with components of equal masses [66]. Panel (a) refers to attractive interspecies interactions, while (b-e) to different growing magnitudes of repulsive interspecies interactions.	25
1.1	Thomas-Fermi approximation compared with numerical solution in 1D. . . . .	39
1.2	Different kind of angular momentum excitations in a superfluid.	55
1.3	Vortex lattice in a rotating Bose-Einstein condensate [34]. . .	58
1.4	Vortex profile resulting from numerical solution of equation (1.82) and comparison with ansatz (1.85). . . . .	60
1.5	Condensate profile with one and two vortices compared to the Thomas-Fermi prediction for no rotation. . . . .	61
1.6	Qualitative phase diagram for anharmonically confined systems.	66
1.7	Wilson loop (1.122) revealing the acquisition of a phase factor when translating along a closed loop. . . . .	74
2.1	An example of a pathological system in which imaginary time propagation achieves nonetheless the true ground state. Despite the density being initialised in the local minimum $B$ (solid black line), the system will eventually evolve towards the true minimum $A$ when propagated in imaginary time. The potential is shown in red. The dashed blue line refers to the building up of a nonzero density in the true minimum $A$ due to numerical errors, as explained in the text. . . . .	85



2.2	A plot of the error as a function of imaginary time step for different methods (arbitrary units). The accuracy of the Javanainen-Ruostekoski Strang splitting (2.29) described in [71] for real time propagation does not carry over to imaginary time propagation. In imaginary time the method is first order accurate. On the other hand, it is possible to see (right) that a different procedure (2.45) can be used which attains second order accuracy. . . . .	95
3.1	1D system with open boundary conditions. . . . .	105
3.2	1D system with periodic boundary conditions. Here site $N + 1$ corresponds to site 1. . . . .	106
3.3	Schematic dynamics on the 2D system in the Landau gauge. A particle tunnelling acquires the phases $\theta_x$ and $\theta_y$ given in (3.2). For a system respecting periodic boundary conditions one has $\psi_{N+1} \equiv \psi_1$ . On the other hand, a system respecting twisted boundary conditions has $\psi_{N+1} \equiv e^{i\Theta_x}\psi_1$ , where the twisting phase is as given in (3.18). . . . .	109
3.4	Convergence of the lattice model aspect ratio to the continuum value $\mathcal{R} = \sqrt{3}$ for increasing number of computational points $N = N_x N_y$ . The simulation considers a periodic unit cell containing two vortices. . . . .	121
3.5	Plot of the inhomogeneity parameter defined in equation (3.59). The stationary points corresponding to triangular and square lattices are labelled. . . . .	123
3.6	Numerical solutions for $N_v = 4$ and $N_v = 1$ leading to triangular and square lattices. The aspect ratios are $R = 2/\sqrt{3}$ and $R = 1$ respectively. . . . .	124

- 
- 3.7 Numerical results of the dimensionless inhomogeneity parameter  $\beta$  (3.58) characterising the interaction energy of the system as a function of the aspect ratio of the computational unit cell. Excellent agreement is found between the numerical results and the analytical expression  $\beta^A$  in the lowest Landau level regime. . . . . 125
- 3.8 The energy per particle of systems with two and eight vortices in the computational unit cell,  $\tilde{E}_2$  and  $\tilde{E}_8$ , as a function of the ratio  $\mathcal{R}$ . The former provides an upper bound for the latter. The triangular lattices corresponding to the ground states are degenerate and the arrangements of the vortices in each of the ground states of the eight-vortex system are shown. . . . . 126
- 4.1 Depiction of bound vortex pairs for species with masses  $m_1 > m_2$  [116]. Within a certain locking radius  $r_c$  the vortices of the two species form bound pairs which rotate together at the driving frequency, while the two superfluids adapt their rotational rate so as to allow for equal vortex densities. Outside the disk defined by  $r_c$ , the pairs become unbound, both vortices and the superfluids rotate at the driving frequency and the two vortex densities become unequal. . . . . 130
- 4.2 Schematic depiction of the regular vortex lattice ground state configurations attainable for a binary system of rotating condensates [118]. When the triangular vortex lattices associated with each mass ratio (and hence vortex density ratios) are commensurate, then the overlapping of these such triangular lattices provides the ground state configuration of the system. The triangular lattices associated with the mass ratio  $m_1/m_2$  are not commensurate. For this reason the configuration minimising the total energy is not a combination of two triangular lattices but a combination of two square lattices instead. . . . 133

- 
- 4.3 Schematic depiction of bounded pairs of vortices (a) and multiply quantised vortices (b), in the heavier species. The configuration of the vortices in the lighter species as well as that of the bounded pairs and of the multiply quantised vortices is triangular. . . . . 134
- 5.1 Two possible ways of overlapping two triangular lattices with equal lattice constant. The square and circle marks refer to points (vortices) corresponding to different lattices. In (a) is what we refer to as *interlaced triangular lattices*, while in (b) are shown two *interlaced oblique lattices*. . . . . 139
- 5.2 Schematic description of the algorithmic procedure. The equations of motion in the top left of the figure are obtained by Wick-rotating the Gross-Pitaevskii equations to imaginary time  $\tau = it$ . . . . . 146
- 5.3 The diagram defines the parameters  $R = |\mathbf{v}_2|/|\mathbf{v}_1|$ ,  $\eta$  and  $\mathbf{r}$ . . . . . 147
- 5.4 Two equivalent unit cells tiling a system made of two interlaced square lattices. . . . . 148
- 5.5 Results from the early work of Mueller and Ho [66]. The relation of the parameters used in these plots with those used in our treatment can be understood by comparing with Fig. 5.6. . . . . 149

- 5.6 Extension of the results from [66]. When varying  $\alpha$ , the parameter  $R$  describes the second order transition transforming a square lattice into a rectangular lattice; the parameter  $\eta$  instead, experiences at first a jump, signalling a first order transition responsible for the transformation of the triangular lattice into the oblique lattice. Further observing the behaviour of  $\eta$ , it is possible to spot where another second order transition occurs, continuously transforming the oblique lattice into the square lattice. For components of equal masses one always obtains minimisers satisfying  $r_1 = r_2$ . At the occurrence of the first order transition  $r_1$  experiences a discontinuity as well: this permits the transition from the triangular to the square configurations. The beginning of the immiscible regime area is highlighted in grey. . . . . 151
- 5.7 Phase diagram describing the ground states of two interacting superfluids of equal masses and same particle number per unit cell  $\mathcal{N}_1 = \mathcal{N}_2$ . The abscissa represents the intraspecies interaction strength (which is assumed to be the same for both species) while the ordinate the interaction strength amongst the two different species. The area of the phase space below  $T_2$  is characterised by the parameter  $\phi$ , while that above is characterised by  $R$ . Transition  $T_1$  is of first order, while  $T_2$  and  $T_3$  are second order transitions. For completeness the trivial attractive regime ( $\alpha < 0$ ) is included as well, showing a ground state consisting of two overlapping triangular lattices. . . . . 155
- 5.8 Linear phase boundaries in the miscible regime.  $\bar{T}_1$  marks the boundary between the triangular phase and the oblique phase,  $\bar{T}_2$  divides the oblique and the square phases and  $\bar{T}_3$  is the last phase boundary leading to the rectangular phase. . . . . 156

6.1	Geometrical significance of Lösschian numbers. In a triangular lattice, the distance from the origin of the elements of every set of points equidistant from the origin, is given by the square root of a Lösschian number. . . . .	163
6.2	On the left: two non-commensurate triangular lattices with corresponding mass ratio $m_2/m_1 = 2$ . In the presence of non-commensurability one would in practice observe geometrical frustration. On the right: two commensurate triangular lattices with $m_2/m_1 = 3$ . . . . .	164
6.3	Geometrical significance of (6.12). In a square lattice, the distance from the origin of the elements of every set of points equidistant from the origin, is given by the square root of the sum of squares (6.12). . . . .	165
6.4	Phase diagram for two rotating superfluids with atomic mass ratio $m_2/m_1 = 2$ . The intra-species interaction strengths are taken so as to satisfy $\ell_\Omega^{(1)}/\xi^{(1)} = \ell_\Omega^{(2)}/\xi^{(2)} \equiv \ell_\Omega/\xi$ . As discussed in the text, this system does not have a commensurate ground state for small inter-species interactions. One should hence expect to observe frustration in this regime. For stronger interactions one finds instead two novel vortex configurations: the snub-square lattice and the honeycomb lattice. . . . .	167
6.5	Phase diagram for two rotating superfluids with atomic mass ratio $m_2/m_1 = 2$ . Here the intraspecies interactions are taken so as to have equal healing lengths in each component $\xi^{(1)} = \xi^{(2)} \equiv \xi$ . . . . .	168
6.6	The continuous transformation of the Square-SnubSquare lattices into the Triangular-Hexagonal lattices, occurring between the transition boundaries $T_2$ and $T_3$ . . . . .	169



# List of Tables

3.1	Minimum and local maximum of the inhomogeneity parameter $\beta^A$ corresponding to triangular and square lattices respectively. . . . .	123
6.1	Commensurate ground states for different mass ratios. For each lattice it is given its symmetry classification in IUC notation. We denoted by ' $\frac{1}{n}$ Triangular' the triangular lattice with unit cell an $n$ th of the unit cell area of the lattice denoted as 'Triangular'. . . . .	170





# Introduction

“What kind of computer are we going to use to simulate physics?”

---

Richard P. Feynman, *Simulating Physics with Computers*, 1981

It was June 1924 when Satyendra Nath Bose, until then a relatively unknown Indian physicist, sent a letter to Albert Einstein describing his work on the quantum statistics of quanta of light, a kind of particle later named *bosons* by P.A.M. Dirac in honour of the Indian physicist. Just a month later, Einstein would extend this work to ideal gases [4], and a year later led him to speculate on the existence of what today is known as Bose-Einstein Condensation, a purely quantum mechanical phase transition occurring when, at sufficiently low temperatures, a macroscopic fraction of the system falls into the lowest energy quantum state. In 1938 [5], Fritz London proposed that Bose-Einstein condensation might be responsible for a perplexing phenomenon that had been observed since the beginning of the century in  $^4\text{He}$  at low temperatures, namely superfluidity [6]; Heike Kamerlingh Onnes had already liquefied helium in 1908, which allowed him to cool down mercury to temperatures low enough to observe superconductivity, granting him the Nobel price in 1913. However, today it is known that in liquid helium, the

fraction of the system which is condensed is only about 10%. London's work was followed in 1941 by Lev Landau's revolutionary two-fluid model [7], and in 1946 by Nikolay Bogolyubov's. The theoretical understanding was furthered by the subsequent work of David Gross and Lev Pitaevskii, one of Landau's pupils. But it wasn't until June 1995 that Bose-Einstein was actually achieved in a laboratory.

Seventy-one years after Bose's letter, in June 1995, Eric Cornell and Carl Wieman at the JILA lab in Boulder cooled a gas of Rubidium ( $^{87}\text{Rb}$ ) atoms to 170nK, and shortly after Wolfgang Ketterle at MIT did the same with Sodium atoms ( $^{23}\text{Na}$ ), thereby producing the first atomic condensates, which led to the Nobel price in 2001 and paved the way for more theoretical and experimental exciting research.

The following decades saw a significant growth in interest for the topic, a growth also fostered by the rapid advances in cooling technology, which enabled for accurate and precise probing of such systems. Furthermore, it

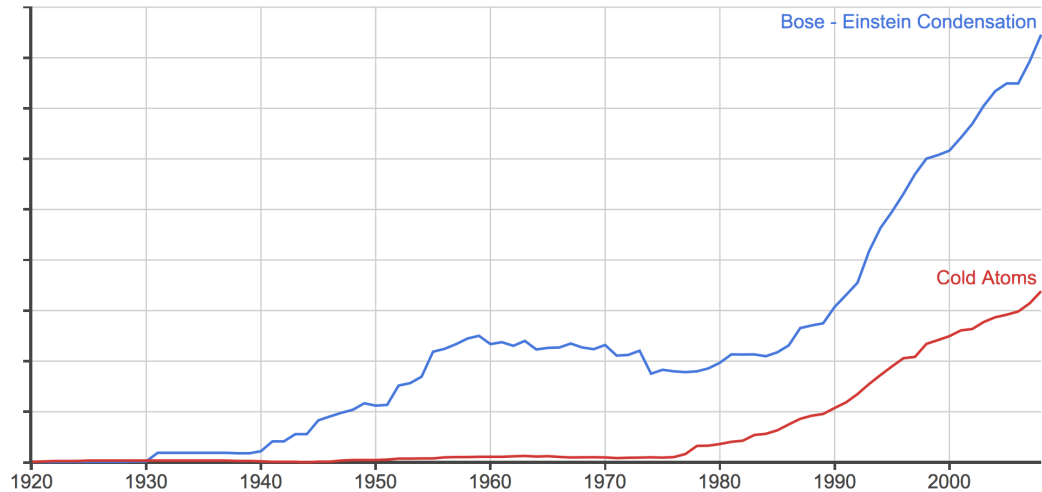


Figure 0.1: Interest in the literature (as rate of occurrence of the topics) for *Bose-Einstein Condensation* and *Cold Atoms* in time [8].

was soon realised [9] that inter-atomic interactions could be tuned, from attractive to repulsive, through the use of so-called Feshbach resonances, which

made cold gases much more than just a simple experimental demonstration. Confining ultracold atomic gases into optical lattices [10], a technique which introduced the prospect of more exotic potential, tight spatial confinement and reduced dimensionality as well as synthetic dimensions [11], opened up the investigation of a most diverse range of systems and theoretical models, and to the creation of quantum simulators, the viability of which was firstly envisaged by R.P. Feynman in the early eighties. The prospect of realising a quantum simulator was effectively brought to reality by the more recent introduction of synthetic gauge fields [12, 13], which allowed the study a broader class of systems, under both Abelian and non-Abelian gauge fields. In recent years, about a dozen<sup>1</sup> different atomic species have been shown to condense at low enough temperatures, as well as molecules, composite particles and quasiparticles, including, inter alia, magnons (quantised spin-waves in magnetic materials)[22], excitons (electron-hole pairs)[23] and polaritons (photon-exciton entangled states)[24].

## Quantum Fluids

Although the relation between Bose-Einstein condensation and superfluidity is not univocal, the two are intimately connected. The term *superfluidity* was originally coined by Pyotr Kapitza to describe the anomalous absence of viscosity observed in <sup>4</sup>He below the characteristic lambda point (this is the so called He-II phase occurring at  $T < T_\lambda \approx 2.17\text{K}$ ) by his group in Moscow [25] and by John F. Allen and Donald Misener in Cambridge in 1938 [26]. A few decades later, Lee, Osheroff and Richardson [27, 28] found that <sup>3</sup>He enters a superfluid phase as well, below 2.7mK. No other superfluids were thereafter discovered, until the realisation of Bose-Einstein condensation in ultracold dilute atomic gases in 1995.

---

<sup>1</sup>Amongst others, <sup>7</sup>Li (1995) [14], H (1998) [15], <sup>85</sup>Rb (2000) [16], <sup>41</sup>K (2001) [17], <sup>133</sup>Cs (2003) [18], <sup>174</sup>Yb (2003) [19], <sup>52</sup>Cr (2005) [20], <sup>39</sup>K (2007) [21].

Among the most peculiar effects of superfluidity is the existence of a critical velocity for dissipation, a property observed from the earliest experiments and firstly explained by Landau. Although such a property has been observed in Bose-Einstein condensates [29], it is not a defining property of a condensate: one suitable example here, is that of an ideal Bose gas for which the critical velocity is expected to vanish, hence depriving the system of its lack of viscosity; another, that of a condensate in a random potential [30]. Such systems, exhibiting Bose-Einstein condensation but lacking superfluidity are known as Bose Glasses. The converse might be true as well: it is indeed possible to find systems lacking condensation but exhibiting all the defining properties of superfluidity; probably the simplest example of such a system is that of a 1D gas at low temperatures.

Other defining properties of superfluidity include phase coherence – a straightforward consequence of which is interference [31, 32]–, and the unusual response to rotation. A quantum fluid cannot in fact rotate as a classical fluid, and acquires angular momentum through the nucleation of vortices carrying quantised angular momentum. These effects have also been observed in Bose-Einstein condensates [33, 34].

## Quantum Vortices

Quantum vortices exist, as predicted in the late forties by Lars Onsager<sup>2</sup> and independently by Feynman in 1955 [35], due to the quantisation of the circulation, and appear as zero density lines in the density of the superfluid. In 1957, Alexei Abrikosov, taking the lead from Onsager and Feynman’s work, studied the energetics of different lattice configurations in the lowest Landau limit, arriving to the claim that the energy is minimised by a periodic square array of quantum vortices. Shortly after, it was shown [36] that a wrong assumption had misled Abrikosov, and that the correct struc-

---

<sup>2</sup>Noticed by F. London in his book *Superfluids*, Wiley (1954)

ture minimising the energy is that of a periodic triangular array of quantum vortices. Nonetheless, despite Abrikosov's wrong prediction, the correct triangular configuration bears today his name. The experimental proof of this result came in the late sixties [37, 38] and Abrikosov was granted the Nobel price in 2003, sharing it with two other major players, who gave invaluable contribution to the physics of superfluidity: Vitaly L. Ginzburg and Anthony J. Leggett. Abrikosov's triangular configuration is known to be stable at any

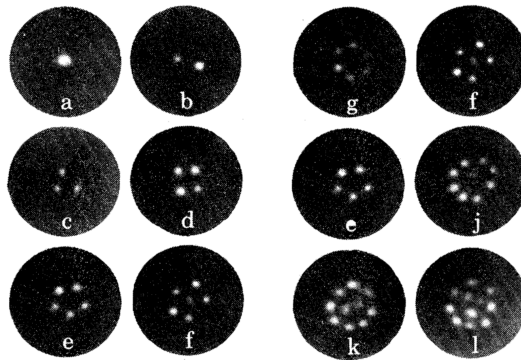


Figure 0.2: Early imaging of stable vortex configurations in superfluid  $^4\text{He}$  [39].

given interspecies interaction strength. The physics is however very much enriched when considering two or more interacting superfluids. Here the configurations are not necessarily triangular anymore, and it is possible to achieve both complex vortex lattices at the variation of the interaction parameters, and lattices made of multiply quantised vortices, which are usually otherwise unstable against decay into singly quantised vortices.

## How to create a vortex

The experimental observation of vortices in superfluid  $^4\text{He}$ , dates back to 1956 [40], the creation of which could be achieved by cooling Helium while rotating it in its non-superfluid phase I. However, it was not until 1999 that the first observation of vortices in a BEC was made at the JILA group in Boulder,

Colorado [41], following a method proposed earlier that year [42], known as *phase imprinting*. In order to overcome technical difficulties associated with condensing the system while in rotation, a procedure was instead proposed to generate vortices from a non-rotating condensate. Considering a two-level system (such as one made by the two hyperfine levels of  $^{87}\text{Rb}$ ), in which each state is confined in a separate harmonic potential, and simultaneously applying an electromagnetic field coupling the two states, so as to cause atoms to cycle between levels, one can obtain one component with a quantised vortex, circulating around the second non-rotating component. Notice that,

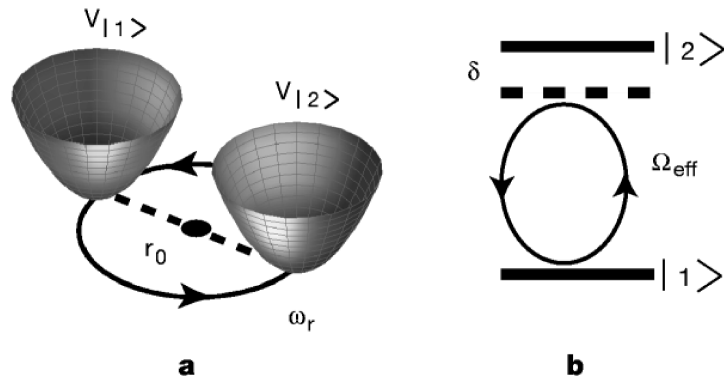


Figure 0.3: In the method proposed by [42], the two traps  $V_{|1\rangle}$  and  $V_{|2\rangle}$  are rotated about each other at a frequency  $\omega_r$ , while the transition between states  $|1\rangle$  and  $|2\rangle$  are driven at the effective frequency  $\Omega_{\text{eff}} = \sqrt{\Omega^2 + \delta^2}$ . Here  $\Omega$  is the Rabi frequency at which the population would oscillate between the two states if the detuning  $\delta$  was absent. A singly quantised vortex can be obtained when  $\omega_r \approx \Omega_{\text{eff}} \approx \delta$ .

in contrast to the one-component  $U(1)$  order parameter (as for He-II) which has the topology of a circle, the coupled two-component system effectively behaves as an  $SU(2)$  spin- $\frac{1}{2}$  system with the topology of a sphere. As a consequence the latter system is not required to exhibit quantised vorticity, as it is instead true for the on-component system [43].

The vortex creation is specifically achieved by transferring the system adiabatically to a spherical trap, rotating a beam around the condensate,

thus inducing an AC Stark shift on one of the two components, as shown in Fig. 0.4, and finally turning off the Rabi coupling at the appropriate moment, thereby leaving a  $2\pi$  winding of the phase in this component. The vortex

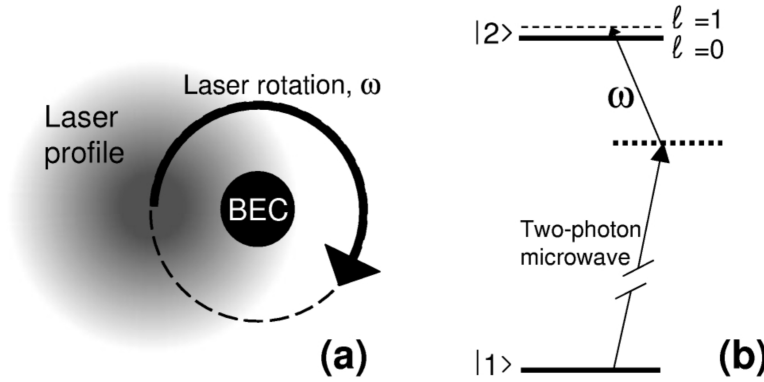


Figure 0.4: The detuned off-resonance laser gives rise to a rotating gradient in the AC Stark shift, thus imprinting a  $2\pi$  winding of the phase in the condensate [41].

core in this system is much larger than the natural healing length, due to the core being filled with the non-rotating component. Its size clearly depends on the fraction of the non-rotating component, and has been found to reach up to  $10\mu m$ , thus allowing for non-destructive imaging with visible light. This is particularly important if one is interested in tracking the motion of the vortex.

In the same experiment, the JILA group was also able to remove the non-rotating component in the core through an intense laser pulse, so as to leave a single component with one singly quantised vortex with core size of order of the healing length  $\xi \approx 0.2\mu m$ . By imaging the two component system first, removing the core, turning of the confining trap so that the condensate expands ballistically, and imaging the expanded vortex core, it was made possible to measure the precession rate of the empty-core vortex: these measurements were found to consistently agree with the theoretical predictions [44].

It is also worth mentioning the existence of a different elegant and sophisticated procedure to imprint a geometrical Berry phase [45], which relies on engineering a spatially dependent phase contingent on the path of a slowly varying magnetic field [46]. With this method it has also been possible to create vortices with two and four units of circulation [47]; however, as we will argue later, in a bulk condensate, these are energetically unstable against decay into singly quantised vortices.

What is probably the most popular method, pioneered by the ENS group in Paris and by the MIT group [48, 34], consists instead in mechanically stirring the condensate through a laser beam. This method in particular, allowed for the creation of many vortices (in the order of hundreds) thus making it possible to observe the Abrikosov lattice. Cornell's group at JILA was instead to achieve condensation of a rotating cloud of atoms, in analogy with the process of cooling  $^4\text{He}$  in the rotating bucket; moreover, although as metastable states, they achieved the first giant vortices containing up to 60 phase singularities [49, 50]. Finally, Anderson's group in Arizona [51], was also able to achieve the creation of vortex-antivortex pairs by sweeping the condensate through a laser beam obstacle.

## Vortex lattices

In agreement with theoretical predictions, large arrays of vortices respect the Feynman relation for the vortex density  $\rho_v = \frac{\Omega m}{\pi \hbar}$  (see Chapter 1), and the lattice formed rotates around the axis of rotation so as to simulate rigid rotation. The two characteristic lengths of the system, namely the healing length and the intervortex spacing  $\ell \approx 2\sqrt{\frac{1}{\pi\rho_v}}$  (again, cf. Chapter 1) are helpful to define two defining regimes of the system. One is the *Thomas-Fermi* (or *Coulomb*) regime, in which the interaction and confining energies are both large compared with the gradient energy associated with variations in the density, and consequently  $\ell \gg \xi$ . On the other hand, when the interaction is weak, or equivalently for large rotation rates, one defines the *lowest Landau*



*level* (LLL) regime. Here the vortex cores overlap, so that the healing length is in the order of  $\ell$  or greater, and the energy associated with density variations is far from negligible. The linearised one-body problem is then exactly solvable, and, as we will discuss in more detail later, equivalent to Landau's original problem of an electron in a uniform magnetic field (hence the name LLL regime, which is sometimes also referred to as *mean field quantum Hall* regime). For a single component system, the Abrikosov lattice is known to be stable in both these regimes and in between. Despite theoretical predictions of circular lattice distortions near the boundary of a finite condensate, experiments with many vortices found instead a high degree of regularity [52].

Small perturbations of the vortex lattice were first studied by Tkachenko in the mid sixties [53]: the triangular lattice was shown to support stable normal modes, which in the limit of long-wavelengths effectively consists of transverse phonons with linear dispersion relation. Such Tkachenko oscillations were reported in liquid  $^4\text{He}$  [54], but it was not until recently that a conclusive demonstration of their existence was obtained [55].

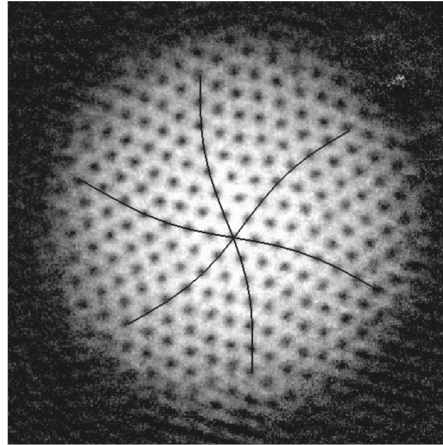


Figure 0.5: Tkachenko oscillations of the vortex lattice in Bose-Einstein condensate [55]. The black lines are sines fitted to the vortex lattice distortion.

It is however possible to find more exotic configurations when considering

strong long-range interactions. One such example is that of  $^{52}\text{Cr}$ , an atom with large magnetic dipole moment [20]. When dipolar interactions are sufficiently strong, in addition to the common Abrikosov phase, one can find a square configuration, a stripe crystal (or rectangular), and a bubble crystal phase [56].

## Condensates in rotating optical lattices

Very much interest was drawn to the effect of a pinning optical lattice on the vortex configuration [57, 58]: this is in fact a phenomenon of remarkable importance as naturally arising in systems such as multicomponent condensates, in the context of high temperature superconductors [59, 60], and in neutron stars where the pinning and unpinning of superfluid vortices in the highly degenerate neutron matter to the outer stellar crust, is thought to be responsible for pulsar glitches (sudden changes in the star's rotational frequency)[61, 62]. Furthermore, recent proposals also put forward the pinning of vortices in superfluids as a method to engineer the braiding of Majorana bound states in topological superconductors [63].

The nature of the ground states here depends both on the densities of vortices and pinning sites, which also raises the problem of commensurability [64], as we will discuss in the last chapters of this manuscript. The pinning of vortices in atomic condensates can be achieved by rotating optical lattices [65], and depending on the condensate's coupling strength and the depth of the pinning sites, one can observe transitions between the Abrikosov lattice and phases where the vortices are pinned to the underlying optical lattice, with a range of different structures, including the stable accommodation of vortices with multiple units of circulation within one pinning site.

## Systems with multiple components

As we will extensively discuss in the later chapters, one finds more complex configurations when considering systems with multiple components, although the Abrikosov lattice is always favoured in the lighter or more strongly interacting component, for large enough couplings.

The first results in the classification of ground states for a mixture of two interacting condensates with components of equal masses were obtained in the lowest Landau level by [66] and are summarised in Fig. 0.6: one finds the ground state consists of two overlapping triangular lattices in the attractive interspecies interaction case, and of two interlaced triangular, oblique, square, or rectangular lattices in the case of repulsive interspecies interaction. We will discuss extensively of these results and of their extension away from the lowest Landau level regime in chapters 5 and 6.

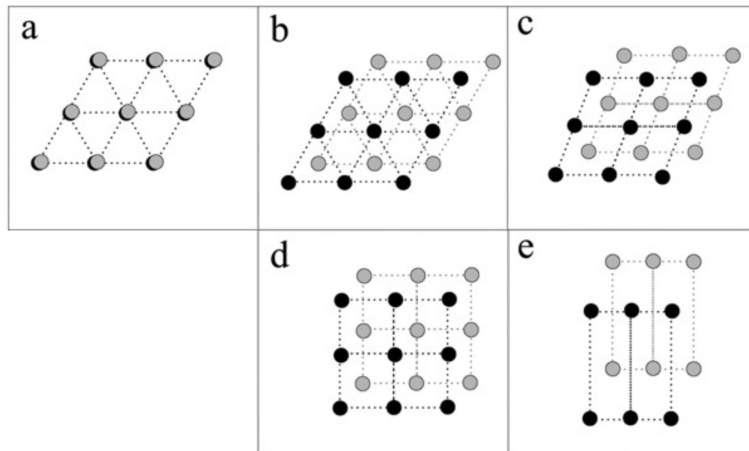


Figure 0.6: Predicted ground state configurations for a mixture of two condensates with components of equal masses [66]. Panel (a) refers to attractive interspecies interactions, while (b-e) to different growing magnitudes of repulsive interspecies interactions.

In these systems, one usually finds great and accurate experimental control over the interaction parameters, which allows to study a whole range of

lattice configurations and to move continuously from miscible to segregated phases [67]. However, the relative populations of each component are usually constant.

Until about a decade ago, most experiments would trap atomic condensates with hyperfine spins  $F = 2$  or  $F = 1$  magnetically. A system of condensed spin- $F$  bosons is described by the spinor field operator  $\hat{\psi}_m$  such that  $\langle \hat{\psi}_m(\mathbf{r}, t) \rangle = \zeta_m(\mathbf{r}, t)\psi(\mathbf{r}, t)$ , where  $m$  labels  $F_z$  ( $-F \leq m \leq F$ ),  $\psi$  is a scalar, and  $\zeta_m^\dagger \cdot \zeta_m = 1$ . When trapped magnetically, the atomic spins are maximally aligned along the magnetic field, so that the dynamics of  $\langle \hat{\psi}_m \rangle$  is completely determined by the scalar  $\psi$ . One can instead trap the system optically [68], thus leaving the spin degrees of freedom unconstrained. Moreover, the populations of the spin components are no longer constant, and the population balance can vary via spin exchange collisions. The physics is thus even more enriched in spinor systems. As an example, spin-1 systems (such as  $^{23}\text{Na}$ ,  $^{39}\text{K}$ ,  $^{87}\text{Rb}$ ), depending on the different scattering lengths at play, can exist in either a *polar* phase, in which the system tries to minimise the local spin density  $\langle \hat{\mathbf{S}} \rangle = 0$ , or a *ferromagnetic* phase, where the system acts to maximise the total spin, so that the expectation  $\langle \hat{\mathbf{S}} \rangle$  acquires a non-zero value. Different topological momentum carrying excitations exist in the form of spin-textures, varying in the two phases: in polar systems these are known as  $\pi$ -*disclinations* of the polar phase (half-quantum vortices), while in the ferromagnetic case one finds core-less vortices, also known as *skyrmions* [69, 70].

## Outline of this thesis

This thesis constitutes a study of perfect vortex lattices in superfluids. Common approaches involve either analytical treatment in experimentally restrictive regimes, or the direct simulation of the system within an harmonic trapping potential. The latter approach in particular, is both inefficient and

inconvenient, since the harmonic trap distorts the vortex lattice. We aim instead at simulating such systems in a manner which allows access to any interaction regime, while preserving the exact shape of the lattice.

The present thesis comprises the research published in [1], where we describe a novel computational scheme to investigate the lowest energy states of rotating superfluid systems. This work constitutes the bulk of Chapter 3 and some of Chapter 2. A second contribution [2], describes an extension of the above mentioned method, to multicomponent systems, extends results by [66] providing a complete characterisation of the phase diagram for superfluids whose components have equal masses, and discusses on the results in the regime of strong interactions, demonstrating that a simple linear relation for the phase boundaries can be obtained in this limit. These results are presented in Chapter 5. Finally, Chapter 6 contains the work recently submitted for publication on Phys.Rev.Lett. [3], in which the method for multicomponent system is applied to mixtures with non unitary mass ratios, predicting new exotic lattice configurations.

The thesis is organised as it follows.

- **Chapter 1** is a broad introduction to superfluidity and Bose-Einstein condensation. The properties of single vortices are also discussed. In the last section we discuss on the symmetries of the system, specifically with particular attention to the Magnetic Translation group arising from the synthetic gauge field associated with rotation. Finally we show how standard periodic boundary conditions should not be a preferred choice for rotating systems, demonstrating that a more natural and suitable choice exist, namely *Twisted Boundary conditions*.
- **Chapter 2** is devoted to an overview of the numerical methods used. In particular, a description is given of the *imaginary time propagation* method, indispensable to the search for the lowest energy states, and *split-step methods* needed for time propagation. We explain why the imaginary time method in its standard form, is in principle applicable

to linear systems only. We further argue that the method is however applicable to the non-linear case of our interest (namely that of the Gross-Pitaevskii equation), by showing the energy is monotonically decreasing in imaginary time. The same argument applies to split-step methods: the standard procedure giving a second order method for linear problems, does not apply directly for non-linear ones; a second order method for the non-linear problem of interest was already presented in [71], but this method is shown to lose accuracy when propagating in imaginary time. We provide here a different split-step method which is second-order accurate in imaginary time.

- In **Chapter 3**, we introduce a non-linear anisotropic Hofstadter model, showing it reduces to the continuum Gross-Pitaevskii theory describing the system in the continuum limit; moreover, we discuss on different approaches to the implementation of the required twisted boundary conditions. Specifically, we introduce a generalisation of the Fourier transform which extends its action of diagonalisation over systems with periodic boundary conditions to systems respecting twisted boundary conditions: this is the *Magnetic Fourier Transform*. After discussing the positive implications of this transform for the discrete model, we test the method against the early results of Abrikosov and Kleiner *et al.* [72, 36], obtained in the Lowest Landau limit. We further extend these results to stronger interaction regimes.
- **Chapter 4** describes the results for mixtures of two superfluids under attractive interactions. In particular, we show that a lattice of multiply quantised vortices is attainable in this regime. The chapter is included both for completeness and to demonstrate the applicability of the method introduced in Chapter 3 to a broader class of problems.
- **Chapter 5** gives a generalisation of the method from Chapter 3 to multicomponent systems. This involves a non trivial constraint on the boundary conditions of the additional component(s). Then, we proceed

to extend the results Mueller and Ho [66] obtained in the Lowest Landau limit for two components whose constituents have equal masses, and we thereby provide a complete characterisation of the whole phase diagram. Finally we consider the limit of strong interaction (Coulomb limit), to find that a simple linear relation can be found for the phase boundaries.

- **Chapter 6** is dedicated to the case of a mixture of two superfluids with a non unitary mass ratio. We start from some general considerations concerning the commensurability of the two systems. We further present a characterisation of the phase diagram for the particular case  $m_2/m_1 = 2$ , and finally we give an overview of the possible exotic lattice configurations attainable for higher mass ratios. A generalisation of the expression for the phase boundaries provided in the previous chapter is also given.





# Chapter 1

## Bose-Einstein Condensation, Superfluidity and Symmetries

This first chapter is devoted to the introduction of the background concepts needed to build up the models presented in the rest of this thesis. A brief description of the physical significance of Bose-Einstein condensation will be given, starting from a statistical argument, then introducing the standard argument for condensation in non-interacting systems, and finally looking at this phenomenon in an interactive perspective, and in the scenario of condensates of different species interacting with each other. The superfluid properties of such a system will also be discussed, together with the implications for what concerns their response to rotation. Finally we will discuss on the symmetries of the system. This discussion will prove particularly relevant for the construction of the models, which will be approached in Chapter 3.

### 1.1 Bose-Einstein Condensation

The concepts underpinning the process of Bose-Einstein condensation can be grasped at once from a concise statistical argument. If one considers the problem of distributing  $\mathcal{N}$  particles among  $S$  states so that the  $j$ th state

contains  $n_j$  particles, he will find substantially different answers depending on whether the particles under consideration are distinguishable or indistinguishable. If, as it is done classically, the particles are *distinguishable*, then there are  $\mathcal{N}! / \prod_{j=1}^S n_j!$  different possible configurations. On the other hand, if the particles are indistinguishable there is only one configuration possible (assuming there are no extra constraints, as it is for the bosonic case). When the discrepancy becomes particularly evident, i.e. when  $\mathcal{N} \geq S$ , the configurations in which more particles occupy the same state have a higher relative weight. This result, although not particularly rigorous, is remarkably instructive and very general. No mention was in fact made of thermal equilibrium nor interaction; regardless of these considerations, bosons, because of their very own nature, have a tendency to cluster together.

### 1.1.1 Non-interacting systems

We will now discuss the case of an ideal, i.e. non-interacting, Bose gas. The mean occupation number of single particle states of energy  $\epsilon_j \leq \epsilon_{j+1}$ , at temperature  $T$  and with chemical potential  $\mu$ , is given by the Bose distribution

$$\langle n_\nu \rangle = \left( e^{\frac{\epsilon_\nu - \mu}{k_B T}} - 1 \right)^{-1}. \quad (1.1)$$

It is worth noticing that for large temperature  $T$ , the effect of the quantum statistics becomes negligible, and one obtains back the Boltzmann distribution  $f(\epsilon_\nu) \xrightarrow{T \rightarrow \infty} \exp[-(\epsilon_\nu - \mu)/k_B T]$  known from classical mechanics. One implication of this result, inter alia, is that, in order to observe the quantum nature of the system, it is either necessary to have low temperatures or high densities at fixed temperature.

If the energy of the ground state is set to zero  $\epsilon_0 = 0$ , it is evident that in order to avoid unphysical negative occupation numbers, the chemical potential must remain negative. We can now consider the total particle

number, which can be obtained from the distribution function as

$$\mathcal{N} = \sum_{\nu} f(\epsilon_{\nu}). \quad (1.2)$$

For large particle numbers, one may replace the sum in the above expression, with an integral over the single-particle energy, taking care to include the lowest energy state explicitly, lest obtain problematic and unphysical results:

$$\mathcal{N} \approx f(\epsilon_0) + \int_0^{\infty} d\epsilon f(\epsilon) g(\epsilon). \quad (1.3)$$

Here  $g(\epsilon)$  is the density of states, an expression for which can be obtained recalling that, due to Heisenberg uncertainty relation, there is one quantum state per phase space cell of volume  $(2\pi\hbar)^3$ . Writing for the real space volume  $\mathcal{V} = \Delta x \Delta y \Delta z$ , and for the volume in momentum space containing states with momentum less than  $p$  as  $\frac{4}{3}\pi p^3$ , it is possible to write the total number of states with energy less than  $\frac{p^2}{2m}$  as

$$G(\epsilon) = \frac{\mathcal{V} \frac{4}{3}\pi p^3}{(2\pi\hbar)^3} = \mathcal{V} \frac{\sqrt{2}}{3\pi^2 \hbar^2} (m\epsilon)^{3/2}, \quad (1.4)$$

so that the density is given by

$$g(\epsilon) = \frac{dG(\epsilon)}{d\epsilon} = \mathcal{V} \frac{\sqrt{2}}{3\pi^2 \hbar^2} (m)^{3/2} \sqrt{\epsilon}. \quad (1.5)$$

More generally, it is possible to write  $g(\epsilon) = c_{\alpha} \epsilon^{\alpha-1}$ , where  $c_{\alpha}$  is a constant and  $\alpha = d/2$  for the homogeneous case in  $d$  dimension, or  $\alpha = d$  for the harmonic oscillator case in  $d$  dimensions [73].

If we now assume to keep the temperature fixed, while adding more particles, we find that in general the density  $n$  will rise as

$$n = \frac{f(\epsilon_0)}{\mathcal{V}} + \frac{c_{\alpha}}{\mathcal{V}} \int_0^{\infty} d\epsilon \frac{\epsilon^{\alpha-1}}{e^{\frac{\epsilon-\mu}{k_B T}} - 1}. \quad (1.6)$$

Moreover, because an increase in the particle number must be followed by an increase in the chemical potential, we find that in the limit  $\mathcal{N} \rightarrow \infty$ , the chemical potential must approach its upper limit  $\mu = 0$  (from below). Then, for the second term in (1.6), usually referred to as the *critical density*  $n_c$ , one finds

$$\begin{aligned} n_c &= \frac{c_\alpha}{\mathcal{V}} \int_0^\infty d\epsilon \frac{\epsilon^{\alpha-1}}{e^{\frac{\epsilon}{k_B T}} - 1} = \frac{(k_B T)^\alpha c_\alpha}{\mathcal{V}} \int_0^\infty dx \frac{x^{\alpha-1}}{e^x} \\ &= \frac{(k_B T)^\alpha c_\alpha}{\mathcal{V}} \zeta(\alpha) \Gamma(\alpha), \end{aligned} \quad (1.7)$$

where we have made the substitution  $x = \epsilon/k_B T$ , and where  $\Gamma(x)$  is the Gamma function and  $\zeta(z)$  the Riemann zeta function. For  $\alpha = 3/2$  for instance, one finds  $\zeta(\alpha)\Gamma(\alpha) \approx 2.315$ .

Therefore, one can see that increasing the number of particles  $\mathcal{N}$ , the chemical potential  $\mu$  approaches zero, the second term in (1.6) approaches the critical density  $n_c$ , and the remaining particles start falling all in the lowest energy state. This process, also attainable with similar arguments in the limit  $T \rightarrow 0$ , is known as Bose-Einstein condensation [74].

Let us finally notice, that since  $n_c \sim \zeta(\alpha)\Gamma(\alpha)$ , the process of condensation might be forbidden for systems of certain dimensionalities. In particular, because the Riemann zeta functions diverges in  $\alpha = 1$  and is negative on the domain  $[0, 1)$ , and the Gamma function diverges in  $\alpha = 0$ , one finds condensation at finite temperatures, only for an harmonically confined system in dimensions  $d > 1$ , or for a homogeneous system with dimensions  $d > 2$ .

More rigorous results concerning the existence of the process of condensation for more realistic systems can of course be obtain [75, 76] as a function of the number of particles, the strength of interaction, etc., but are out of the scope of this thesis.

### 1.1.2 Interacting systems: the Gross-Pitaevskii equation

For a fully condensed system, all particles occupy the same (normalised) single particle state  $\phi(\mathbf{r})$ , and the wavefunction describing the condensate in the mean field approach (Hartree-Fock) is a symmetrised product of the single particle wave functions

$$\Psi(\mathbf{r}_1, \mathbf{r}_2, \dots, \mathbf{r}_N) = \prod_{j=1}^N \phi(\mathbf{r}_j). \quad (1.8)$$

In addition, the interactions are typically well approximated at low energies, by a constant effective interaction in momentum space  $g = 4\pi\hbar^2 a/m$  (with  $a$  the s-wave scattering length), which in coordinate space, translates to the effective contact potential of the form  $g\delta(\mathbf{r}_j - \mathbf{r}_k)$ . The corresponding Hamiltonian then can be written as

$$H = \sum_{j=1}^N \left( \frac{\mathbf{p}_j^2}{2m} + V(\mathbf{r}_j) \right) + g \sum_{j<k} \delta(\mathbf{r}_j - \mathbf{r}_k); \quad (1.9)$$

introducing the scaled quantity  $\psi(\mathbf{r}) = \sqrt{N}\phi(\mathbf{r})$ , known as the *condensate wave function*, and neglecting terms of order  $1/N$ , which is safe for large  $N$ , it is possible to write the expectation value of the Hamiltonian (1.9), corresponding to the energy associated with the state (1.8), as

$$E[\psi] = \int d\mathbf{r} \left[ \frac{\hbar^2}{2m} |\nabla\psi(\mathbf{r})|^2 + V(\mathbf{r})|\psi(\mathbf{r})|^2 + \frac{g}{2} |\psi(\mathbf{r})|^4 \right]. \quad (1.10)$$

An expression for the wave function can now be obtained by minimising this energy functional with respect to independent variations of  $\psi$  and  $\psi^*$  subject

to the constant normalisation condition

$$\mathcal{N} = \int d\mathbf{r} |\psi(\mathbf{r})|^2; \quad (1.11)$$

this constraint can be accounted for by a Lagrange multiplier  $\mu$ , i.e. the chemical potential ensuring constancy of the total particle number. Writing the variations in the wave function as  $\psi \rightarrow \psi + \delta\psi$ , and dropping the explicit dependence on  $\mathbf{r}$ , we find<sup>1</sup>

$$\delta(E - \mu\mathcal{N}) = \int d\mathbf{r} \left[ \frac{\hbar^2}{2m} \nabla\psi \nabla\delta\psi^* + V\psi\delta\psi^* + g|\psi|^2\psi\delta\psi^* - \mu\psi\delta\psi^* \right] + c.c., \quad (1.12)$$

and finally equating to zero the variation of the quantity  $E - \mu\mathcal{N}$  with respect to  $\psi^*$ , one obtains the so-called time independent Gross-Pitaevskii equation<sup>2</sup>[77, 78]:

$$-\frac{\hbar^2}{2m} \nabla^2\psi + V\psi + g|\psi|^2\psi = \mu\psi, \quad (1.13)$$

thereby greatly simplifying the full many-body problem into a single non-linear differential equation. In the limit of a non-interacting system, it is worth noticing that (1.13) reduces to the Schrödinger equation, as the interaction strength vanishes, and the chemical potential becomes the mean energy per particle.

The Gross-Pitaevskii equation, similarly to its linear counterpart, the Schrödinger equation, has a time-dependent version in which the chemical potential  $\mu$  is replaced by  $i\hbar\partial_t$ ; this can be justified on the basis of Bogoliubov microscopic theory through Heisenberg time evolution equation, or alterna-

---

<sup>1</sup>Disregarding terms of order higher than  $\delta\psi$ . In particular we have used:  $\nabla(\psi + \delta\psi)\nabla(\psi^* + \delta\psi^*) = |\nabla\psi|^2 + \nabla\psi\nabla\delta\psi^* + \nabla\psi^*\nabla\delta\psi + \nabla\delta\psi\nabla\delta\psi^*$ , and similarly for  $(\psi + \delta\psi)(\psi^* + \delta\psi^*)$ .

<sup>2</sup>Here we have made use of the integration by parts  $\langle \nabla\psi | \nabla\psi \rangle = -\langle \psi | \nabla^2\psi \rangle$ .

tively, from an action principle<sup>3</sup> [73]. The time dependent Gross-Pitaevskii equation then reads

$$i\hbar\partial_t\psi = -\frac{\hbar^2}{2m}\nabla^2\psi + V\psi + g|\psi|^2\psi. \quad (1.14)$$

### Conservation of the energy

A property of foremost importance that the equation of motion (1.14) must respect, is that of energy conservation. We will now briefly show that this is indeed the case.

One way to prove the energy is conserved in time is to look at the Lagrangian associated with the energy (1.10). Confirming that such a quantity is invariant under time translations  $t \rightarrow t + \delta t$ , one can invoke Noether theorem to find that the energy is the associated conserved quantity. However, more concisely and directly, one can consider the time evolution (1.14) in terms of the hermitian Hamiltonian operator  $H = H_0 + g\rho$ , using *bra-ket* notation, as

$$\begin{aligned} i\hbar|\dot{\psi}\rangle &= (H_0 + g\rho)|\psi\rangle, \\ i\hbar\langle\dot{\psi}| &= -\langle\psi|(H_0 + g\rho), \end{aligned} \quad (1.15)$$

where we have introduced the density  $\rho = |\psi|^2$ , and where  $H_0 = -\frac{\hbar^2}{2m}\nabla^2 + V$  is the linear Schrödinger Hamiltonian. The dot denotes, as usual, a time

---

<sup>3</sup> $\delta \int_{t_1}^{t_2} L dt = 0$ , where the Lagrangian is given by  $L = \frac{i\hbar}{2} \int d\mathbf{r} (\psi^* \partial_t \psi - \psi \partial_t \psi^*) - E$ .

derivative. Then,

$$\begin{aligned}
 \frac{dE}{dt} &= \langle \dot{\psi} | H_0 | \psi \rangle + \langle \psi | H_0 | \dot{\psi} \rangle + g \left( \langle \dot{\psi} | \rho | \psi \rangle + \langle \psi | \rho | \dot{\psi} \rangle \right) \\
 &= \frac{1}{i\hbar} \left( -\langle \psi | H H_0 | \psi \rangle + \langle \psi | H_0 H | \psi \rangle \right) + \frac{g}{i\hbar} \left( -\langle \psi | H \rho | \psi \rangle + \langle \psi | \rho H | \psi \rangle \right) \\
 &= \frac{g}{i\hbar} \left( \langle \psi | [H_0, \rho] | \psi \rangle + \langle \psi | [\rho, H_0] | \psi \rangle \right) \\
 &= 0,
 \end{aligned} \tag{1.16}$$

as expected.

### Particle number conservation

Another important quantity which is conserved in the time evolution of equations (1.14) is the total number of particles  $\mathcal{N} = \langle \psi | \psi \rangle$ . This can be readily shown by explicitly taking the time derivative:

$$\begin{aligned}
 \frac{d\mathcal{N}}{dt} &= \langle \dot{\psi} | \psi \rangle + \langle \psi | \dot{\psi} \rangle \\
 &= -\frac{1}{i\hbar} \langle \psi | H | \psi \rangle + \frac{1}{i\hbar} \langle \psi | H | \psi \rangle = 0,
 \end{aligned} \tag{1.17}$$

consistently with the normalisation condition (1.11).

### 1.1.3 Time-independent solutions and characteristic lengths

Although the achievement of the Gross-Pitaevskii equation has provided a great simplification over the original many-body problem, this is still a non-linear differential equation with no exact solution. One needs therefore, in general, to resort to numerical methods.

However, there are a few cases in which we can approximate (1.14) and still get a good estimate of the wave function. Consider for instance, the case of an harmonically trapped system, so that  $V(\mathbf{r}) = \frac{m\omega^2}{2} r^2$ . When the number



of particles  $N$  is large, and interactions are repulsive, the contribution of the kinetic energy becomes negligible [73], and one can approximate (1.13) by  $(V + g\rho)\psi = \mu\psi$ , which has solution

$$\psi_{TF} = \begin{cases} \sqrt{(\mu - V)/g} & \text{if } V < \mu \\ 0 & \text{if } V > \mu \end{cases}. \quad (1.18)$$

This result, commonly referred to as Thomas-Fermi approximation, provides a useful analytic tool for theoretical description of a condensate. Figure 1.1 shows the good agreement of the Thomas-Fermi approximation with a numerical solution for the 1D problem in the harmonic trapping potential. The boundary of the system is then given by  $V = \mu$ , which, for a system with spherical symmetry, provides a way to estimate the extension of the cloud: this is the so called *Thomas-Fermi radius*

$$R_{TF} = \sqrt{\frac{2\mu}{m\omega^2}}. \quad (1.19)$$

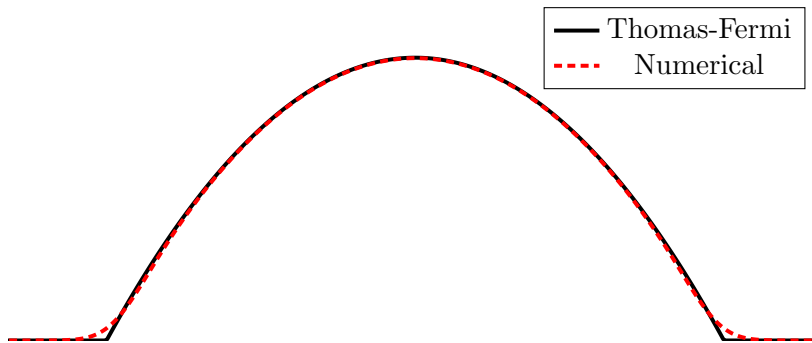


Figure 1.1: Thomas-Fermi approximation compared with numerical solution in 1D.

The concept of radius of the condensate allows one to obtain an approximation for the chemical potential by plugging (1.18) into the normalisation

condition for the wavefunction

$$\int d\mathbf{r} |\psi(\mathbf{r})|^2 = \mathcal{N}. \quad (1.20)$$

Depending on the dimensionality  $d$  of the system, this leads

$$\mu_{TF} = \begin{cases} \frac{1}{2} (3g\omega\mathcal{N}\sqrt{m})^{2/3} & \text{if } d = 1 \\ \sqrt{gm\omega^2\mathcal{N}/\pi} & \text{if } d = 2 \\ \frac{m^{3/5}}{2} (15g\omega^3\mathcal{N}/4\pi)^{2/5} & \text{if } d = 3 \end{cases}. \quad (1.21)$$

We conclude this discussion on the characteristics of the time-independent system, introducing another important parameter which will be useful throughout the rest of this work, namely the *healing length*  $\xi$ , also known as *correlation length*. The healing length, gives a scale of how the density of the condensate changes near a local perturbation. In particular, we denote by  $\xi$  the order of spatial variations, so that the kinetic energy in the Gross-Pitaevskii balances with the interaction energy. Writing  $\hbar^2/2m\xi$  for the kinetic energy, and  $g\bar{\rho}$  for the interaction energy, one finds the following expression for the healing length of the condensate

$$\xi = \sqrt{\frac{\hbar^2}{2mg\bar{\rho}}}, \quad (1.22)$$

with  $\bar{\rho} = \mathcal{N}/\mathcal{V}$  the average density. The healing length is then the distance over which the wave function heals over defects, such as, for instance, vortices, as we will see later.

As we have mentioned, in the Thomas-Fermi regime we can neglect the energy contribution coming from the kinetic term in (1.10) [79]. For a homogeneous system we can then approximate the ground state as  $E_0 = \bar{\rho}g\mathcal{N}/2$ . Thus, in contrast with the case of an ideal gas, a bosonic system experiences

a non vanishing pressure at zero temperature:

$$P = -\frac{\partial E_0}{\partial \mathcal{V}} = \frac{g\bar{\rho}^2}{2}. \quad (1.23)$$

Moreover, one can find a finite compressibility as well

$$\frac{\partial \bar{\rho}}{\partial P} = \frac{1}{g\bar{\rho}}, \quad (1.24)$$

and using through the hydrodynamic relation

$$\frac{\partial \bar{\rho}}{\partial P} = \frac{1}{mc^2}, \quad (1.25)$$

find an expression for the sound velocity

$$c = \sqrt{\frac{g\bar{\rho}}{m}}. \quad (1.26)$$

This expression (1.26) for the velocity of sound is in agreement with that found in the Bogoliubov dispersion relation for elementary excitations [79, 73]

$$\epsilon(p) = \sqrt{\frac{g\bar{\rho}}{m}p^2 + \left(\frac{p^2}{2m}\right)^2}, \quad (1.27)$$

which in the long wavelength limit (i.e. for small momenta  $p \ll mc$ ) takes the phonon-like form

$$\epsilon(p) = cp. \quad (1.28)$$

In the opposite limit of short wavelengths,  $p \gg mc$ , the dispersion relation (1.27) approaches the free particle relation

$$\epsilon(p) \approx \frac{p^2}{2m} + g\bar{\rho}. \quad (1.29)$$

It is worth noticing that the healing length defined in (1.22) can be also defined in terms of the speed of sound as

$$\xi = \frac{1}{\sqrt{2}} \frac{\hbar}{mc}. \quad (1.30)$$

## 1.2 Mixtures of condensates

We now turn our attention to multicomponent systems. The simplest multicomponent system is one consisting of a mixture of two different atomic species [80]. These systems are sometimes known as *scalar mixtures*. Another possibility is that of a mixture of the same isotopes, but in different hyperfine states [81], which has recently become experimentally amenable with the advent of optical trapping techniques [68]. The introduction of extra degrees of freedom in this latter case, due to the possibility of each component to transition into the other hyperfine state, makes the treatment of these systems more complicated, and we shall concern ourselves only with the case of scalar mixtures.

Let us then start considering a mixture of two different condensates, each described by the wave functions  $\psi_1$  and  $\psi_2$ . One can then write the overall wavefunction for the composite system as

$$\Psi = \prod_{j=1}^{\mathcal{N}_1} \phi_1(\mathbf{r}_j) \prod_{k=1}^{\mathcal{N}_2} \phi_2(\mathbf{r}_k), \quad (1.31)$$

analogously to what was done for the single component problem (1.8), and with obvious notation for the single particle wave functions of the first component  $\phi_1$  and second component  $\phi_2$ . Following the same procedure as before, we introduce the two scaled condensate wave functions  $\psi_1 = \sqrt{\mathcal{N}_1} \phi_1$  and  $\psi_2 = \sqrt{\mathcal{N}_2} \phi_2$ , and find that neglecting terms of order  $1/\mathcal{N}_1$  and  $1/\mathcal{N}_2$ , the

total energy of the system is described by the following functional

$$E = \int d\mathbf{r} \left[ \frac{\hbar^2}{2m_1} |\nabla\psi_1|^2 + \frac{\hbar^2}{2m_2} |\nabla\psi_2|^2 + V_1 |\psi_1|^2 + V_2 |\psi_2|^2 + \frac{g_1}{2} |\psi_1|^4 + \frac{g_2}{2} |\psi_2|^4 + g_{12} |\psi_1|^2 |\psi_2|^2 \right], \quad (1.32)$$

from which, through the variational principle used in Sec. 1.1.2, follow the equations of motion, namely the two coupled GPEs

$$\begin{aligned} i\hbar \frac{\partial\psi_1}{\partial t} &= \left( -\frac{\hbar^2}{2m_1} \nabla^2 + V_1 + g_1 |\psi_1|^2 + g_{12} |\psi_2|^2 \right) \psi_1, \\ i\hbar \frac{\partial\psi_2}{\partial t} &= \left( -\frac{\hbar^2}{2m_2} \nabla^2 + V_2 + g_2 |\psi_2|^2 + g_{12} |\psi_1|^2 \right) \psi_2. \end{aligned} \quad (1.33)$$

The interaction strength between atoms of the same kind is here quantified by  $g_i$ , while the interspecies interaction is quantified by  $g_{12}$ ; the latter can be found to be [73]

$$g_{12} = 2\pi\hbar^2 a_{12} \frac{m_1 + m_2}{m_1 m_2}, \quad (1.34)$$

with  $a_{12}$  the scattering lengths between the two different species, and where  $m_1$ ,  $m_2$  are the masses of the constituents of the first and second component respectively. The system preserves the total energy as well as the number of particles for each species individually.

Let us consider now spatial variations of the energy (neglecting contributions from the kinetic energy, i.e. being under diluteness conditions): for a solution to be stable we must require that the energy increases for these

deviations. The first order variation is found to be

$$\begin{aligned}\delta E &= \int d\mathbf{r} \left[ \sum_i \frac{\partial \mathcal{E}}{\partial \rho_i} \delta \rho_i \right] \\ &= \int d\mathbf{r} \left[ \sum_i \mu_i \delta \rho_i \right] = 0,\end{aligned}\tag{1.35}$$

where  $\mathcal{E}$  is as usual the integrand of (1.32), the energy density. In the previous equation we have used the fact that  $\partial_{\rho_i} \mathcal{E} = \mu_i$  with  $\mu_i$  the chemical potential of the  $i$ th species, and that

$$\delta \left( \int \rho_i d\mathbf{r} \right) = \delta \mathcal{N}_i = 0,\tag{1.36}$$

because of particle number conservation. The second order variation leads to the following quadratic form instead

$$\begin{aligned}\delta^2 E &= \frac{1}{2} \int d\mathbf{r} \left[ \frac{\partial^2 \mathcal{E}}{\partial \rho_1^2} (\delta \rho_1)^2 + \frac{\partial^2 \mathcal{E}}{\partial \rho_2^2} (\delta \rho_2)^2 + 2 \frac{\partial^2 \mathcal{E}}{\partial \rho_1 \partial \rho_2} \delta \rho_1 \delta \rho_2 \right] \\ &= \frac{1}{2} \int d\mathbf{r} \left[ \frac{\partial \mu_1}{\partial \rho_1} (\delta \rho_1)^2 + \frac{\partial \mu_2}{\partial \rho_2} (\delta \rho_2)^2 + \left( \frac{\partial \mu_1}{\partial \rho_2} + \frac{\partial \mu_2}{\partial \rho_1} \right) \delta \rho_1 \delta \rho_2 \right] \\ &= \frac{1}{2} \left[ \langle \delta \boldsymbol{\rho} | \nabla_{\boldsymbol{\rho}} \boldsymbol{\mu} | \delta \boldsymbol{\rho} \rangle \right],\end{aligned}\tag{1.37}$$

where we have introduced the following matrix

$$\nabla_{\boldsymbol{\rho}} \boldsymbol{\mu} = \begin{pmatrix} \frac{\partial \mu_1}{\partial \rho_1} & \frac{\partial \mu_2}{\partial \rho_1} \\ \frac{\partial \mu_1}{\partial \rho_2} & \frac{\partial \mu_2}{\partial \rho_2} \end{pmatrix},\tag{1.38}$$

and the vector  $|\delta \boldsymbol{\rho}\rangle \equiv (\delta \rho_1, \delta \rho_2)^T$ . Then, for the quadratic form to be positive definite we must require the trace and the determinant of (1.38) to be strictly

positive; from this we obtain the following conditions

$$\frac{\partial \mu_i}{\partial \rho_i} > 0, \quad \frac{\partial \mu_1}{\partial \rho_1} \frac{\partial \mu_2}{\partial \rho_2} > \frac{\partial \mu_1}{\partial \rho_2} \frac{\partial \mu_2}{\partial \rho_1} = \left( \frac{\partial \mu_1}{\partial \rho_2} \right)^2 = \left( \frac{\partial \mu_2}{\partial \rho_1} \right)^2. \quad (1.39)$$

Recalling once again that we are working in a regime where the kinetic energy can be neglected, one can find that  $\partial_{\rho_i} \mu_i = g_i$  and  $\partial_{\rho_1} \mu_2 = \partial_{\rho_2} \mu_1 = g_{12}$ , so that the above translate into

$$\begin{aligned} g_1 &> 0, \\ g_2 &> 0, \\ g_1 g_2 &> g_{12}^2. \end{aligned} \quad (1.40)$$

These give the necessary and sufficient conditions for stability, and in particular, the first and second conditions ensure the stability against collapse of each component, while the third enforces stability against phase separation. For this reason the third condition in (1.40) is also known as the *miscibility/immiscibility condition*. Further, it is possible to show that the conditions (1.40), ensure the resilience of the overall uniformity of the system [73, 82].

Finally, let us show more in detail how the above condition gives rise to a transition between an homogeneous and inhomogeneous phases. The total energy of the inhomogeneous state can be written as

$$E_{\text{in}} = \sum_{j=1,2} g_j \frac{\mathcal{N}_j^2}{\mathcal{V}_j}, \quad (1.41)$$

where  $\mathcal{V}_j$  is the volume occupied by the  $j$ th component. The total volume is then  $\mathcal{V} = \mathcal{V}_1 + \mathcal{V}_2$ . A similar expression for the energy associated with the homogeneous state can be written:

$$E_{\text{ho}} = \frac{g_1}{2} \frac{\mathcal{N}_1^2}{\mathcal{V}} + \frac{g_2}{2} \frac{\mathcal{N}_2^2}{\mathcal{V}} + g_{12} \frac{\mathcal{N}_1 \mathcal{N}_2}{\mathcal{V}}. \quad (1.42)$$

When the intra-species strength is sufficiently small, any variation in the

densities increases the total energy, which implies that excitations are stable, and the homogeneous state is the ground state. This might not be true however when the intra-species strength is larger: in particular we can see that there exist a state with lower energy. Let us proceed minimising  $E_{\text{in}}$  with respect to the two components volumes, so as to obtain the following expressions:

$$\begin{aligned}\mathcal{V}_1 &= \frac{\mathcal{V}}{1 + \sqrt{\frac{g_2 \mathcal{N}_2}{g_1 \mathcal{N}_1}}}, \\ \mathcal{V}_2 &= \frac{\mathcal{V}}{1 + \sqrt{\frac{g_1 \mathcal{N}_1}{g_2 \mathcal{N}_2}}};\end{aligned}\tag{1.43}$$

moreover the two components' densities can then be written as

$$\begin{aligned}\bar{\rho}_1 &= \left(1 + \sqrt{\frac{g_2 \mathcal{N}_2}{g_1 \mathcal{N}_1}}\right) \frac{\mathcal{N}_1}{\mathcal{V}}, \\ \bar{\rho}_2 &= \sqrt{\frac{g_2}{g_1}} \bar{\rho}_1.\end{aligned}\tag{1.44}$$

Here  $\bar{\rho}_j$  are the average densities of the two condensates. Further, the energy for the inhomogeneous state is now written as

$$E_{\text{in}} = \frac{g_1 \mathcal{N}_1^2}{2 \mathcal{V}} + \frac{g_2 \mathcal{N}_2^2}{2 \mathcal{V}} + \sqrt{g_1 g_2} \frac{\mathcal{N}_1 \mathcal{N}_2}{\mathcal{V}}.\tag{1.45}$$

Thus we can compute the difference between the energy associated with the homogeneous and inhomogeneous states:

$$E_{\text{ho}} - E_{\text{in}} = (g_{12} - \sqrt{g_1 g_2}) \frac{\mathcal{N}_1 \mathcal{N}_2}{\mathcal{V}}.\tag{1.46}$$

The miscibility/immiscibility condition in (1.40) then follows directly [79, 82]. Let us therefore notice that, although this result can also be obtained from a dynamical stability argument [79, 83], the above energetic stability argu-



ment is sufficient in order to determine the miscibility/immiscibility transition point.

The collective excitations for a system with  $m = m_1 = m_2$ , can be found with the usual Bogoliubov procedure, which in the case of a mixture of two components leads to a generalisation of (1.27) [79, 73]:

$$\varepsilon^{(\pm)}(p) = \sqrt{\frac{p^2}{2m} \left( \frac{p^2}{2m} + 2mc_{\pm}^2 \right)}, \quad (1.47)$$

where the squared density sound velocity  $c_+^2$  and spin sound velocity  $c_-^2$  are eigenvalues of

$$\frac{1}{m} \begin{pmatrix} g_1 \bar{\rho}_1 & g_{12} \sqrt{\bar{\rho}_1 \bar{\rho}_2} \\ g_{12} \sqrt{\bar{\rho}_1 \bar{\rho}_2} & g_2 \bar{\rho}_2 \end{pmatrix}, \quad (1.48)$$

corresponding to modes in which the two condensates move in phase (density modes) or out of phase (spin modes). The two sound velocities read:

$$c_{\pm}^2 = \frac{1}{2m} \left[ g_1 \bar{\rho}_1 + g_2 \bar{\rho}_2 \pm \sqrt{(g_1 \bar{\rho}_1 + g_2 \bar{\rho}_2)^2 + 4(g_{12}^2 - g_1 g_2) \bar{\rho}_1 \bar{\rho}_2} \right]. \quad (1.49)$$

For  $g_{12}^2 > g_1 g_2$  one has  $c_-^2 < 0$ , which means that  $\varepsilon^{(-)}(p)$  becomes imaginary for long wavelengths, leading to dynamical instability, in agreement with our energetic argument above. Further, notice that in the simplified case in which  $g = g_1 = g_2$ , and  $\bar{\rho} = \bar{\rho}_1 = \bar{\rho}_2$ , the velocities above take the simple form  $c_{\pm} = \frac{\bar{\rho}}{m}(g \pm g_1 2)$ .

In analogy with the definition of the healing length in (1.30), one can now define the density and spin healing lengths for the mixture as

$$\xi_{\pm} = \sqrt{\frac{\hbar^2}{2mc_{\pm}^2}}. \quad (1.50)$$

Notice in particular that, approaching the miscibility/immiscibility boundary  $\alpha = 1$ , while the density healing length  $\xi_+$  slowly decays because of the increasing density sound velocity  $c_+$ , the spin healing length  $\xi_-$  diverges.

Even more generally, when considering different constituents' masses  $m_2 \neq m_1$ , one finds the following dispersion relation [73]:

$$\varepsilon^{(\pm)}(p) = \sqrt{\frac{p^2}{2\sqrt{m_1 m_2}} \left( \frac{p^2}{4\sqrt{m_1 m_2}} \frac{m_2^2 + m_1^2}{m_1 m_2} + 2\sqrt{m_1 m_2} c_{\pm}^2 \right)}, \quad (1.51)$$

where the sound velocities are now given by

$$c_{\pm}^2 = \frac{g_1 \bar{\rho}_1}{2m_1} + \frac{g_2 \bar{\rho}_2}{2m_2} \pm \frac{1}{2\sqrt{m_1 m_2}} \sqrt{\left( \frac{p^2}{4\sqrt{m_1 m_2}} \frac{m_2^2 - m_1^2}{m_1 m_2} + g_1 \bar{\rho}_1 \sqrt{\frac{m_2}{m_1}} - g_2 \bar{\rho}_2 \sqrt{\frac{m_1}{m_2}} \right)^2 + 4g_{12}^2 \bar{\rho}_1 \bar{\rho}_2}. \quad (1.52)$$

One can then write an expression for the two density and spin healing lengths which accounts for different components' masses. These expressions offer a natural way to characterise the phase transitions of the system, such as those described in chapters 5 and 6.

### 1.2.1 SU(2) symmetric point

For the case of equal interaction strength  $g_1 = g_2 = g_{12} \equiv g$ , the system enters into a particularly symmetric state: the energy becomes in fact invariant under SU(2) rotations of the condensate wave function [70]. The interaction energy density can indeed be written as

$$\mathcal{E}_I = \frac{g}{2} (\rho_1^2 + \rho_2^2 + 2\rho_1 \rho_2) = \frac{g}{2} (\rho_1 + \rho_2)^2. \quad (1.53)$$

Equivalently, defining the overall wave function

$$\Psi = \begin{pmatrix} \psi_1 \\ \psi_2 \end{pmatrix}, \quad (1.54)$$

the interaction energy density can be written concisely as

$$\mathcal{E}_I = \frac{g}{2} (\Psi^\dagger \Psi)^2. \quad (1.55)$$

The main consequence of this result, is that at the  $SU(2)$  symmetric point, which demarcates the boundary between the miscible and immiscible phases, the two components will behave as a single component with wave function  $\Psi$ . This result allows to conclude, for instance, that the ground state of a system under rotation at the  $SU(2)$  point will consist of a triangular vortex lattice (as a combination of the individual vortex lattices of each component), as it is expected for a rotating single component superfluid. This is indeed the case, as we will argue in Chapter 5.

In order to make the  $SU(2)$  invariance of the system manifest, it is beneficial to reparametrise the condensate wave function as a function of the total density  $\rho = \rho_1 + \rho_2$  and the polar and azimuthal angles  $\theta$  and  $\phi$ :

$$\Psi = \begin{pmatrix} \psi_1(\mathbf{r}) \\ \psi_2(\mathbf{r}) \end{pmatrix} = \sqrt{\rho} e^{i\chi} \begin{pmatrix} \sin(\frac{\theta}{2}) e^{i\phi/2} \\ \cos(\frac{\theta}{2}) e^{-i\phi/2} \end{pmatrix}, \quad (1.56)$$

where  $\chi$  is a global phase. Then at the  $SU(2)$  symmetric point, the system is invariant under rotations of the polar and azimuthal angles  $\theta$  and  $\phi$  as well as the global phase  $\chi$ . A departure from this highly symmetric point, is expected to yield anisotropies in the energy [84]. Although probably not expected, the  $SU(2)$  symmetric point is experimentally particularly relevant. One example is the mixture of two  $^{87}\text{Rb}$  hyperfine states  $|1\rangle = |F=1, m_F=-1\rangle$  and  $|2\rangle = |F=2, m_F=1\rangle$ , for which  $g_1 = 100.44\bar{a}$ ,  $g_2 = 95.47\bar{a}$  and  $g_{12} = 98.09\bar{a}$ ,

where  $\bar{a} = 4\pi\hbar^2 a_0 / m_{87\text{Rb}}$ ,  $m_{87\text{Rb}}$  is the rubidium isotope's atomic mass, and  $a_0$  is the Bohr radius [85].

### 1.3 Quantum Fluid Dynamics of the Gross-Pitaevskii equation

In order to shed more light on the physical behaviour of condensates, one may consider reformulating the Gross-Pitaevskii equation in a different form. The usual linear Schrödinger equation can be recast in a system of fluid-dynamics-like equations, as it was firstly shown by Madelung [86]. The formalism used, also known as Madelung transformations, can be extended to general non-linear Schrödinger equations [87]. In particular we are interested in the applications of such methods to the Gross-Pitaevskii equation [79, 73, 88]. Consider the multiplication of the Gross-Pitaevskii equation (1.14) by  $\psi^*$ ,

$$i\hbar\psi^*\frac{\partial\psi}{\partial t} = -\frac{\hbar^2}{2m}\psi^*\nabla^2\psi + V\rho + g\rho^2, \quad (1.57)$$

where  $\rho(\mathbf{r}) = |\psi(\mathbf{r})|^2$  is the density. Subtracting (1.57) from its complex conjugate we immediately obtain a *continuity equation* for the particle density:

$$\frac{\partial\rho}{\partial t} + \nabla \cdot \mathbf{j} = 0, \quad (1.58)$$

where the momentum density is given by

$$\mathbf{j} = \frac{\hbar}{2i} (\psi^*\nabla\psi - \psi\nabla\psi^*). \quad (1.59)$$

Drawing analogies from classical fluid mechanics, we can then identify the *superfluid velocity* as  $\mathbf{v} = \mathbf{j}/m\rho$ . Writing the wave function in terms of its amplitude and its phase as  $\psi = \sqrt{\rho}e^{i\phi}$ , and plugging this ansatz into the

### 1.3. Quantum Fluid Dynamics of the Gross-Pitaevskii equation 51

expression for the superfluid velocity, we obtain the following expression

$$\mathbf{v} = \frac{\hbar}{m} \nabla \phi. \quad (1.60)$$

This condition heavily constricts the possible motion of a condensate, which is said to correspond to potential flow, where the quantity  $\hbar\phi/m$  is referred to as the *velocity potential*. Provided that the phase  $\phi$  is not singular, the condensate is therefore irrotational, since

$$\nabla \times \mathbf{v} = \frac{\hbar}{m} \nabla \times \nabla \phi = 0. \quad (1.61)$$

The phase  $\phi$  on its own has no physical significance: the state is always defined up to a phase, which reflects the gauge invariance of the system<sup>4</sup>; however, as we can see, once we have fixed the gauge, differences of phases do have a significance. We will discuss more on this in the next sections.

A substitution of  $\psi = \sqrt{\rho}e^{i\phi}$  into the Gross-Pitaevskii equation generates a set of two equations which can be found by splitting the GPE into its real and imaginary parts. The imaginary part results in (1.58), whereas the real part leads to

$$-\hbar \frac{\partial \phi}{\partial t} = -\frac{\hbar^2}{2m\sqrt{\rho}} \nabla \sqrt{\rho} + \frac{1}{2} m \mathbf{v}^2 + V + g\rho, \quad (1.62)$$

or, taking the gradient

$$D_t \mathbf{v} = \nabla \left( \frac{\hbar^2}{2m\sqrt{\rho}} \nabla \sqrt{\rho} - V - g\rho \right), \quad (1.63)$$

where  $D_t$  is the so-called material derivative given by the time derivative plus a self-advective term  $D_t = m\partial_t + m\mathbf{v}\nabla$ . The left hand side comes in

---

<sup>4</sup>See Chapter 1, Sec. 1.5.

particular from the relation

$$\frac{1}{2}\nabla\mathbf{v}^2 = \mathbf{v}\nabla\mathbf{v} + \mathbf{v} \times (\nabla \times \mathbf{v}), \quad (1.64)$$

and from the realisation that the latter can be further simplified for irrotational  $\mathbf{v}$ . Equation (1.63) is analogous to the inviscid Navier-Stokes equation, also known as Euler equation.

To sum up, we just showed that the Gross-Pitaevskii equation can be rewritten as a set of equations analogous to well known equations in fluid dynamics, namely

$$\begin{cases} \frac{\partial\rho}{\partial t} + \nabla \cdot \mathbf{j} = 0 \\ D_t\mathbf{v} = \nabla \left( \frac{\hbar^2}{2m\sqrt{\rho}} \nabla^2 \sqrt{\rho} - V - g\rho \right) \end{cases} \quad (1.65)$$

The argument of the gradient in the second equation is referred to as *quantum pressure* and describes forces due to spatial variations in  $\rho$ . In particular this term can be shown to derive directly from Heisenberg uncertainty principle [79].

## 1.4 Rotation of superfluids

Some of the most interesting properties of a superfluid, are related to the non classical manner in which superfluids react to rotation. We have already discussed about the irrotationality of the system due to the motion of the condensate corresponding to a potential flow. We will now consider what are the consequences of the introduction of rotation in a superfluid by analysing the problem from a rotating frame of reference.

Recalling that the infinitesimal generator of rotations is the angular momentum operator  $\mathbf{L}$ , we can write a general rotation around the axis  $\mathbf{u}$  as

$R_{\mathbf{u}}(\theta) = \exp(-i\theta\mathbf{u} \cdot \mathbf{L})$ . In order to consider the action of an operator under rotation we can consider a wave function  $\psi$  and its rotated counterpart  $\tilde{\psi} = R_{\mathbf{u}}\psi$ . Given an operator  $A$  acting on such a wave function, one finds that this operator is transformed in the rotating frame as

$$R_{\mathbf{u}}(A\psi) = R_{\mathbf{u}}AR_{\mathbf{u}}^\dagger R_{\mathbf{u}}\psi = R_{\mathbf{u}}AR_{\mathbf{u}}^\dagger \tilde{\psi}. \quad (1.66)$$

Thus, we infer that a quantum system described by the Hamiltonian  $H_0$  with a rotationally invariant confining potential, will be described under rotation by a time dependent Hamiltonian  $H(t) = R_{\Omega}H_0R_{\Omega}^\dagger$ . The time dependence is here introduced through the time varying angle  $\theta = \Omega t$ , so that the rotation operator reads  $R_{\Omega} = \exp(-it\Omega \cdot \mathbf{L}/\hbar)$ . If  $\tilde{\psi}$  is the wave function describing the system governed by this time-dependent Hamiltonian  $i\hbar\partial_t\tilde{\psi} = H(t)\tilde{\psi}$ , then we can consider its counterpart in the rotating frame  $\psi = R_{\Omega}^\dagger\tilde{\psi}$  and find the associated equation of motion by considering its time evolution:

$$\begin{aligned} i\hbar\partial_t\psi &= i\hbar(\partial_t R_{\Omega}^\dagger)\tilde{\psi} + i\hbar R_{\Omega}^\dagger\partial_t\tilde{\psi} \\ &= i\hbar(i\Omega \cdot \mathbf{L}/\hbar)R_{\Omega}^\dagger\tilde{\psi} + R_{\Omega}^\dagger H(t)\tilde{\psi} \\ &= -\Omega \cdot \mathbf{L}R_{\Omega}^\dagger\tilde{\psi} + R_{\Omega}^\dagger R_{\Omega}H_0R_{\Omega}^\dagger\tilde{\psi} \\ &= (H_0 - \Omega \cdot \mathbf{L})\psi. \end{aligned} \quad (1.67)$$

Assuming rotation along the  $z$ -axis, the energy functional in the rotating frame then reads:

$$E = \int d\mathbf{r} \left[ \frac{\hbar^2}{2m} |\nabla\psi|^2 + V|\psi|^2 + \frac{g}{2} |\psi|^4 - \Omega\psi^* L_z\psi \right], \quad (1.68)$$

where  $L_z = (xp_y - yp_x) = -i\hbar(x\partial_y - y\partial_x)$  is the  $z$ -component of the angular momentum operator  $\mathbf{L} = \mathbf{r} \times \mathbf{p}$ , with  $\mathbf{p} = -i\hbar\nabla$  the canonical momentum.

The equations of motion are consequently changed into

$$i\hbar \frac{\partial \psi}{\partial t} = \left( -\frac{\hbar^2}{2m} \nabla^2 + V + g|\psi|^2 - \Omega L_z \right) \psi. \quad (1.69)$$

Because of the introduction of the rotation term  $\Omega L_z$ , the energy functional (1.68) is not guaranteed to be lower bounded, i.e. the existence of a ground state is not necessarily guaranteed to exist, being constrained by the values of the angular velocity  $|\Omega|$ ; we will discuss further this important detail in the following Sec. 1.4.3.

It has already been mentioned that a superfluid does not respond in an ordinary way to rotations. This has far-reaching consequences. After the discovery of Bose-Einstein condensation in atomic gases, a lot of effort was spent studying of rotating condensate to match the theoretical predictions on superfluid states [44]. The main reason for these characteristic properties is that superfluids have their motion constrained by the potential flow of the superfluid velocity:

$$\mathbf{v} = \frac{\hbar}{m} \nabla \phi. \quad (1.70)$$

As we have already mentioned, this implies the velocity field is irrotational  $\nabla \times \mathbf{v} = 0$ , as long as the phase is not singular. At low angular velocities the superfluid part of a cloud of condensed atoms will remain at rest. However, such irrotational state may become energetically unfavourable for a higher angular velocity: considering the energy  $E$  and  $\langle \mathbf{L} \rangle$ , which is the expectation value of the angular momentum in the laboratory frame and the energy in the rotating frame  $E_{\text{rot}}$ , the system will tend to minimise

$$E^{\text{rot}} = E - \langle \boldsymbol{\Omega} \cdot \mathbf{L} \rangle, \quad (1.71)$$

which shows that there might be states energetically more favourable than the irrotational state. Considering the ground state energy  $E_0$  and the first



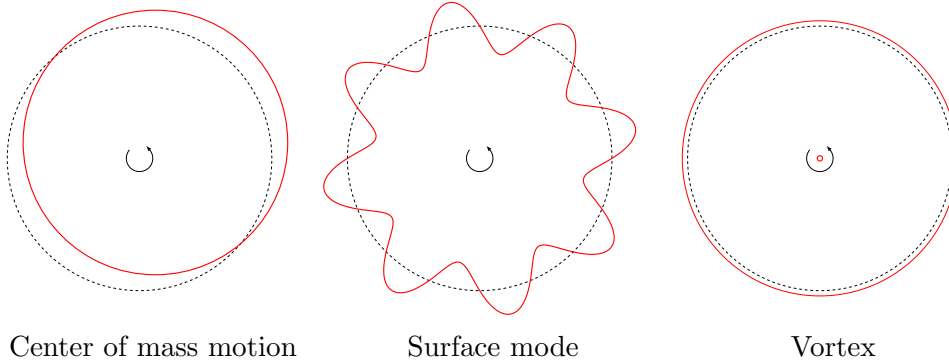


Figure 1.2: Different kind of angular momentum excitations in a superfluid.

excited state energy  $E_1$  and comparing them in the rotating frame we find

$$\Delta E^{\text{rot}} = E_1^{\text{rot}} - E_0^{\text{rot}} = E_1 - E_0 - \Omega L, \quad (1.72)$$

where we have picked an axis of rotation so as to have only one component of  $\boldsymbol{\Omega}$  and  $\langle \mathbf{L} \rangle$ . The excited state becomes energetically favourable when the difference above is negative, so that it turns into the actual ground state. This argument brings us then to define the critical value

$$\Omega > \Omega_c = \frac{E_1 - E_0}{L}, \quad (1.73)$$

known as the critical angular velocity. For any  $\Omega < \Omega_c$  the ground state will be the irrotational ground state, while for  $\Omega > \Omega_c$  one can expect more interesting kinds of excited state, allowing the condensate to acquire angular momentum.

Contributions to the  $\langle \boldsymbol{\Omega} \cdot \mathbf{L} \rangle$  term can be achieved through three kind of excitations: oscillations of the centre of mass, surface modes and vortices; these excitations are depicted in Fig.1.2. We will focus in particular on the latter. From the requirement of single valuedness of the wave functions, it follows that changes in phase  $\Delta\phi$  around any closed contour, must be integer

multiples of  $2\pi$ :

$$\Delta\phi = \oint \nabla\phi \cdot d\mathbf{l} = 2\pi n. \quad (1.74)$$

Consequently, one finds the quantisation condition for the circulation  $\Gamma$ :

$$\Gamma = \oint \mathbf{v} \cdot d\mathbf{l} = \frac{\hbar}{m} 2\pi n, \quad (1.75)$$

a concept firstly put forward by Onsager and Feynman [89, 90]. The only way the requirements of irrotationality and that of existence of non-zero angular momentum can then be simultaneously fulfilled, is if the phase  $\phi$  is singular. The circulation around such a singularity is then  $\Gamma_v = 2\pi n\hbar/m$  and the excitation forming in such conditions is what we call a *quantum vortex*. The quantum number  $n$ , often referred to as the *charge* of the vortex, is commonly restricted to  $n = 1$  in equilibrium. Indeed, as we will see later, multiply-quantised vortices ( $n > 1$ ) are commonly unstable against decay into singly quantised vortices.

### 1.4.1 Density of vortices

In his seminal work [90], Feynman arrived at the conclusion that the lowest energy state for an irrotational fluid with a given angular momentum, is a vortex lattice with a  $2\pi$  winding of the phase around each vortex. Given the superfluid velocity (1.70) it is straightforward to see that the superfluid cannot rotate as a rigid body since  $\nabla \times \mathbf{v} = 0$ , as it was discussed. That is, the velocity field is irrotational, unless the phase  $\phi$  of the order parameter has a singularity. On the other hand, the vortex lattice can only rotate as a rigid body in equilibrium. Hence, on average, the region of the superfluid that is packed with vortices rotates as a rigid body. This allows to estimate a relation between the angular velocity  $\boldsymbol{\Omega}$ , and the number of vortices  $N_v$ , in the ground state.

Let  $D$  be a region of area  $A$  packed with  $N_v$  vortices, and assume, on average, rigid body rotation so that  $\mathbf{v} = \boldsymbol{\Omega} \times \mathbf{r}$ . As usual  $\partial D$  denotes the boundary of  $D$ . Then, it is possible to compute the circulation of the velocity as in (1.75):

$$\begin{aligned}
\Gamma_{\partial D} &= \oint_{\partial D} \mathbf{v} \cdot d\mathbf{l} = \int_D \nabla \times \mathbf{v} \cdot d\mathbf{D} = \int_D \nabla \times (\boldsymbol{\Omega} \times \mathbf{r}) \cdot d\mathbf{D} \\
&= \int_D \nabla \cdot (\mathbf{r}\boldsymbol{\Omega}^T - \boldsymbol{\Omega}\mathbf{r}^T) \cdot d\mathbf{D} \\
&= \int_D [\boldsymbol{\Omega}(\nabla \cdot \mathbf{r}) - (\boldsymbol{\Omega} \cdot \nabla)\mathbf{r}] \cdot d\mathbf{D} \\
&= \int_D (3\boldsymbol{\Omega} - \Omega_j \partial_j \mathbf{r}) \cdot d\mathbf{D} = \int_D (3\boldsymbol{\Omega} - \boldsymbol{\Omega}) \cdot d\mathbf{D} \\
&= 2\boldsymbol{\Omega}A,
\end{aligned} \tag{1.76}$$

where we have used Stokes' theorem, and the identities  $\nabla \times (A \times B) = \nabla \cdot (BA^T - AB^T)$  and  $\nabla \cdot (AB^T) = B(\nabla \cdot A) + (A \cdot \nabla)B$ . Recalling now that the circulation around a single vortex is  $\Gamma_v = 2\pi\hbar/m$ , we can also compute the circulation on  $\partial D$  as

$$\Gamma_{\partial D} = N_v \Gamma_v = \frac{2\pi\hbar}{m} N_v. \tag{1.77}$$

Therefore, introducing the density of vortices  $\rho_v = N_v/A$ , and equating (1.76) with (1.77), one obtains the well known *Feynman relation* [90, 91] for the density of vortices

$$\rho_v = \frac{m\boldsymbol{\Omega}}{\pi\hbar}. \tag{1.78}$$

Looking at the above (1.78), one can notice that it is possible to write it in

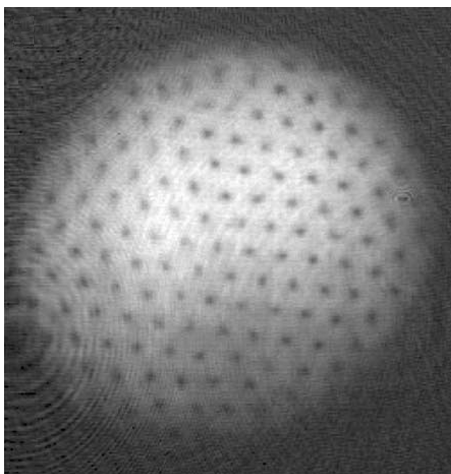


Figure 1.3: Vortex lattice in a rotating Bose-Einstein condensate [34].

terms of a parameter with dimensions of length:

$$\rho_v = \frac{1}{2\pi\ell_\Omega^2}, \quad (1.79)$$

where, in close analogy with the *magnetic length* in quantum Hall systems<sup>5</sup>, we define

$$\ell_\Omega = \sqrt{\frac{\hbar}{2m\Omega}}. \quad (1.80)$$

The length scale  $\ell_\Omega$  provides a measure of the characteristic separation between vortices.

The two length scales characterising the system are then the healing length  $\xi$  and the magnetic length  $\ell_\Omega$ . We point out that their ratio, clearly a dimensionless quantity, can be used to extract an expression for the inter-

---

<sup>5</sup>As we will argue in Sec. 1.5 of this chapter as well as in Chapter 5, it is possible to reformulate equations (1.68) and (1.69) so as to make the gauge invariance of the system apparent. It will then be manifest the full analogy between our system and that of a charged particle in a magnetic field of strength  $B = 2m\Omega/e$ , with  $e$  the charge of the particle.

action strength  $g$  as

$$g = \left(\frac{\ell_\Omega}{\xi}\right)^2 \pi \frac{\rho_v \hbar^2}{\bar{\rho} m}. \quad (1.81)$$

Therefore, the dimensionless ratio  $\ell_\Omega/\xi$  can be taken as a characteristic measure of the interaction strength. This will prove convenient in the following chapters where we will often refer to this ratio to characterise interactions.

### 1.4.2 Properties of Single Vortices

If we consider a system with cylindrical symmetry we can write an equation for the density only, since the phase  $\phi$  will depend only on the azimuthal angle  $\varphi$ . In particular we can insert  $\psi = \sqrt{\rho}e^{i\phi} = fe^{in\varphi}$  into the time independent GPE (1.13) to find

$$\mu f = -\frac{\hbar^2}{2m} \left[ \frac{1}{r} \frac{\partial}{\partial r} \left( r \frac{\partial f}{\partial r} \right) + \frac{\partial^2 f}{\partial z^2} - \frac{n^2 f}{r^2} \right] + Vf + gf^3, \quad (1.82)$$

where we have used  $\nabla^2 \equiv \frac{1}{r} \frac{\partial}{\partial r} \left( r \frac{\partial}{\partial r} \right) + \frac{\partial^2}{\partial z^2} + \frac{1}{r^2} \frac{\partial^2}{\partial \varphi^2}$ . Let us briefly study the ground state of this result in a limiting case: taking  $V = 0$ ,  $n = 1$ , large distances ( $\partial_r f = 0$ ,  $1/r^2 = 0$ ) and remembering that the ground state has no  $z$ -dependence (which implies  $\partial_z f = 0$ ) we get

$$\mu f = gf^3, \quad (1.83)$$

so that we have the following solution

$$\rho = \frac{\mu}{g}. \quad (1.84)$$

At short distances the solution is linear, since the centrifugal term proportional to  $1/r^2$  dominates the dynamics. By rescaling  $f$  by  $f_0^2 = \rho$ , i.e. the density far away from the vortex core, and  $r$  by the healing length of the

condensate, we can make equation (1.82) adimensional and solve it numerically. The result is show in Fig.1.4; the latter also shows a comparison with the following ansatz

$$\rho = \rho_0 \left(1 - e^{-r^2/\lambda^2}\right), \quad (1.85)$$

where  $\lambda = 1.781\xi$  [92]. At this point it is worth mentioning that the in-

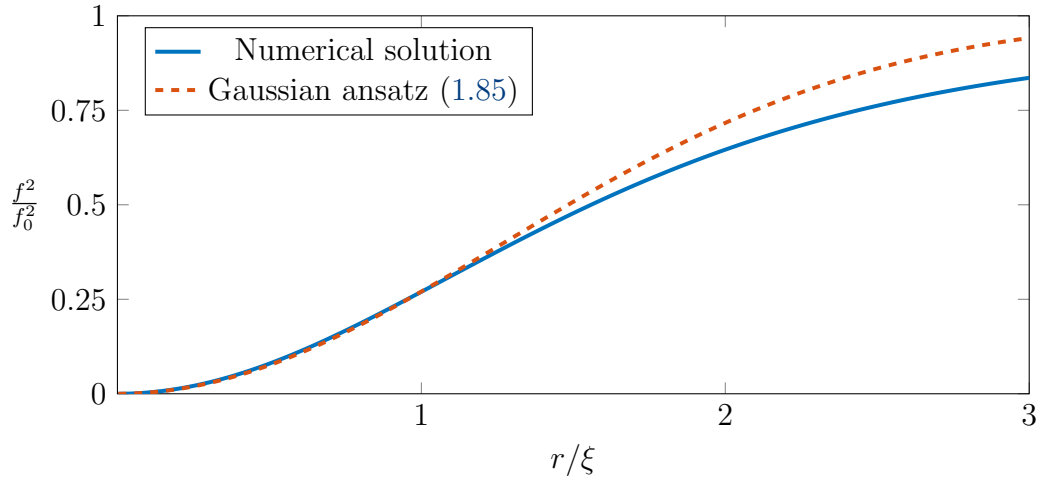


Figure 1.4: Vortex profile resulting from numerical solution of equation (1.82) and comparison with ansatz (1.85).

roduction of vortices, directly affects the spatial extent of the condensate. The condensate profile is not well approximated by the Thomas-Fermi profile (1.18) any longer, as it can be deduced from the results of numerical simulations depicted in Fig. 1.5. Of course a more accurate Thomas-Fermi approximation can be obtained neglecting the kinetic energy term; assuming again the confining potential to be harmonic with frequency  $\omega$  one finds [93]:

$$\rho_{TF} = \frac{1}{g} \left[ \mu - \frac{m}{2}(\omega^2 - \Omega^2)r^2 \right] \theta(R_{TF}(\Omega) - r) \quad (1.86)$$

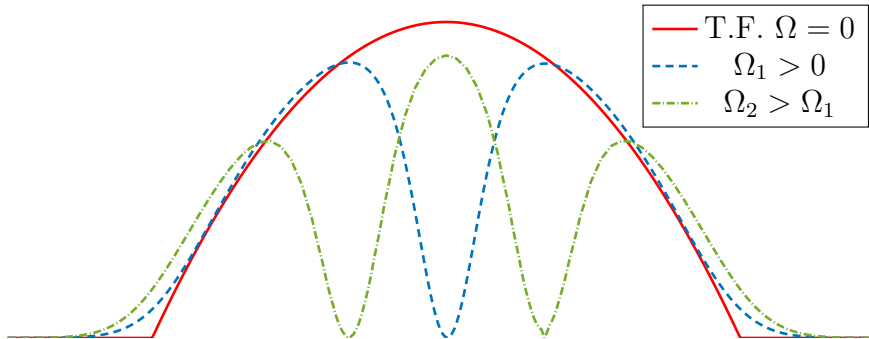


Figure 1.5: Condensate profile with one and two vortices compared to the Thomas-Fermi prediction for no rotation.

where  $\theta(x)$  is the *Heaviside theta function*, and the Thomas-Fermi radius is

$$R_{TF}(\Omega) = \frac{\sqrt{\frac{2\mu}{m\omega^2}}}{(1 - \frac{\Omega^2}{\omega^2})^{1/4}} = \frac{R_{TF}(0)}{(1 - \frac{\Omega^2}{\omega^2})^{1/4}}. \quad (1.87)$$

Now one can easily find the energy with the same procedures as explained before and compare it with the one associated to a uniform gas; we find that the energy per unit length is

$$\epsilon = 2\pi \int_0^\Lambda r dr \left[ \frac{\hbar^2}{2m} \left( \frac{\partial f}{\partial r} \right)^2 + \frac{\hbar^2}{2m} \frac{f^2}{r^2} + \frac{g}{2} f^4 \right]. \quad (1.88)$$

$\Lambda$  is a cutoff which needs to be introduced since the integral diverges logarithmically, but which has to be large compared with the characteristic size of the vortex, i.e. the healing length  $\xi$ ; the cutoff can be taken to be of the order of the Thomas-Fermi radius  $R_{TF}$  [79]. More in general, one must require  $\Lambda \gg \xi$ . At first approximation we can find the energy  $\epsilon_\nu$  associated with the single vortex state by subtracting the energy  $\epsilon_0$  associated with  $\Omega = 0$ , from (1.88). Assuming that  $\log(\Lambda/\xi) \gg 1$ , and that the other terms in the energy

can be neglected, it is possible to find [73]

$$\epsilon_\nu = \epsilon - \epsilon_0 \approx \frac{\pi \hbar^2}{m} \rho \log \left( \frac{\Lambda}{\xi} \right). \quad (1.89)$$

For a multiply-quantised vortex one can instead find that the core size becomes  $|n|\xi$  [73]. A similar approach allows then to find a similar expression for the energy associated with a multiply-quantised vortex:

$$\epsilon_\nu^n \approx n^2 \frac{\pi \hbar^2}{m} \rho \log \left( \frac{\Lambda}{|n|\xi} \right). \quad (1.90)$$

This result is particularly interesting as it permits to see that singly quantised vortices are more energetically favourable. Indeed, vortices with more than one quanta of circulation require more energy than a collection of vortices with a single quantum of circulation:

$$\epsilon_\nu^n \geq n \epsilon_\nu^1. \quad (1.91)$$

The above results can be generalised to account for vortex-vortex interactions. For two vortices separated by a distance  $d \gg \xi$ , with charges  $n_1$  and  $n_2$ , the interaction potential energy can be found to be [73]

$$\epsilon_{\text{int}} \approx \frac{2\pi n_1 n_2 \hbar^2 \rho}{m} \log \left( \frac{\Lambda}{d} \right). \quad (1.92)$$

The cutoff must again be the largest length scale  $\Lambda \gg d \gg \xi$ , and for system with many vortices one can take  $d$  on the order of the magnetic length  $\ell_\Omega$ . As long as this is the case, namely that the logarithmic accuracy holds ( $\log(\Lambda/\xi) \gg 1$ ), the above expression for the interaction energy gives a *Coulomb-like* force between two vortices, which, for positive interaction couplings  $g > 0$ , is repulsive for vortex charges with the same signs, attractive otherwise. Since  $\xi \sim g^{-1/2}$ , one finds that such a *Coulomb regime* holds as long as the intra-species interactions are large. In the following we will refer



equivalently to this regime as Coulomb regime or strong interaction limit.

Finally, let us notice that from the above results, it follows that vortices with  $|n| > 1$  are metastable states, and should not be expected to appear in the ground state of rotating homogeneous systems; rather one should expect the contribution to the circulation to derive from several singly quantised vortices. Nonetheless, it is possible to observe such vortices with multiple quanta of circulation in inhomogeneous systems under anharmonic trapping potentials [73, 94], as we will briefly explain later.

### 1.4.3 Existence of ground states and their nature under rotation

Let us now briefly consider the case of a superfluid trapped in an harmonic potential. It can be shown that the problem of minimisation of the energy functional  $E[\psi]$ , has a solution  $E[\psi_0]$  if and only if  $|\Omega| < \omega$ , where  $\Omega$  is the angular velocity and  $\omega$  the trapping frequency; in this case  $\psi_0$  is the ground state of the system. When the system is at rest, the ground state is symmetric and unique up to a complex phase; introducing angular momentum, i.e. when  $\Omega$  exceeds its critical value  $\Omega_c$ , the symmetry breaks: at this point one finds the minimiser is not unique any more, and an infinitely degenerate ground state arises. Moreover, it is possible to show that no solution to the minimisation problem exist when  $|\Omega| > \omega$ . In particular one finds

$$\inf_{\psi} E[\psi] = -\infty. \quad (1.93)$$

In order to demonstrate this statement, let us consider, without loss of generality, the linear case in which the system is governed by the rotating Schrödinger Hamiltonian operator

$$H = \frac{\mathbf{p}^2}{2m} + \frac{m\omega^2}{2}\mathbf{r}^2 - \Omega L_z, \quad (1.94)$$

with  $L_z = xp_y - yp_x$ . The first two terms correspond to the quantum harmonic oscillator and can therefore be written together as

$$\frac{1}{2}(\mathbf{p}^2 + \omega^2 \mathbf{r}^2) = \hbar\omega (\mathbf{c}^\dagger \mathbf{c} + 1) \quad (1.95)$$

where  $\mathbf{c}$  is the standard lowering ladder operator

$$\mathbf{c} = \sqrt{\frac{m\omega}{2\hbar}} \left( \mathbf{r} + \frac{i}{m\omega} \mathbf{p} \right), \quad (1.96)$$

such that  $[c_\alpha, c_\alpha^\dagger] = 1$ . Inverting the relations for the operator  $\mathbf{c}$  and its hermitian conjugate  $\mathbf{c}^\dagger$ , one has the expressions

$$\begin{aligned} \mathbf{r} &= \sqrt{\frac{\hbar}{2m\omega}} (\mathbf{c}^\dagger + \mathbf{c}), \\ \mathbf{p} &= i\sqrt{\frac{\hbar m\omega}{2}} (\mathbf{c}^\dagger - \mathbf{c}). \end{aligned} \quad (1.97)$$

It is then evident that  $L_z$  can be written in terms of the components of  $\mathbf{c} = (a, b)^\top$ , resulting in

$$L_z = xp_y - yp_x = -i\hbar (a^\dagger b - b^\dagger a). \quad (1.98)$$

Therefore, the Hamiltonian operator (1.94) can be written as

$$\begin{aligned} H &= \hbar\omega (a^\dagger a + b^\dagger b + 1) + i\hbar\Omega (a^\dagger b - b^\dagger a) \\ &= \hbar (a^\dagger, b^\dagger) \begin{pmatrix} \omega & i\Omega \\ -i\Omega & \omega \end{pmatrix} \begin{pmatrix} a \\ b \end{pmatrix} + \hbar\omega \\ &= \hbar (a^\dagger, b^\dagger) \underbrace{(\omega \mathbb{1} - \Omega \sigma_y)}_{\mathcal{M}} \begin{pmatrix} a \\ b \end{pmatrix} + \hbar\omega. \end{aligned} \quad (1.99)$$

Matrix  $\mathcal{M}$  has trace  $\text{tr}[\mathcal{M}] = 2\omega$  and determinant  $\det[\mathcal{M}] = \omega^2 - \Omega^2$ ; it can thus be diagonalised into

$$\begin{pmatrix} \omega - \Omega & 0 \\ 0 & \omega + \Omega \end{pmatrix}, \quad (1.100)$$

by the following change of basis

$$\begin{aligned} \alpha &= \frac{1}{\sqrt{2}}(a + ib), \\ \beta &= \frac{1}{\sqrt{2}}(a - ib). \end{aligned} \quad (1.101)$$

In this basis, the angular momentum operator reads  $L_z = \hbar(\beta^\dagger\beta - \alpha^\dagger\alpha)$ . Finally, the Hamiltonian can be put into the revealing form

$$H = \hbar(\omega + \Omega)\alpha^\dagger\alpha + \hbar(\omega - \Omega)\beta^\dagger\beta + \hbar\omega. \quad (1.102)$$

Confirming that  $[\alpha, \alpha^\dagger] = 1$  and  $[\beta, \beta^\dagger] = 1$ , we recognise  $\alpha$  and  $\beta$  as ladder lowering operators and  $\alpha^\dagger\alpha$ ,  $\beta^\dagger\beta$  as particle number operators of clockwise and counter-clockwise rotations. The ground state of the system is therefore not guaranteed to exist. More specifically, when  $\Omega > \omega$ , the energy has no lower bound, as claimed in (1.93), which leads to instability. The reason for this result can be found in fact that the centrifugal effective potential, which grows quadratically as the trapping potential, can eventually overcome the trap's confining forces.

### Anharmonic confinement

In order to get around this problem, one can employ anharmonic trapping. Since the trapping potential is always strong enough to contain the rotating condensate, a condensate which is confined anharmonically is expected to give rise to a rich variety of phases. The physics of anharmonic trapped

condensates can be summed up qualitatively by the schematic phase diagram presented in Fig. 1.6 [95]. We can distinguish three different phases: arrays

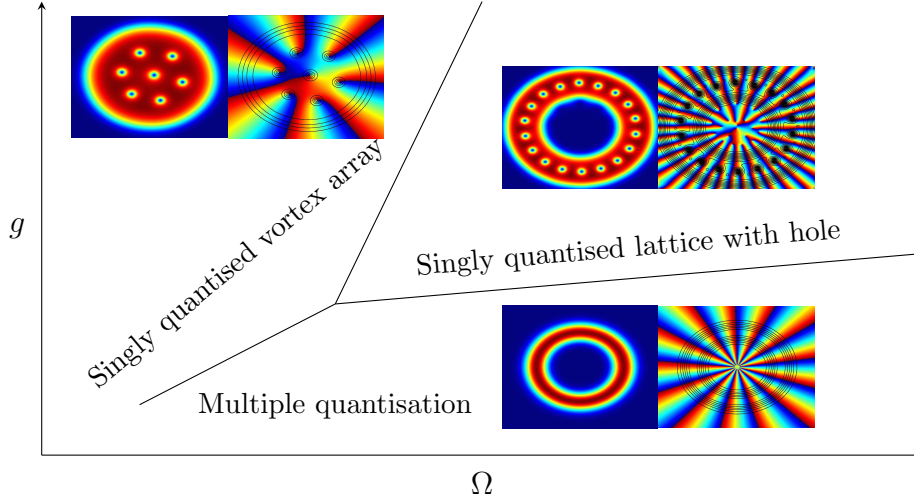


Figure 1.6: Qualitative phase diagram for anharmonically confined systems.

of singly quantised vortices arranged in a triangular lattice, vortex lattices with a finite radius hole in the centre such that the density is zero but the vorticity is not, and giant multiply-quantised vortices.

Formal accounts which have investigated this phase diagram under diverse anharmonic potential [96, 97], have accurately described the transition between the different regimes [98, 99, 100]. Nonetheless, the phase diagram can be qualitatively understood unambiguously in terms of the effective potential, arising from the joint action of anharmonic potential and the effective centrifugal potential. We consider for simplicity a quartic potential, so that the resulting effective potential can be written as

$$V_{eff} \propto (kr^4 - \Omega_{eff}^2 r^2), \quad (1.103)$$

with  $\Omega_{eff} \propto |\Omega|$ . This effective potential has a mexican hat shape and the size of the hat's crown in the middle is controlled by the parameter  $\Omega_{eff}$ . Increasing  $|\Omega|$  makes the condensate drift away from the centre of the trap

and arrange into a ring shape. For weak interacting regimes, a state made of multiply-quantised vortices is always the minimiser of the energy functional [94]; for larger interaction strengths and small  $|\Omega|$  (and consequently  $\Omega_{\text{eff}}$ ) we find instead triangular arrays of singly-quantised vortices. Finally, for large rotating frequencies  $\Omega$  and strong interactions, one finds a lattice of vortices carrying a single quantum of circulation, arranged around a hole at the centre of the condensate [101]. The ‘hole’ differs from a multiply-quantised vortex in that the former consists in a depleted region created by a cluster of vortices which do not however necessarily overlap. This can be better understood observing the phase of the states depicted in Fig. 1.6.

## 1.5 Symmetries of the system

Let us consider again the Gross-Pitaevskii equation (1.69) under rotation. Upon the introduction of the gauge field  $\mathcal{A}_s = \Omega m(-y, x)$ , the rotation term can be written as

$$-\Omega\psi^\dagger L_z\psi = \frac{i\hbar}{m}\psi^\dagger \mathcal{A}_s^\dagger \nabla\psi. \quad (1.104)$$

Notice that  $\nabla \times \mathcal{A}_s = 2\Omega m\hat{z}$ , and  $\mathcal{A}_s^\dagger \mathcal{A}_s = m^2\Omega^2 r^2$ , so that it is possible to write the energy as

$$E = \int dx dy \left[ \frac{1}{2m} |(-i\hbar\nabla - \mathcal{A}_s)\psi|^2 + \frac{1}{2}m\omega_{\text{eff}}^2 r^2 |\psi|^2 + \frac{g}{2}|\psi|^4 \right], \quad (1.105)$$

where we have introduced the effective harmonic oscillator frequency  $\omega_{\text{eff}} = \sqrt{\omega^2 - \Omega^2}$ . In fact:

$$\begin{aligned}
 & \int dx dy \left[ \frac{1}{2m} |(-i\hbar\nabla - \mathcal{A}_s)\psi|^2 \right] = \\
 & = \int dx dy \left[ \frac{\hbar^2}{2m} |\nabla\psi|^2 + \frac{1}{2m} \mathcal{A}_s^\dagger \psi^\dagger \mathcal{A}_s \psi + \frac{i\hbar}{2m} (\psi^\dagger \mathcal{A}_s^\dagger \nabla\psi - \mathcal{A}_s \psi \nabla\psi^\dagger) \right] \\
 & = \int dx dy \left[ \frac{\hbar^2}{2m} |\nabla\psi|^2 + \frac{m\Omega^2 r^2}{2} |\psi|^2 + \frac{i\hbar}{m} \psi^\dagger \mathcal{A}_s^\dagger \nabla\psi \right] \\
 & = \int dx dy \left[ \frac{\hbar^2}{2m} |\nabla\psi|^2 + \frac{m\Omega^2 r^2}{2} |\psi|^2 - \Omega \psi^\dagger L_z \psi \right],
 \end{aligned} \tag{1.106}$$

where, in the second line, we have used integration by parts. The energy in (1.105) is rearranged in a particularly convenient way. First of all it allows to draw a clear analogy with charged particles in a magnetic field<sup>6</sup>, whose Hamiltonian is identical to (1.105) in the joint limit of weak interactions and rapid rotation (so that  $g \approx 0$  and  $\omega_{\text{eff}} \approx 0$ ); this analogy allows to make use of a set of techniques and well known concepts useful to our problem, as we have already done in Sec. 1.4.1 and as we are going to do in the following Sec. 1.5.1. Furthermore, the form of equation (1.105) makes the gauge invariance of the system manifest: the energy functional is indeed invariant under the gauge transformation

$$\begin{aligned}
 \psi & \rightarrow e^{\frac{i}{\hbar}\lambda}\psi, \\
 \mathcal{A}_s & \rightarrow \mathcal{A}_s + \nabla\lambda,
 \end{aligned} \tag{1.107}$$

---

<sup>6</sup>The Hamiltonian for a particle of charge  $e$  in a magnetic field is given by

$$H = \frac{1}{2m} (p - e\mathbf{A})^2,$$

where  $\mathbf{A}$  is the vector potentials so that the magnetic field is given by  $\mathbf{B} = \nabla \times \mathbf{A}$ . Thus, under the analogy with the rotating superfluid, we have that the magnetic field is related to the angular velocity as  $B = 2m\Omega/e$ .

with the pure gauge  $\lambda$  being an arbitrary function of the  $xy$ -coordinates. The gauge invariance is easily checked as

$$\begin{aligned}
|(-i\hbar\nabla - \mathcal{A}_s)\psi|^2 &\rightarrow \left|(-i\hbar\nabla - \mathcal{A}_s - \nabla\lambda)e^{\frac{i}{\hbar}\lambda}\psi\right|^2 \\
&= \left|-i\hbar\psi\left(\frac{i}{\hbar}\nabla\lambda\right)e^{\frac{i}{\hbar}\lambda} - i\hbar e^{\frac{i}{\hbar}\lambda}\nabla\psi - \mathcal{A}_s e^{\frac{i}{\hbar}\lambda}\psi - \nabla\lambda e^{\frac{i}{\hbar}\lambda}\psi\right|^2 \\
&= \left|e^{\frac{i}{\hbar}\lambda}(\nabla\lambda - i\hbar\nabla - \mathcal{A}_s - \nabla\lambda)\psi\right|^2 \\
&= |(-i\hbar\nabla - \mathcal{A}_s)\psi|^2.
\end{aligned}
\tag{1.108}$$

This gauge freedom allows for a choice of the gauge which best suits the problem at hand. The previously defined gauge field  $\mathcal{A}_s$  is known as symmetric gauge. Another common choice is the so called Landau gauge obtained from the symmetric gauge by choosing  $\lambda = \Omega mxy$ , so that  $\mathcal{A}_L = 2m\Omega(0, x)$ . In what follows we will write the vector potential in an arbitrary gauge as  $\mathcal{A} = \mathcal{A}_L + \nabla\lambda$ , leaving  $\lambda$  unspecified but noting that we may return to the original symmetric gauge by putting  $\lambda = -\Omega mxy$ . This will make apparent which quantities are gauge invariant. For instance, since the effective magnetic field,  $B \equiv \epsilon_{ij}\partial_i\mathcal{A}_j = 2m\Omega$  (summation is implicit over repeated indices), defined in analogy with quantum Hall systems, is independent of  $\lambda$ , it is a gauge invariant quantity. This connection in particular, makes evident that the role played by the Coriolis force in the rotation frame is the same as that played by the Lorentz force on a charged particle in a magnetic field.

### 1.5.1 Landau levels

Consider now the limit of rapid rotation, so as to make the effective frequency  $\omega_{\text{eff}}$  vanishing. In this limit the centrifugal and centripetal terms contributing to the total energy are completely balanced and the system can effectively be thought of as uniform in the plane perpendicular to the axis of rotation.

One can then realise that in the limit of weak interactions (so that  $\xi \gg \ell_\Omega$ ), it is possible to find a closed form solution to (1.105). Continuing with the analogy, similarly to what was done by Landau [102] for the case of a charged particle in a magnetic field, we start considering the Hamiltonian operator

$$H = \frac{1}{2m}(\mathbf{p} - \mathcal{A}_L)^2 = \frac{1}{2m} [p_x^2 + (p_y - 2\Omega m x)^2], \quad (1.109)$$

associated with the energy functional obtained from (1.105) by enforcing the approximation  $\omega_{\text{eff}} = 0$ , valid in the limit  $N_v \gg 1$ , and fixing the gauge to the Landau gauge  $\mathcal{A}_L$ . Here  $\mathbf{p} = -i\hbar\nabla$  is the canonical momentum operator. Clearly the Hamiltonian commutes with the momentum operator  $p_y$ , so that the two possess a complete set of common eigenfunctions. Therefore we can replace the operator  $p_y$  with its eigenvalue  $\hbar k_y$

$$\begin{aligned} H &= \frac{p_x^2}{2m} + \frac{1}{2m}(k_y - 2\Omega m x)^2 \\ &= \frac{p_x^2}{2m} + \frac{1}{2}m(2\Omega)^2\left(x - \frac{\hbar k_y}{2\Omega m}\right)^2, \end{aligned} \quad (1.110)$$

which can be recognised in this form as the Hamiltonian of a quantum oscillator with angular frequency  $2\Omega$ , and the minimum of the harmonic potential shifted by  $\hbar k_y/2\Omega m$  (clearly such a translation does not affect the energy). Then, one can immediately write down its energy spectrum:

$$E_n = 2\hbar\Omega \left( n + \frac{1}{2} \right), \quad n \geq 0. \quad (1.111)$$

In particular the ground state energy, which we will refer to as Lowest Landau Level (LLL), is given by  $E_0 = \hbar\Omega$ . Moreover, it is important to notice that the system is highly degenerate with respect  $k_y$ . Such a degeneracy is however lifted by the existence of non-zero interactions.



### 1.5.2 The Magnetic Translation Group and Twisted Boundary Conditions

The Hamiltonian operator as presented in (1.109), is also indicative of another important symmetry of the system. The kinetic momentum operator entering (1.109) is given by  $\mathbf{P} = \mathbf{p} - \mathcal{A}_L$ . It is then clear that the hamiltonian is not translational invariant. In particular, in the Landau gauge we have  $[\tilde{T}(\mathbf{R}), P_y] \neq 0$ , where  $\tilde{T}(\mathbf{R}) = \exp(\frac{i}{\hbar}\mathbf{p} \cdot \mathbf{R})$  is the standard translation operator, with the canonical momentum as infinitesimal generator. More generally, given a different choice for the gauge, one finds  $[\tilde{T}(\mathbf{R}), P_j] \neq 0$ . Now, one would like to find a set of operators which generalises the concept of translation and with respect to which the Hamiltonian is invariant. Consider then the two operators

$$\begin{aligned}\Pi_x &= p_x - 2\Omega my, \\ \Pi_y &= p_y.\end{aligned}\tag{1.112}$$

These operators clearly commute with the kinetic momenta (and therefore with the Hamiltonian):  $[\Pi_j, P_k] = 0$ . From these one can define the Magnetic Translation Operators (MTOs) as

$$T(\mathbf{R}) = e^{\frac{i}{\hbar}\mathbf{\Pi} \cdot \mathbf{R}},\tag{1.113}$$

which, when acting on quantities involving only coordinates, operate in complete analogy with the standard translation operators:

$$T(\mathbf{R})f(\mathbf{r})T^{-1}(\mathbf{R}) = f(\mathbf{r} + \mathbf{R}).\tag{1.114}$$

The operators (1.112) are specific to the Landau gauge. We can find a more general expression for the  $\Pi_j$  operators which applies for any choice of the gauge. To do so, let us introduce two arbitrary functions of the  $xy$ -

coordinates  $f(x, y)$  and  $g(x, y)$ , and write the operators in their general form as

$$\begin{aligned}\Pi_x &= p_x - 2\Omega my + f, \\ \Pi_y &= p_y + g.\end{aligned}\tag{1.115}$$

The kinetic momenta are now  $P_x = p_x - \partial_x \lambda$  and  $P_y = p_y - 2\Omega mx - \partial_y \lambda$ , with  $\lambda$  the pure gauge. The conditions  $[\Pi_j, P_k] = 0$  then yield

$$\begin{aligned}[\Pi_x, P_x] &= i\hbar \partial_x^2 \lambda + i\hbar \partial_x f, \\ [\Pi_x, P_y] &= i\hbar \partial_x \partial_y \lambda + i\hbar \partial_y f, \\ [\Pi_y, P_x] &= i\hbar \partial_y \partial_x \lambda + i\hbar \partial_x g, \\ [\Pi_y, P_y] &= i\hbar \partial_y^2 \lambda + i\partial_y g,\end{aligned}\tag{1.116}$$

where we have made use of the standard commutation relations  $[r_j, p_j] = i\hbar$ ,  $[p_j, f] = -i\hbar \partial_j f$ . Setting the first two equations to zero one finds  $f = -\partial_x \lambda$ . Similarly the last two equations lead to  $g = -\partial_y \lambda$ . Therefore, the  $\Pi_j$  operators in a general gauge are

$$\begin{aligned}\Pi_x &= p_x - 2\Omega my - \partial_x \lambda, \\ \Pi_y &= p_y - \partial_y \lambda.\end{aligned}\tag{1.117}$$

These are infinitesimal generators of the magnetic translation operators  $T(\mathbf{R})$  defined in (1.113), elements of the so called Magnetic Translation Group (MTG) [103, 104].

The first property to note with regards to the infinitesimal generators  $\Pi_j$  as defined in equation (1.117), is their commutation relation. In fact, if the infinitesimal generators of the standard translations (the canonical momenta) commute with each other, for the operators in (1.117) one finds

$$[\Pi_x, \Pi_y] = -2i\hbar \Omega m.\tag{1.118}$$

Notice that this quantity is gauge invariant, as it can be inferred by the lack of dependency on  $\lambda$ . This property, translates to MTOs which one can expect not to commute in general, in contrast again to what happens for the standard translation operators. It is possible to explicitly compute the commutator

$$[T(\mathbf{R}), T(\mathbf{R}')] = e^{\frac{i}{\hbar}\mathbf{\Pi}\cdot\mathbf{R}} e^{\frac{i}{\hbar}\mathbf{\Pi}\cdot\mathbf{R}'} - e^{\frac{i}{\hbar}\mathbf{\Pi}\cdot\mathbf{R}'} e^{\frac{i}{\hbar}\mathbf{\Pi}\cdot\mathbf{R}}. \quad (1.119)$$

More specifically, from the Baker-Campbell-Hausdorff formula we have

$$\begin{aligned} \log\left(e^{\frac{i}{\hbar}\mathbf{\Pi}\cdot\mathbf{R}} e^{\frac{i}{\hbar}\mathbf{\Pi}\cdot\mathbf{R}'}\right) &= \frac{i}{\hbar}\mathbf{\Pi}\cdot\mathbf{R} + \frac{i}{\hbar}\mathbf{\Pi}\cdot\mathbf{R}' - \frac{1}{2\hbar^2}[\mathbf{\Pi}\cdot\mathbf{R}, \mathbf{\Pi}\cdot\mathbf{R}'] \\ &= \frac{i}{\hbar}\mathbf{\Pi}\cdot(\mathbf{R} + \mathbf{R}') + \frac{i\Omega m}{\hbar}(\epsilon_{ij}R_iR'_j), \end{aligned} \quad (1.120)$$

so that

$$\begin{aligned} [T(\mathbf{R}), T(\mathbf{R}')] &= e^{\frac{i}{\hbar}\mathbf{\Pi}\cdot(\mathbf{R}+\mathbf{R}')} e^{\frac{i\Omega m}{\hbar}(\epsilon_{ij}R_iR'_j)} - e^{\frac{i}{\hbar}\mathbf{\Pi}\cdot(\mathbf{R}+\mathbf{R}')} e^{-\frac{i\Omega m}{\hbar}(\epsilon_{ij}R_iR'_j)} \\ &= 2ie^{\frac{i}{\hbar}\mathbf{\Pi}\cdot(\mathbf{R}+\mathbf{R}')} \sin\left(\frac{\Omega m}{\hbar}\epsilon_{ij}R_iR'_j\right). \end{aligned} \quad (1.121)$$

It is interesting to notice that although the expressions for the magnetic translations depend on the choice of the gauge, the commutator of two magnetic translations is again gauge invariant. Another quantity which can be shown to be gauge invariant is the composition of magnetic translations  $T_y^{-1}(R_y)T_x^{-1}(R_x)T_y(R_y)T_x(R_x) = e^{\frac{i}{\hbar}2\Omega m R_x R_y}$  (here and after we use the notation  $T_j(R) \equiv T(R\hat{\mathbf{x}}_j)$ ).

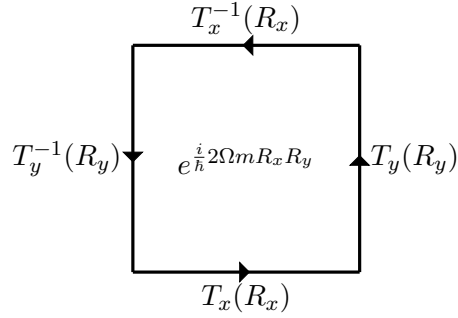


Figure 1.7: Wilson loop (1.122) revealing the acquisition of a phase factor when translating along a closed loop.

This quantity is known as the Wilson loop<sup>7</sup>:

$$\begin{aligned}
 W_\gamma &= \exp \left[ \frac{i}{\hbar} \oint_{\gamma=\partial D} \mathcal{A} d\gamma \right] = \exp \left[ \frac{i}{\hbar} \iint_D \nabla \times \mathcal{A} dD \right] \\
 &= \exp \left[ \frac{2i\Omega m}{\hbar} \iint_D dD \right] \\
 &= \exp \left[ \frac{i}{\hbar} 2\Omega m R_x R_y \right],
 \end{aligned} \tag{1.122}$$

where  $D = R_x R_y$  is the area enclosed by the closed line  $\gamma$ , and  $\partial D$  its boundary (i.e  $\gamma$  itself). This procedure reveals the acquisition of a phase when magnetically translating along a closed loop. This phase factor is of great importance and it is closely connected with the commutator (1.121). Before discussing more on the importance of this phase factor, let us introduce one further property of the system.

Consider then the description of a periodic system by a unit cell of size  $L_x \times L_y$ . Naively, it would feel natural to impose periodic boundary condi-

<sup>7</sup>We are ignoring here the path ordering operator since the gauge field  $\mathcal{A}$  commutes with itself at different times (there is no time dependance at all).

tions. This is usually done by requiring

$$\begin{aligned}\tilde{T}(L_x)\psi(x, y) &= \psi(x, y), \\ \tilde{T}(L_y)\psi(x, y) &= \psi(x, y);\end{aligned}\tag{1.123}$$

recall that the operators  $\tilde{T}$  used here are the standard translation operators generated by the canonical momenta. Imposing periodic boundary conditions has the effect of making the order of the MTG finite, and the momenta quantised:

$$k_j = \frac{2\pi}{L_j}n, \quad n \in \mathbb{Z}.\tag{1.124}$$

This is not ideal as the lowest non-zero momentum might be quite large. A workaround, [105] consists in employing the so called twisted boundary conditions, as it was found in early work [106], which enforce the acquisition of a phase ‘twist’ over a period:

$$\tilde{T}(L_j)\psi(x, y) = e^{i\Theta_j}\psi(x, y),\tag{1.125}$$

so that arbitrary momenta can be attained by varying the *twisting phases*  $\Theta_j$ :

$$k_j = \frac{2\pi}{L_j}n + \frac{\Theta_j}{L_j}, \quad n \in \mathbb{Z}.\tag{1.126}$$

The correct twisted boundary conditions can be achieved by employing the correct translation operators, namely the MTOs with infinitesimal generators (1.117), as

$$\begin{aligned}\psi(x, y) &= T(L_x)\psi(x, y), \\ \psi(x, y) &= T(L_y)\psi(x, y).\end{aligned}\tag{1.127}$$

Notice that it is then possible to write  $T(L_j) = e^{-i\Theta_j} \tilde{T}(L_j)$ , and extract an expression for the  $\Theta_j$ s from the definition of the MTOs, given that under periodic boundary conditions  $\tilde{T}(L_j) = 1$ . It is also worth noticing that although the assumption of periodicity of the wavefunction  $\psi$  has been relaxed, the observable density  $\rho = |\psi|^2$  retains its periodicity; moreover the Hamiltonian operator  $H = \frac{\mathbf{P}^2}{2m} + g\rho$  is still self-adjoint over the space of functions satisfying the twisted boundary conditions.

Let us now compute the twisted boundary conditions (1.127) explicitly. At first, it is essential to notice that an MTO transforms under a gauge transformation as

$$T_j \rightarrow e^{i\lambda/\hbar} T_j e^{-i\lambda/\hbar}. \quad (1.128)$$

Let us check this is the case for the specific case of the MTO  $T_y$  in the Landau gauge. We have already found that in the new gauge obtained through the pure gauge  $\lambda$ , the operator  $T_y^L$  transforms as

$$T_y^L(R_y) = e^{\frac{i}{\hbar} R_y p_y} \rightarrow T_y = e^{\frac{i}{\hbar} R_y (p_y - \partial_y \lambda)}. \quad (1.129)$$

Here we explicitly labeled the MTO in the Landau gauge as  $T_y^L$  to avoid confusion. It is now possible to use the Zassenhaus formula

$$e^{t(A+B)} = e^{tA} e^{tB} e^{-\frac{t^2}{2}[A,B]} e^{\frac{t^3}{3!}(2[B,[A,B]]+[A,[A,B]])} \dots \quad (1.130)$$

to expand (1.129). Computing the commutators

$$\begin{aligned} [p_y, -\partial_y \lambda] &= i\hbar \partial_y^2 \lambda, \\ [p_y, i\hbar \partial_y^2 \lambda] &= \hbar^2 \partial_y^3 \lambda, \\ &\vdots \\ [p_y, [\dots, [p_y, -\partial_y \lambda]]] &= -(-i\hbar)^n \partial_y^{n+1} \lambda, \end{aligned} \quad (1.131)$$

one can expand (1.129) with (1.130) to find

$$\begin{aligned}
T_y(R_y) &= e^{\frac{i}{\hbar}R_y(p_y - \partial_y \lambda)} = e^{\frac{i}{\hbar}R_y p_y} e^{-\frac{i}{\hbar}R_y \partial_y \lambda} e^{\frac{R_y^2}{2\hbar^2}[p_y, -\partial_y \lambda]} e^{\frac{-iR_y^3}{\hbar^3 6}(2[-\partial_y \lambda, [p_y, -\partial_y \lambda]] + [p_y, [p_y, -\partial_y \lambda]])} \dots \\
&= e^{\frac{i}{\hbar}R_y p_y} e^{-\frac{i}{\hbar}R_y \partial_y \lambda} e^{\frac{i}{2\hbar}R_y^2 \partial_y^2 \lambda} e^{\frac{-iR_y^3}{\hbar^3 6}([p_y, i\hbar \partial_y^2 \lambda])} \dots \\
&= e^{\frac{i}{\hbar}R_y p_y} e^{-\frac{i}{\hbar}R_y \partial_y \lambda} e^{\frac{i}{2\hbar}R_y^2 \partial_y^2 \lambda} e^{\frac{-i}{6\hbar}R_y^3 \partial_y^3 \lambda} \dots \\
&= T_y^L(R_y) \exp \left[ \frac{i}{\hbar} \sum_{n=1}^{\infty} \frac{1}{n!} (-R_y \partial_y)^n \lambda \right] \\
&= T_y^L(R_y) \exp \left[ \frac{i}{\hbar} \sum_{n=0}^{\infty} \frac{1}{n!} \left( -\frac{i}{\hbar} R_y p_y \right)^n \lambda - \frac{i}{\hbar} \lambda \right] \\
&= T_y^L(R_y) \exp \left[ \frac{i}{\hbar} e^{-\frac{i}{\hbar} R_y p_y} \lambda - \frac{i}{\hbar} \lambda \right] = T_y^L(R_y) e^{\frac{i}{\hbar} T_y^{L\dagger}(R_y) \lambda} e^{-\frac{i}{\hbar} \lambda} \\
&= e^{\frac{i}{\hbar} T_y^L(R_y) T_y^{L\dagger}(R_y) \lambda} T_y^L(R_y) e^{-\frac{i}{\hbar} \lambda} \\
&= e^{\frac{i}{\hbar} \lambda} T_y^L(R_y) e^{-\frac{i}{\hbar} \lambda}.
\end{aligned} \tag{1.132}$$

Taking now one further step, it is possible to find  $T_y(R_y) = e^{\frac{i}{\hbar}[\lambda(x,y) - \frac{i}{\hbar}\lambda(x,y+R_y)]} T_y^L(R_y)$ . Applying the transformation rule (1.128) to  $T_x^L$ , we find also the second boundary condition in a general gauge. To sum up, the required twisted boundary conditions finally are:

$$\begin{aligned}
\psi(x, y) &= T_x(L_x) \psi(x, y) = e^{-\frac{i}{\hbar} 2\Omega m y L_x} e^{-\frac{i}{\hbar} [\lambda(x+L_x, y) - \lambda(x, y)]} \psi(x + L_x, y), \\
\psi(x, y) &= T_y(L_y) \psi(x, y) = e^{-\frac{i}{\hbar} [\lambda(x, y+L_y) - \lambda(x, y)]} \psi(x, y + L_y),
\end{aligned} \tag{1.133}$$

or equivalently

$$\begin{aligned}
\psi(x, y) &= e^{-i\Theta_x} \psi(x + L_x, y), \\
\psi(x, y) &= e^{-i\Theta_y} \psi(x, y + L_y),
\end{aligned} \tag{1.134}$$

with

$$\begin{aligned}\Theta_x &= \frac{1}{\hbar} [2\Omega m y L_x + \lambda(x + L_x, y) - \lambda(x, y)], \\ \Theta_y &= \frac{1}{\hbar} [\lambda(x, y + L_y) - \lambda(x, y)].\end{aligned}\tag{1.135}$$

These boundary conditions impose an important quantisation condition on  $\Omega$ . When restricted our analysis to a periodic unit cell, consistency requires that  $\psi = T_x(L_x)T_y(L_y)\psi = T_y(L_y)T_x(L_x)\psi$  and therefore  $[T_x(L_x), T_y(L_y)] = 0$ . Similarly, the requirement of single-valuedness of the wavefunction imposes the constraint  $W_\gamma = \mathbb{1}$  on the above mentioned Wilson loop. Such requirements are all satisfied when

$$\frac{2}{\hbar}\Omega m L_x L_y = 2\pi n, \quad n \in \mathbb{Z}.\tag{1.136}$$

Rearranging the terms in the expression above, recalling Feynman's relation (1.78), we recognise the integer  $n$  as a familiar quantity:

$$\frac{n}{L_x L_y} = \frac{\Omega m}{\pi \hbar} \equiv \rho_v.\tag{1.137}$$

The quantisation integer  $n \equiv N_v$  corresponds to the number of vortices in the unit cell.

Going back again to the analogy with a charged particle in a magnetic field, we realise that this quantisation condition exists in complete analogy to the quantisation of the magnetic field in quantum Hall systems.



# Chapter 2

## Numerical Methods

Many-particle systems are hard to describe analytically due to their complex nature and hence usually numerical solutions are necessary. This need drives, amongst others, the birth of a multitude of numerical methods for obtaining the solution to the Schrödinger equation and its non-linear versions, which find applications in a growing range of fields. In particular we are interested in one of those non-linear versions, namely the Gross-Pitaevskii equation. Analytical solutions to the Gross-Pitaevskii equation are known only in a few particular cases, some of which we have discussed in the previous chapter. With this motivation in mind, in this chapter we approach the study of split-step numerical methods. Split-step methods fall under the category of pseudospectral methods, which are in general faster than finite difference methods (such as the Crank-Nicolson methods, for instance): this is, of course, at the expense of losing accuracy; however the great power of these methods is the ease of implementation and the small computational power required. The founding idea consists of splitting the Gross-Pitaevskii equation into two parts in order to isolate position and momentum operators, and then evolving the wavefunction by one step in position space and subsequently in momentum space, alternating. This requires employment of a fast Fourier transform (FFT) algorithm in order to switch from position

to momentum space and vice versa; for this reason such methods are also known as split-step Fourier methods, or SSFM, and can be extensively found in the literature.

The Chapter will start considering a clever and powerful method to compute the ground state of a general system, known as imaginary time propagation. This method is conceived for linear systems but, as we will see, it can be directly applied to non-linear problems as well. We will then introduce split-step methods for linear systems, giving a few caveats for their implementation. In particular, we will demonstrate that the standard approach loses accuracy for the non-linear problem at hand as well as for the case of propagation in imaginary time, but we will be able to restore the correct order of accuracy through a simple adaptation of the method.

## 2.1 Imaginary Time propagation

The problem of finding the ground state can be quite hard and only a few exactly-solvable cases exist. However, it is possible to approach such a problem by seeking a solution to the corresponding equation of motion in imaginary time  $\tau = it$ , whose solutions are formally obtained through the propagator  $\exp(-\tau H)$ . In general, any initial condition, under the action of the operator  $\exp(-\tau H)$ , will in this way converge asymptotically to the ground state for  $\tau \rightarrow \infty$ . This technique, usually employed for linear Schrödinger systems, is known by the name of *imaginary time propagation*. As we shall see, the extension to non-linear systems is not trivial, but can be done in practice at no extra cost.

Let us consider for the moment the case of a system described by an arbitrary linear Hamiltonian  $H$ ; then, the equation of motion is

$$i\hbar \frac{d\psi}{dt} = H\psi. \tag{2.1}$$

An important property of  $H$  is its hermiticity, from which it follows that its eigenvalues are real and non-negative. Moreover, the corresponding eigenfunctions  $\phi_n$  form a complete orthonormal set, giving an orthonormal basis of the underlying Hilbert space. Consequently, it is possible to expand the wavefunction as

$$\psi = \sum_n c_n \phi_n, \quad (2.2)$$

where  $c_n = \langle \phi_n | \psi \rangle$ , and write its time evolution in terms of the eigenstates and eigenvalues of  $H$  as

$$\psi(t) = \sum_n c_n e^{-iE_n t/\hbar} \phi_n, \quad (2.3)$$

where  $\phi_n$  is such that  $H\phi_n = E_n\phi_n$ . A Wick rotation of the time parameter  $t = -i\tau$  transforms (2.1) into a diffusion type equation, and its unitary time evolution (2.3) into an exponential decay:

$$\psi(\tau) = \sum_n c_n e^{-E_n \tau/\hbar} \phi_n. \quad (2.4)$$

As one can see, when propagating forward in the imaginary time  $\tau$ , each eigenfunction will decay exponentially to zero, with a rate of decay proportional to its corresponding eigenvalue  $E_n$ . Therefore all the states will die off exponentially faster than the ground state:

$$\frac{\psi_n(\tau)}{\psi_0(\tau)} \propto e^{-\tau(E_n - E_0)/\hbar}. \quad (2.5)$$

As a consequence, the proportion of the ground state will increase with increasing imaginary time: indeed we have the limit

$$\lim_{\tau \rightarrow \infty} \frac{\langle \psi(\tau) | c_0 \psi_0(\tau) \rangle}{\langle \psi(\tau) | \psi(\tau) \rangle} = \lim_{\tau \rightarrow \infty} \frac{c_0^2 e^{-2\tau E_0/\hbar}}{c_0^2 e^{-2\tau E_0/\hbar} + \sum_n c_n^2 e^{-2\tau E_n/\hbar}} = 1, \quad (2.6)$$

which means that for large  $\tau$  we obtain

$$\psi(\tau) = c_0 e^{-\tau H/\hbar} \psi_0(0) + \mathcal{O}(e^{-\tau(E_1-E_0)/\hbar}). \quad (2.7)$$

Notice that the ground state is found up to a constant factor. It is therefore necessary to normalise after each imaginary time propagation. In conclusion, the ground state can be written as

$$\psi_0 = \lim_{\tau \rightarrow \infty} \frac{\psi(\tau)}{\sqrt{\langle \psi(\tau) | \psi(\tau) \rangle}}. \quad (2.8)$$

Theoretically, this procedure works only by choosing an initial condition which overlaps with the ground state, i.e. if  $c_0 \neq 0$ . However, in practice one finds that the ground state is achieved even if  $c_0 = 0$ : this is due to the small numerical errors which might artificially create such an overlap at any point in the imaginary time propagation procedure. Of course, such initial conditions require more time to achieve convergence, and an appropriate choice of the initial state can significantly speed up the algorithm.

### 2.1.1 Imaginary time propagation for non-linear systems

The procedure we have just described is particularly suited to explain the idea behind the imaginary time propagation procedure. This however, relies on the assumption that a complete set of orthonormal eigenstates exist. This might not be guaranteed in the nonlinear case. In order to see whether the imaginary time propagation indeed drives a state to the lowest energy eigenfunction of the Hamiltonian operator, we can proceed as it follows. Consider the evolution  $|\dot{\psi}\rangle = -H|\psi\rangle$  where  $H$  now is nonlinear, obtained by the Wick rotation  $\tau = it$  of the Gross-Pitaevskii equation, under the

constraint of constant normalisation

$$\int |\psi|^2 d\mathbf{r} \equiv \langle \psi | \psi \rangle = \mathcal{N}. \quad (2.9)$$

The dot denotes here a derivative with respect to  $\tau$  multiplied by the reduced Plank constant:  $\dot{\psi} \equiv \hbar \frac{d\psi}{d\tau}$ . The process of normalisation (2.9) amounts to multiplication of the wavefunction by a factor:  $\psi \rightarrow e^{-\lambda(t)}\psi$ . Because of this reason, it is equivalent to solving the following:

$$\hbar \partial_\tau \psi = -H\psi - \dot{\lambda}\psi. \quad (2.10)$$

The equation of motion in imaginary time and its complex conjugate

$$\begin{aligned} |\dot{\psi}\rangle &= -\left(H - \dot{\lambda}\right) |\psi\rangle, \\ \langle \dot{\psi}| &= -\langle \psi| \left(H - \dot{\lambda}\right), \end{aligned} \quad (2.11)$$

can be multiplied now by  $\langle \psi|$  and  $|\psi\rangle$  respectively and then summed, to obtain:

$$\partial_\tau \langle \psi | \psi \rangle = 2 \langle \psi | \left( H - \dot{\lambda} \right) | \psi \rangle = 0. \quad (2.12)$$

This allows us to obtain an expression for the time derivative of the parameter  $\lambda$ :

$$\dot{\lambda} = \frac{\langle \psi | H | \psi \rangle}{\langle \psi | \psi \rangle}. \quad (2.13)$$

Writing for the energy  $E = \langle \psi | H | \psi \rangle$ , it becomes apparent that (2.13) represents the energy per particle — a quantity, we recall, which is conserved in real time but not in imaginary time. Considering now the specific case of the Gross-Pitaevskii equation, we can write the Hamiltonian as a sum of its linear and non-linear terms:  $H = H_0 + g\rho$ , where  $\rho = \psi^2$  denotes the density.

Taking for simplicity  $\mathcal{N} = \langle \psi | \psi \rangle = 1$ , the imaginary-time variation of the energy can then be found as it follows:

$$\begin{aligned}
\frac{dE}{d\tau} &= \langle \dot{\psi} | H_0 | \psi \rangle + \langle \psi | H_0 | \dot{\psi} \rangle + \frac{g}{2} \left( \langle \dot{\psi} | \rho | \psi \rangle + \langle \psi | \dot{\rho} | \psi \rangle + \langle \psi | \rho | \dot{\psi} \rangle \right) \\
&= -\langle \psi | \left( (H_0 + g\rho - \dot{\lambda}) H_0 \right) | \psi \rangle - \langle \psi | H_0 \left( H_0 + g\rho - \dot{\lambda} \right) | \psi \rangle + g \left( \langle \dot{\psi} | \rho | \psi \rangle + \langle \psi | \rho | \dot{\psi} \rangle \right) \\
&= -2\langle H_0^2 \rangle - g\langle \rho H_0 + H_0 \rho \rangle + 2\dot{\lambda}\langle H_0 \rangle - g \left( \langle (H_0 + g\rho - \dot{\lambda}) \rho \rangle + \langle \rho (H_0 + g\rho - \dot{\lambda}) \rangle \right) \\
&= -2\langle H_0^2 \rangle - 2g\langle \rho H_0 + H_0 \rho \rangle - 2g^2\langle \rho^2 \rangle + 2g\dot{\lambda}\langle \rho \rangle + 2\dot{\lambda}\langle H_0 \rangle \\
&= -2\langle (H_0 + g\rho)^2 \rangle + 2 \left( \langle H_0^2 \rangle + 2g\langle H_0 \rangle \langle \rho \rangle + g^2\langle \rho^2 \rangle \right) \\
&= -2 \left[ \langle (H_0 + g\rho)^2 \rangle - \langle H_0 + g\rho \rangle^2 \right] = -2 \left( \langle H^2 \rangle - \langle H \rangle^2 \right) \\
&= -2 \left\langle \left( H - \langle H \rangle \right)^2 \right\rangle \leq 0
\end{aligned} \tag{2.14}$$

This result shows that the energy is a monotonically decreasing function of the imaginary time  $\tau$ , which is reassuring. Therefore, in the long imaginary-time limit the system is guaranteed to converge at least to a local minimum. This in turns should lead the system to eventually converge to the ground state (in most cases) even if there is no initial overlap with it, or if the system is initialised in a local minimum: once a state  $\phi_j$  satisfying the equality above is achieved, any numerical error which drives the system into a higher energy state will be smoothed out by the imaginary time propagation bringing the state back to the state  $\phi_j$ ; on the other hand, any numerical error driving the system to a lower energy state will necessarily make the imaginary time propagation procedure drive the state to a lower energy state. An example of such a process is presented in the following Fig. 2.1. Despite the system being initialised in the local minimum  $B$ , numerical errors can build up a non-zero density in the global minimum  $A$ , thus decreasing the overall energy. The system will eventually evolve towards the true minimum. Notice that this happens independently of the space separation between  $A$  and  $B$ , or

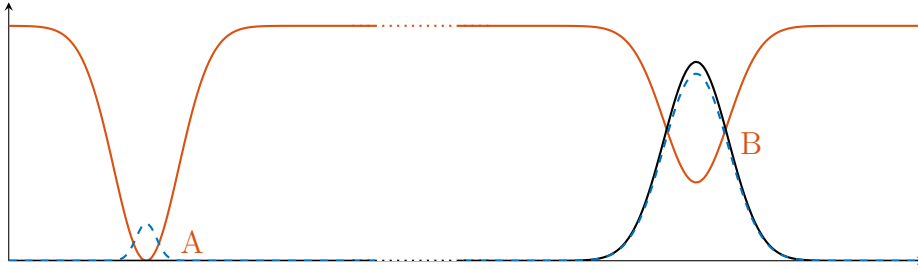


Figure 2.1: An example of a pathological system in which imaginary time propagation achieves nonetheless the true ground state. Despite the density being initialised in the local minimum  $B$  (solid black line), the system will eventually evolve towards the true minimum  $A$  when propagated in imaginary time. The potential is shown in red. The dashed blue line refers to the building up of a nonzero density in the true minimum  $A$  due to numerical errors, as explained in the text.

the magnitude of the potential between the two minima. In fact, the same would happen if considering a particle inside an infinite box potential, and an adjacent box potential with lower energy. This is because the process does not occur through tunnelling, but exclusively thanks to the accumulation of numerical errors and can thus be sped up by employing a larger time step. This heuristic argument does not clearly have universal validity, but it probably fails only in presence of very pathological systems and initial states; empirically, we do not find any initial condition which would not eventually converge to the true ground state, even though we cannot rule out the existence of one in which the imaginary time propagation would not be able to drive the system out of a local minimum.

Although this argument guarantees the eventual convergence in most scenarios, still it does not guarantee an effective rate of convergence. As mentioned before, it is better, in terms of efficiency, to start the propagation in imaginary time from a state overlapping with the ground state. In practice, it is convenient to initialise the wavefunction with random complex values so that it is statistically guaranteed the presence of any possible state.

Now that we have a method to achieve the ground state by propagating in

imaginary time, we need an algorithm to actually compute the propagation. The method we chose is a pseudo-spectral method, and we are now going to explain in detail how it works.

## 2.2 Methods for propagation in time

The problem of solving the time dependent GPE can be tackled with several methods, most notably with Crank-Nicolson or other finite difference methods. This class of methods is very powerful as it ensures unitarity for arbitrary time steps; furthermore the time step is limited only by the requirements on the accuracy but not from stability considerations. On the other hand, it is a fairly expensive computational method, of uneasy implementation and not preserving gauge invariance [107]. The alternatives to Crank-Nicolson are various, but we will focus on split-step pseudo-spectral methods. This choice is computationally cheaper and particularly suited for our problem. Unfortunately it does not conserve the total energy but, as we will see, it is possible to implement a workaround which restores unitarity. From now on and for the rest of the Chapter, for the sake of brevity, we will be using units in which  $\hbar = m = 1$ .

### 2.2.1 Time propagation

Split-step methods were originally developed for the case of linear equations such as the linear Schrödinger equation. Consider a system described by the following initial value problem

$$\begin{aligned}\partial_t \psi &= (A + B)\psi, \\ \psi(0) &= \psi_0,\end{aligned}\tag{2.15}$$

with formal solution  $\psi(t) = e^{t(A+B)}\psi_0$ . Split-steps methods aim to approximate the operator  $e^{t(A+B)}$  by an appropriate combination of the operators



$e^{At}$  and  $e^{Bt}$ , when  $[A, B] \neq 0$ . More specifically one can write

$$e^{(A+B)t} = \prod_{i=1}^m e^{a_i A t} e^{b_i B t} + \mathcal{O}(t^p), \quad (2.16)$$

where  $a_i, b_i$  are constants to be determined and where the order  $p$  is obtained for some large enough  $m$ . The values of  $a_i$  and  $b_i$  can be determined by matching the  $p$ -th order expansion of the left and right hand side of (2.16). This procedure is particularly useful because we might know how the operators  $e^{At}$  and  $e^{Bt}$  operate individually but not how  $e^{(A+B)t}$  operates. This is exactly the case in our problem, as we will see later.

A first example, is what is known by the name of Lie splitting:

$$e^{(A+B)t} = e^{At} e^{Bt} + \mathcal{O}(t^2), \quad (2.17)$$

or equivalently

$$e^{t(A+B)} = e^{Bt} e^{At} + \mathcal{O}(t^2), \quad (2.18)$$

which is known to be of order one. In order to verify this, we can look at the error  $\epsilon(t) = \psi_{\text{approx}}(t) - \psi(t)$ , where  $\psi_{\text{approx}}$  is given by the propagation through the approximate *Lie splitting* as  $\psi_{\text{approx}} = e^{At} e^{Bt} \psi_0$ . In details:

$$\begin{aligned} \varepsilon_L(t) &= [e^{At} e^{Bt} - e^{(A+B)t}] \psi_0 \\ &= \left[ \left( 1 + tA + \frac{t^2}{2} A^2 + \mathcal{O}(t^3) \right) \left( 1 + tB + \frac{t^2}{2} B^2 + \mathcal{O}(t^3) \right) + \right. \\ &\quad \left. - \left( 1 + t(A+B) + \frac{t^2}{2} (A+B)^2 + \mathcal{O}(t^3) \right) \right] \psi_0 \\ &= \left[ 1 + tB + \frac{t^2}{2} B^2 + tA + t^2 AB + \frac{t^2}{2} A^2 - 1 - t(A+B) - \frac{t^2}{2} (A+B)^2 + \mathcal{O}(t^3) \right] \psi_0 \\ &= \frac{t^2}{2} [A, B] \psi_0 + \mathcal{O}(t^3). \end{aligned} \quad (2.19)$$

As we can see this method is accurate to first order, exhibiting a local error of the order of  $\mathcal{O}(t^2)$ . A more accurate splitting is instead the following second order method, known as *Strang splitting* [108, 109]:

$$e^{t(A+B)} = e^{\frac{t}{2}B} e^{tA} e^{\frac{t}{2}B} + \mathcal{O}(t^3). \quad (2.20)$$

The Strang splitting is also known as the symmetric split-step method since the operator  $S = e^{\frac{t}{2}B} e^{tA} e^{\frac{t}{2}B}$  preserves time symmetry, i.e.

$$S(t)S(-t) = \mathbb{1}, \quad (2.21)$$

while, as one can easily verify, it is not the case for the operator used in (2.17). As mentioned, the Strang operator  $S$  is able to attain a higher order of accuracy and, by using a bit more algebra, it is possible to show that the associated error is

$$\varepsilon_S(t) = \frac{t^3}{12} ([B, [B, A]] - [A, [A, B]]) \psi_0 + \mathcal{O}(t^4). \quad (2.22)$$

The simplicity of the method allows for an easy implementation in any algebra package such as *Mathematica*: in [71], Javanainen and Ruostekoski, having employed *Mathematica*'s algebra package, report to have obtained coefficients for an expansion up to order  $\mathcal{O}(t^5)$ . The usage of symbolic calculations in carrying out these expansions proves necessary as the expansion becomes intractable with growing orders.

The convergence and stability of the methods can be demonstrated [110], provided that (sufficient and necessary conditions)  $\|e^{tA}\| \leq 1$ ,  $\|e^{tB}\| \leq 1$  and  $\|e^{t(A+B)}\| \leq 1$ .

### 2.2.2 Split-step methods for linear Schrödinger equation

The split-step procedure outlined above becomes particularly interesting when applied in conjunction with Fourier diagonalisation. Let us see what this means in particular for the linear Schrödinger equation:

$$i\frac{\partial}{\partial t}\psi(x, t) = H_0\psi(x, t), \quad (2.23)$$

where the linear Hamiltonian is given by  $H_0 = K + V$ , with the kinetic energy and time-independent potential given by

$$\begin{aligned} K &= -\frac{1}{2}\nabla^2, \\ V &= V(x). \end{aligned} \quad (2.24)$$

Let us consider the Strang splitting  $\psi(t) = e^{-iH_0t}\psi_0 = e^{-iKt/2}e^{-iVt}e^{-iKt/2}\psi_0$ . Recalling that the kinetic energy operator is diagonalised in momentum space, the evaluation of the operator  $e^{-iKt/2}$  is better done in momentum space leading

$$e^{-iKt/2}\psi_0 = \mathcal{F}^{-1}\left[e^{-it\mathbf{k}^2/2}\mathcal{F}[\psi_0]\right], \quad (2.25)$$

where  $\mathcal{F}[\cdot]$  denotes the Fourier transform. Therefore, the whole splitting procedure, combined with the Fourier diagonalisation, amounts to the following operation, performed repeatedly for each time steps  $\Delta t$ :

$$\psi(t + \Delta t) = \mathcal{F}^{-1}\left[e^{-i\Delta t\mathbf{k}^2/2}\mathcal{F}\left[e^{-iV\Delta t}\mathcal{F}^{-1}\left[e^{-i\Delta t\mathbf{k}^2/2}\mathcal{F}[\psi(t)]\right]\right]\right]. \quad (2.26)$$

Such steps can be carried out numerically by employing the readily available FFT algorithms.

### 2.2.3 Split-step methods for the non-linear Gross-Pitaevskii equation in real time

The method outlined above can be generalised almost straightforwardly to the non-linear case, even if caution must be taken in order to preserve the order of accuracy. Let us then consider the particular case of the Gross-Pitaevskii equation:

$$i \frac{\partial \psi}{\partial t} = (H_0 + g |\psi|^2) \psi. \quad (2.27)$$

We could now be tempted to write an effective potential as

$$V_{eff} = V(x) + g |\psi|^2. \quad (2.28)$$

However, this proves inconvenient as the Strang splitting, in this non-linear case, loses its second order accuracy and becomes first order accurate. Javanainen and Ruostekoski [71], suggest instead the following recursive method:

$$\begin{aligned} \psi_0 &= \psi(x, t), \\ \psi_1 &= \exp \left[ \frac{-i \Delta t K}{2} \right] \psi_0, \\ \psi_2 &= \exp \left[ -i \Delta t (V(x) + g |c_0 \psi_0 + c_1 \psi_1|^2) \right] \psi_1, \\ \psi(x, t + \Delta t) &= \exp \left[ \frac{-i \Delta t K}{2} \right] \psi_2. \end{aligned} \quad (2.29)$$

As we can see the method is analogous to the standard Strang splitting, but the crucial difference is the step by step evaluation which allows to use a more “up to date” version of the wavefunction when calculating  $\psi_2$ ; choosing an appropriate linear combination it is in fact possible to regain the second order accuracy. In order to do so, we consider the expansion of the wavefunction

at the first step:

$$\psi(x, t + \Delta t) = \left( 1 + \Delta t \partial_t + \frac{\Delta t^2}{2} \partial_t^2 + \mathcal{O}(\Delta t^3) \right) \psi(x, t), \quad (2.30)$$

where

$$\begin{aligned} \frac{\partial \psi}{\partial t} &= -i (H_0 + g |\psi|^2) \psi, \\ \frac{\partial^2 \psi}{\partial t^2} &= -i (H_0 + g |\psi|^2) \frac{\partial \psi}{\partial t} - ig \psi \left( \psi^* \frac{\partial \psi}{\partial t} + \psi \frac{\partial \psi^*}{\partial t} \right), \\ &\vdots \end{aligned} \quad (2.31)$$

et cetera. Expanding now the exponentials in (2.29) we can try to match the terms in (2.29) with those in (2.30). Once again an algebra package suits this task perfectly. The result one can find, is that the second order accuracy is achieved if and only if  $c_0 = 0$  and  $c_1 = \pm 1$ , which means one has to employ in expansion (2.29) the most recent version of the wavefunction. The authors, in [71], trying different cases, showed that this most recent version of the wavefunction seems to be the best choice, giving the most accurate answer.

It is possible to find this same result following similar considerations: consider the Hamiltonian  $H = K + V$ , where the potential incorporates now the non-linear interaction term,  $V = V(x) + g\rho$ . Denoting by  $\tilde{\rho}$  the density entering the Strang splitting, and consequently  $\tilde{V} = V(\tilde{\rho})$ , the real time propagation achieved by the Strang splitting is given by

$$\begin{aligned} \psi^S(t + \Delta t) &= \left[ e^{-iK\Delta t/2} e^{-i\tilde{V}\Delta t} e^{-iK\Delta t/2} + \mathcal{O}(\Delta t^3) \right] \psi(t) \\ &= \left[ e^{-i\tilde{H}\Delta t} + \mathcal{O}(\Delta t^3) \right] \psi(t) \\ &= \left[ 1 - i\Delta t \tilde{H} - \frac{\Delta t^2}{2} \tilde{H}^2 + \mathcal{O}(\Delta t^3) \right] \psi(t), \end{aligned} \quad (2.32)$$

where clearly  $\tilde{H} = K + \tilde{V}$ . At the same time, from the Gross-Pitaevskii

equation  $\partial_t \psi = -iH\psi$  one finds

$$\psi^{GPE}(t + \Delta t) = \left[ 1 - i\Delta t H - \frac{\Delta t^2}{2} H^2 - i\frac{\Delta t^2}{2} g\partial_t \rho \right] \psi(t), \quad (2.33)$$

where we have made use of the fact that  $\partial_t^2 \psi = (H^2 - ig\partial_t \rho)\psi$ . Subtracting (2.33) and (2.32) and equating this to zero:

$$\begin{aligned} \frac{\psi^S(t + \Delta t) - \psi^{GPE}(t + \Delta t)}{\psi(t)} &= -i\Delta t(\tilde{H} - H) - \frac{\Delta t^2}{2}(\tilde{H}^2 - H^2) + i\frac{\Delta t^2}{2}g\partial_t \rho + \mathcal{O}(\Delta t^3) \\ &= -i\Delta t(\tilde{H} - H) + i\frac{\Delta t^2}{2}g\partial_t \rho + \mathcal{O}(\Delta t^3) \\ &= ig\Delta t(\tilde{\rho} - \rho) - i\frac{\Delta t^2}{2}g\partial_t \rho + \mathcal{O}(\Delta t^3) = 0, \end{aligned} \quad (2.34)$$

where  $\tilde{H}^2 - H^2 = 0 + \mathcal{O}(\Delta t)$ . Thus, to second order in the time step  $\Delta t$ , we find

$$\begin{aligned} \tilde{\rho}(t) &= \rho(t) + \frac{\Delta t}{2}\partial_t \rho(t) \\ &= \rho\left(t + \frac{\Delta t}{2}\right). \end{aligned} \quad (2.35)$$

Therefore, the second order accuracy of the Strang splitting is restored in the non-linear case of the Gross-Pitaevskii equation, as long as a more ‘up to date’ wavefunction is used. Numerically such a wavefunction can be obtained by a simpler first order Lie splitting as

$$\tilde{\rho} = \left| e^{-i\frac{\Delta t}{2}V(\rho)} e^{-i\frac{\Delta t}{2}K} \psi \right|^2. \quad (2.36)$$

As a consequence the correct splitting reads

$$e^{-iH\Delta t} = e^{-i\frac{\Delta t}{2}K} \exp \left[ -i\Delta t V \left( \left| e^{-i\frac{\Delta t}{2}V(\rho)} e^{-i\frac{\Delta t}{2}K} \psi \right|^2 \right) \right] e^{-i\frac{\Delta t}{2}K} + \mathcal{O}(\Delta t^3). \quad (2.37)$$

However, it is possible to simplify this result further. Consider the first order expansion of (2.36), disregarding for simplicity the trapping potential, so that  $V = g\rho$ :

$$\begin{aligned} \left| e^{-i\frac{\Delta t}{2}V(\rho)} e^{-i\frac{\Delta t}{2}K} \psi \right|^2 &= \left| \left( 1 - i\frac{\Delta t}{2}g\rho \right) \left( 1 - i\frac{\Delta t}{2}K \right) \psi \right|^2 + \mathcal{O}(\Delta t^2) \\ &= \left| \left( 1 - i\frac{\Delta t}{2}g\rho - i\frac{\Delta t}{2}K \right) \psi \right|^2 + \mathcal{O}(\Delta t^2) \\ &= \left( \psi^* + i\frac{\Delta t}{2}K\psi^* + i\frac{\Delta t}{2}g\rho\psi^* \right) \left( \psi - i\frac{\Delta t}{2}K\psi - i\frac{\Delta t}{2}g\rho\psi \right) + \mathcal{O}(\Delta t^2) \\ &= \rho + i\frac{\Delta t}{2}(\psi K\psi^* - \psi^* K\psi) + \mathcal{O}(\Delta t^2). \end{aligned} \quad (2.38)$$

Now, it is possible to observe that to first order, (2.36) is equivalent to

$$\begin{aligned} \left| e^{-i\frac{\Delta t}{2}K} \psi \right|^2 &= \left| \left( 1 - i\frac{\Delta t}{2}K \right) \psi \right|^2 + \mathcal{O}(\Delta t^2) \\ &= \left( 1 + i\frac{\Delta t}{2}K \right) \psi^* \left( 1 - i\frac{\Delta t}{2}K \right) \psi + \mathcal{O}(\Delta t^2). \quad (2.39) \\ &= \rho + i\frac{\Delta t}{2}(\psi K\psi^* - \psi^* K\psi) + \mathcal{O}(\Delta t^2), \end{aligned}$$

so that to second order we have

$$\Delta t \left| e^{-i\frac{\Delta t}{2}V(\rho)} e^{-i\frac{\Delta t}{2}K} \psi \right|^2 = \Delta t \left| e^{-i\frac{\Delta t}{2}K} \psi \right|^2 + \mathcal{O}(\Delta t^3). \quad (2.40)$$

Thanks to (2.40), it is then possible to simplify (2.37) into the splitting

$$e^{-iH\Delta t} = e^{-i\frac{\Delta t}{2}K} \exp \left[ -i\Delta t V \left( \left| e^{-i\frac{\Delta t}{2}K} \psi \right|^2 \right) \right] e^{-i\frac{\Delta t}{2}K} + \mathcal{O}(\Delta t^3), \quad (2.41)$$

which corresponds exactly to the procedure (2.29) described in [71].

## 2.2.4 Split-step method for the non-linear Gross-Pitaevskii equation in imaginary time

Unfortunately, the second order method proposed by [71] and discussed so far, works exclusively for real time propagation. When we consider instead propagation in imaginary time, this method loses its second order accuracy although performing better than the standard Lie splitting. This result is shown in Fig. 2.2. Luckily, we can still find a procedure which is second order accurate in imaginary time. Proceeding as it was done before in real time, recalling the Gross-Pitaevskii equation in imaginary time is  $\partial_\tau \psi = -H\psi$ , one finds, as in (2.35), that

$$\tilde{\rho}(\tau) = \rho\left(\tau + \frac{\Delta\tau}{2}\right), \quad (2.42)$$

which can be achieved again numerically with a first order Lie splitting

$$\tilde{\rho} = \left| e^{-\frac{\Delta\tau}{2}V(\rho)} e^{-\frac{\Delta\tau}{2}K} \psi \right|^2. \quad (2.43)$$

However, in imaginary time there is no equivalent for (2.40), i.e. in general

$$\Delta\tau \left| e^{-\frac{\Delta\tau}{2}V(\rho)} e^{-\frac{\Delta\tau}{2}K} \psi \right|^2 \neq \Delta\tau \left| e^{-\frac{\Delta\tau}{2}K} \psi \right|^2 + \mathcal{O}(\Delta\tau^3). \quad (2.44)$$



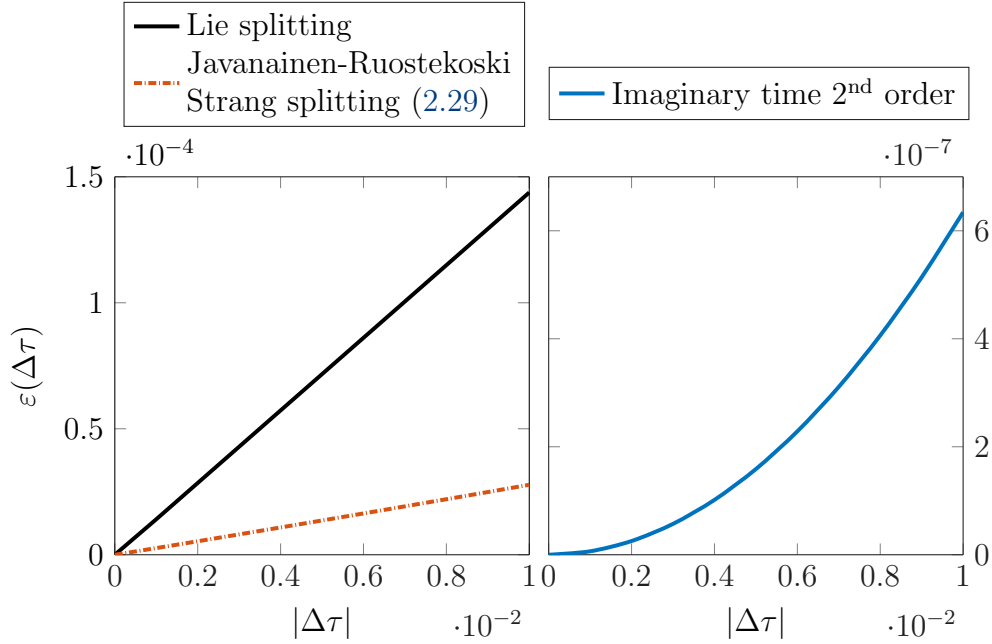


Figure 2.2: A plot of the error as a function of imaginary time step for different methods (arbitrary units). The accuracy of the Javanainen-Ruostekoski Strang splitting (2.29) described in [71] for real time propagation does not carry over to imaginary time propagation. In imaginary time the method is first order accurate. On the other hand, it is possible to see (right) that a different procedure (2.45) can be used which attains second order accuracy.

Thus, in order to attain second order accuracy one must employ the full splitting as

$$e^{-H\Delta\tau} = e^{-\frac{\Delta\tau}{2}K} \exp \left[ -\Delta\tau V \left( \left| e^{-\frac{\Delta\tau}{2}V(\rho)} e^{-\frac{\Delta\tau}{2}K} \psi \right|^2 \right) \right] e^{-\frac{\Delta\tau}{2}K} + \mathcal{O}(\Delta\tau^3). \quad (2.45)$$

Notice that this modification of the splitting procedure, while increasing the accuracy of the method, it does not increase its complexity, introducing only one additional Hadamard product (which has complexity  $\mathcal{O}(n)$ , to be contrasted with the complexity  $\mathcal{O}(n \log n)$  of the *fft* algorithm). In particular,

the whole procedure can be written as:

$$\begin{aligned}
\psi_0 &= \psi(x, t), \\
\psi_1 &= \exp\left[\frac{-\Delta\tau K}{2}\right] \psi_0, \\
\psi_2 &= \exp\left[-\Delta\tau V(|e^{-\frac{\Delta\tau}{2}V(|\psi_1|^2)}\psi_1|^2)\right] \psi_1, \\
\psi(x, \tau + \Delta\tau) &= \exp\left[\frac{-\Delta\tau K}{2}\right] \psi_2.
\end{aligned} \tag{2.46}$$

Equivalently we could have considered the splitting

$$e^{-H\Delta\tau} = e^{-\frac{\Delta\tau}{2}V(\rho_b)}e^{-\Delta\tau K}e^{-\frac{\Delta\tau}{2}V(\rho_a)} + \mathcal{O}(\Delta\tau^3). \tag{2.47}$$

In this case the requirement found is

$$\frac{1}{2}(\rho_a(t) + \rho_b(t)) = \tilde{\rho}(t) = \rho(\tau + \Delta\tau). \tag{2.48}$$

Moreover, the splitting (2.47) can be written as

$$\left(e^{-\frac{\Delta\tau}{2}V(\rho_b)}e^{-\frac{\Delta\tau}{2}K}\right)\left(e^{-\frac{\Delta\tau}{2}K}e^{-\frac{\Delta\tau}{2}V(\rho_a)}\right)\psi = \left(e^{-\frac{\Delta\tau}{2}V(\rho_b)}e^{-\frac{\Delta\tau}{2}K}\right)\psi\left(\tau + \frac{\Delta\tau}{2}\right) + \mathcal{O}(\Delta\tau^2), \tag{2.49}$$

which suggests that to first order in  $\Delta\tau$  we have

$$\begin{aligned}
\rho_b &= \tilde{\rho} + \mathcal{O}(\Delta\tau^2) \\
&= \rho\left(\tau + \frac{\Delta\tau}{2}\right) + \mathcal{O}(\Delta\tau^2)
\end{aligned} \tag{2.50}$$

Therefore, the splitting (2.47) achieves second order accuracy provided that  $\rho_a = \rho_b = \rho(\tau + \Delta\tau/2)$ , or in full

$$e^{-H\Delta\tau} = \exp \left[ -\frac{\Delta\tau}{2} V \left( \left| e^{-\frac{\Delta\tau}{2} K} e^{-\frac{\Delta\tau}{2} V(\rho)} \psi \right|^2 \right) \right] e^{-\Delta\tau K} \cdot \exp \left[ -\frac{\Delta\tau}{2} V \left( \left| e^{-\frac{\Delta\tau}{2} K} e^{-\frac{\Delta\tau}{2} V(\rho)} \psi \right|^2 \right) \right] + \mathcal{O}(\Delta\tau^3). \quad (2.51)$$

As for the other splitting (2.45), only one additional Hadamard is introduced in order to restore the second order accuracy. In particular, no additional Fourier transform is required, thus not affecting the complexity of the whole method to leading order.

Finally let us make a short comment on the time step. Consider for simplicity the error associated with the Lie splitting previously given in equation (2.19). Writing now the Hamiltonian as a sum of its linear and nonlinear parts as  $H = H_0 + g\rho$ , it is straightforward to see that the error, to a first approximation, depends linearly on the interaction strength  $g$ :  $|\epsilon| \sim g|\Delta t^2|$ . It is therefore necessary, when comparing two solutions at two different interacting regimes, that the two time steps are carefully chosen, one larger than the other, so that the accuracy on both solutions is guaranteed to be the same. This will be particularly important when considering transitions between different states, as the boundaries of such transitions are determined by the difference in the energy associated with each state.

## 2.3 Outlook

In conclusion we have described the imaginary time propagation method, proved the energy is monotonically decreasing in imaginary time also for the non-linear Gross-Pitaevskii problem, and found that the method can be employed to seek ground states of the system. Further, we have discussed various split-step methods to propagate in time, demonstrating that the stan-

standard Strang splitting does not retain its second order accuracy when applied to non-linear systems. More specifically, we have shown that the method firstly put forward in [71], restores the second order accuracy in real time. Lastly, we have shown that the latter drops again in accuracy if employed in imaginary time; we have therefore described a method which achieves second order accurate imaginary time propagation and, crucially, at no expense for the algorithmic complexity.

# Chapter 3

## A Discrete Model for Infinite Vortex Lattices

“When one has a particular problem to work out in quantum mechanics, one can minimise the labor by using a representation in which the representatives of the most important abstract quantities occurring in the problem are as simple as possible.”

---

P.A.M. Dirac, from *The Principles of Quantum Mechanics*, 1958.

The most straightforward approach to study systems governed by mean-field Gross-Pitaevskii theory, and the most employed in practice [101, 111, 112], is to directly discretise and solve the equation of motion (1.14) with positive effective frequency  $\omega_{\text{eff}} > 0$ , using numerical techniques such as the Crank-Nicholson method or the standard split-step Fourier method [107]. In this way, the condensate has finite spatial extent being confined by the harmonic trapping potential. For such calculations, one chooses computational

grids sufficiently large, so that the wave function effectively vanishes at the boundary. This makes the boundary conditions involving the phase of the wave function irrelevant, thereby also allowing for the direct application of standard Fourier methods.

However, this approach has substantial drawbacks. First of all, the underlying trapping potential obscures and distorts the configuration of the vortex lattice, as it was shown in [93]. In order to infer the ideal periodic configuration of vortices, one must require the mean inter-vortex spacing  $\ell_\Omega$ , to be much smaller than the size of the condensate. In practice, this means one must numerically simulate systems with at least  $\sim 100$  vortices, which is extremely inefficient given that the space of possible configuration becomes considerably vast with growing number of vortices. Secondly, as we have just mentioned, one needs to take a sufficiently large computational grid so as to ensure the wave function vanishes at the boundaries. This means the computation becomes remarkably inefficient, as many computational grid points are devoted to points of little interest. The method we are going to describe, aims at overcoming such complications. Specifically, we are going to focus on the case where the effective frequency vanishes  $\omega_{\text{eff}} = 0$ , so that the condensate is spatially extended and the ideal vortex lattice is expected to form. We will seek solutions to the Gross-Pitaevskii equation (1.69) which are periodic in  $\rho$ , by enforcing the required twisted boundary conditions (1.133) on the wave function. As a result, unnecessarily large computational domains can be avoided and systems sizes can be chosen on the order of the vortex lattice spacing.

In particular, we start this Chapter by introducing a discrete lattice model whose energy retains the same gauge symmetries as the continuous energy functional and converges to the energy functional as the lattice spacing decreases. Then, motivated by the magnetic translation group, we introduce the so-called magnetic Fourier transform and formulate the continuous Gross-Pitaevskii problem that yields the wave function with the correct periodic

structure. This correct problem arises since the magnetic Fourier transform naturally incorporates twisted boundary conditions which must be satisfied for rotating condensates. We then turn to showing how spatial discretisation of the discrete model can be achieved through a discrete version of the magnetic Fourier transform and how to compute it rapidly using standard fast Fourier transforms. Further, we implement it with the split-step time integration scheme described in the previous Chapter 2. We test the method by showing that it reduces to known results obtained in the lowest-Landau-level regime.

### 3.1 A non-linear Hofstadter model

When confronted with the problem of the energy functional (1.68), one can opt for the direct discretisation of the operators entering (1.68). This procedure has the major drawback of not preserving the hermiticity and gauge symmetry of the system. Instead, a more accurate route to take, consists in choosing an appropriate lattice model which reduces to the energy functional of interest (1.68) in the continuum limit. In doing so, we can require that the discrete Hamiltonian is Hermitian, and that the resulting discrete model inherits the exact gauge symmetry of the continuum model. With this in mind, let us then consider a linear Hofstadter Hamiltonian [113], defined on a square lattice of size  $N_x \times N_y$  which can be written compactly as

$$\mathcal{H} = -w \sum_{\langle j,k \rangle} e^{-\frac{i}{\hbar} \int_{r_j}^{r_k} \mathcal{A} \cdot d\mathbf{r}} \psi_j^* \psi_k, \quad (3.1)$$

where the notation  $\langle i, j \rangle$  denotes sums over closest neighbouring sites  $i$  and  $j$ . The exponential phases factor  $\exp(-\frac{i}{\hbar} \int_{r_j}^{r_k} \mathcal{A} \cdot d\mathbf{r})$  arise from the so-called Peierls substitution [113, 114], needed to correctly incorporate the gauge fields into the lattice model. With an obvious change of notation such that each site is labelled by its In the Landau gauge  $\mathcal{A}_L = 2m\Omega(0, x)$ , we can

write for the Peierls factor

$$\begin{aligned}\theta_x &\equiv \frac{1}{\hbar} \int_{r_{n,l}}^{r_{n+1,l}} \mathcal{A} \cdot d\mathbf{r}, \\ \theta_y &\equiv \frac{1}{\hbar} \int_{r_{n,l}}^{r_{n,l+1}} \mathcal{A} \cdot d\mathbf{r}.\end{aligned}\tag{3.2}$$

With an obvious change of notation, such that the positions on the lattice are determined by the integer values  $n$  and  $l$  according to  $r_{n,l} = (na_x, la_y)$ , with  $a_x, a_y$  the discretisation lattice constants, the previous Hofstadter model (3.1) can be written more explicitly in the Landau gauge  $\mathcal{A}_L = 2m\Omega(0, x)$  as

$$-\sum_{n,l} \left[ w_x (\psi_{n+1,l}^* \psi_{n,l} + \psi_{n,l}^* \psi_{n+1,l}) + w_y (e^{i\theta_y} \psi_{n,l+1}^* \psi_{n,l} + e^{-i\theta_y} \psi_{n,l}^* \psi_{n,l+1}) \right],\tag{3.3}$$

where  $\theta_x = 0$  and  $\theta_y = 2m\Omega a_y x / \hbar$ ; because of the choice of the gauge, particles tunnelling in the  $y$ -direction acquire a phase, while those tunnelling along the  $x$ -direction are unaffected. This, as we will also see later, explains the reason for choosing the Landau gauge, namely the simplification of the problem. Here, we have also allowed for anisotropic tunnelling by introducing the two tunnelling amplitudes  $w_x$  and  $w_y$ . We defer for the moment the discussion on the need for anisotropic tunnelling (Sec. 3.4.2), but state here that it will be of fundamental importance for what follows. The integers  $n$  and  $l$  labelling respectively the  $x$ -direction and the  $y$ -direction on the lattice, are clearly required to satisfy the constraints  $1 \leq n \leq N_x$  and  $1 \leq l \leq N_y$ . In the above (3.3), the first two terms account for nearest-neighbour tunnelling along the  $x$ -direction, while the last two for nearest-neighbour tunnelling along the  $y$ -direction. Now, through the identification  $\psi_{n,l} = \sqrt{a_x a_y} \psi(a_x n, a_y l)$ , expanding to second order, we can indeed check that this lattice Hamiltonian reduces, in the continuum limit, to the linear part of the



Gross-Pitaevskii theory (1.105):

$$\begin{aligned}
& - \int dx dy [w_x \psi^*(x + a_x, y) \psi(x, y) + w_y e^{i\theta_y} \psi^*(x, y + a_y) \psi(x, y) + \text{c.c.}] \\
& \approx - w \int dx dy \left[ w_x \left( \psi^*(x, y) + a_x \partial_x \psi(x, y)^* + \frac{a_x^2}{2} \partial_x^2 \psi^*(x, y) \right) \psi(x, y) + \right. \\
& \quad \left. + w_y e^{i\theta_y} \left( \psi^*(x, y) + a_x \partial_y \psi(x, y)^* + \frac{a_x^2}{2} \partial_y^2 \psi^*(x, y)^* \right) \psi(x, y) + \text{c.c.} \right] \\
& = - \int dx dy \left[ 2(w_x + w_y \cos(\theta_y)) |\psi|^2 + 2w_y i \sin(\theta_y) a_y \psi^* \partial_y \psi \right. \\
& \quad \left. - w_x a_x^2 \partial_x \psi^* \partial_x \psi - w_y a_y^2 \cos(\theta_y) \partial_y \psi^* \partial_y \psi \right] \\
& \approx - \int dx dy \left[ 2(w_x + w_y) |\psi|^2 - w_y \frac{\theta_y^2}{2} |\psi|^2 + 2w_y i \theta_y a_y \psi^* \partial_y \psi \right. \\
& \quad \left. - w_x a_x^2 \partial_x \psi^* \partial_x \psi - w_y a_y^2 \partial_y \psi^* \partial_y \psi \right] \\
& = \int dx dy \left[ \frac{\hbar^2}{2m} |\nabla \psi|^2 + 2m\Omega^2 x^2 |\psi|^2 - 2i\hbar\Omega x \psi^* \partial_y \psi \right] - 2(w_x + w_y) \mathcal{N},
\end{aligned} \tag{3.4}$$

which, up to factors not contributing to the dynamics of the system, is equivalent to

$$\int dx dy \left[ \frac{1}{2m} |(-i\hbar\nabla - \mathcal{A}_L) \psi|^2 \right]. \tag{3.5}$$

In the last line of (3.4), we have made the following choice for the tunnelling parameters:

$$\begin{aligned}
w_x &= \frac{\hbar^2}{2ma_x^2}, \\
w_y &= \frac{\hbar^2}{2ma_y^2}.
\end{aligned} \tag{3.6}$$

Therefore one can write the following expression for the discrete energy which accurately describes, to second order in spatial discretisation, the full Gross-

Pitaevskii theory in the Landau gauge:

$$E_d = - \sum_{n,l} [w_x \psi_{n+1,l}^* \psi_{n,l} + w_y e^{i\theta_y} \psi_{n,l+1}^* \psi_{n,l} + \text{c.c.}] + \sum_{n,l} \frac{\mathcal{U}}{2} |\psi_{n,l}|^4 + 2(w_x + w_y)\mathcal{N}. \quad (3.7)$$

Here we have introduced the on-site interaction  $\mathcal{U} = g/a_x a_y$ , for later convenience. Because in the limit  $\mathcal{U} = 0$  the above reduces to the well-known Hofstadter model (3.1), we will refer to (3.7) as a *generalised Hofstadter model* because of the anisotropic tunnelling and the nonlinearity distinguishing it from (3.1).

We can now write the equations of motion for a system described by the energy functional (3.7), from the variational principle

$$i\hbar\partial_t\psi_{n,l} = \frac{\partial E_d}{\partial\psi_{n,l}^*}, \quad (3.8)$$

which more explicitly, ignoring terms unimportant for the dynamics, reads

$$i\hbar\partial_t\psi_{n,l} = -w_x(\psi_{n+1,l} + \psi_{n-1,l}) - w_y(e^{-i\theta_y}\psi_{n,l+1} + e^{i\theta_y}\psi_{n,l-1}) + \mathcal{U}|\psi_{n,l}|^2\psi_{n,l}. \quad (3.9)$$

One can realise here, that the above equation can be conveniently diagonalised by eigenfunctions of the form  $\tilde{\psi}_{n,l} = e^{-i(k_x a_x n + k_y a_y l)}$ :

$$\begin{aligned} (\tilde{\psi}_{n+1,l} + \tilde{\psi}_{n-1,l}) &= 2\cos(k_x a_x)\tilde{\psi}_{n,l}, \\ (e^{-i\theta_y}\tilde{\psi}_{n,l+1} + e^{i\theta_y}\tilde{\psi}_{n,l-1}) &= 2\cos(k_y a_y - \theta_y)\tilde{\psi}_{n,l}. \end{aligned} \quad (3.10)$$

So that the equations of motion (3.9) are now concisely written as

$$i\hbar\partial_t\tilde{\psi}_{n,l} = -\left[2w_x\cos(k_x a_x) + 2w_y\cos(k_y a_y - \theta_y) + \mathcal{U}|\tilde{\psi}_{n,l}|^2\right]\tilde{\psi}_{n,l}. \quad (3.11)$$

As we have discussed in Sec. 1.5, the system must respect the twisted boundary conditions (1.133). We will discuss in the next section how to implement such boundary conditions.

## 3.2 Twisted Boundary Conditions on the lattice

The only problem we are left with is that concerning the implementation of the twisted boundary conditions (1.133). In particular we are after a term which enforces such boundary conditions allowing us at the same time to retain periodicity over the remaining terms of the Hamiltonian allowing us to diagonalise them in momentum space. We will then start with a simplified 1D problem, which is instructive for the following.

### 3.2.1 1D lattice, Open Boundary Conditions

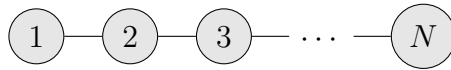


Figure 3.1: 1D system with open boundary conditions.

Consider the system presented in Fig.3.1. Here there is no tunnelling between site  $n = N$  and site  $n = 1$  and vice versa. The Hamiltonian describing such a system is the following:

$$\mathcal{H} = -w \sum_{n=1}^{N-1} (\psi_n^* \psi_{n+1} + \psi_{n+1}^* \psi_n). \quad (3.12)$$

Adding and subtracting a term chosen ad hoc, one can find a term in the Hamiltonian which describes a 1D system with periodic boundary conditions

and diagonalise such a term in momentum space:

$$\begin{aligned}\mathcal{H} &= -w \sum_{n=1}^{N-1} (\psi_n^* \psi_{n+1} + \psi_{n+1}^* \psi_n) - w (\psi_N^* \psi_1 + \psi_1^* \psi_N) + w (\psi_N^* \psi_1 + \psi_1^* \psi_N) \\ &= -w \sum_{n=1}^N (\psi_n^* \psi_{n+1} + \psi_{n+1}^* \psi_n) + w (\psi_N^* \psi_1 + \psi_1^* \psi_N),\end{aligned}\tag{3.13}$$

where with  $\sum$  we denote a sum with periodic boundary conditions, so that  $\psi_{N+1} \equiv \psi_1$ .



Figure 3.2: 1D system with periodic boundary conditions. Here site  $N + 1$  corresponds to site 1.

The first term is promptly diagonalised in momentum space and the Hamiltonian becomes

$$\mathcal{H} = -2w \sum_k \cos(k) \psi_k^* \psi_k + w \begin{pmatrix} \psi_1 \\ \psi_N \end{pmatrix}^\dagger \begin{pmatrix} 0 & 1 \\ 1 & 0 \end{pmatrix} \begin{pmatrix} \psi_1 \\ \psi_N \end{pmatrix}.\tag{3.14}$$

Since the splitting of the Hamiltonian operator will allow us to consider the time evolution of each term independently, we can focus our attention on the evolution of the second term only: the operator splitting can be then done as before. The evolution of the second term in (3.14) is then described by the following equation

$$i\partial_t \begin{pmatrix} \psi_1 \\ \psi_N \end{pmatrix} = w \begin{pmatrix} 0 & 1 \\ 1 & 0 \end{pmatrix} \begin{pmatrix} \psi_1 \\ \psi_N \end{pmatrix},\tag{3.15}$$

which leads to the propagator

$$\begin{aligned} \mathcal{P}(1; N) &= e^{-iw \begin{pmatrix} 0 & 1 \\ 1 & 0 \end{pmatrix} \Delta t} \\ &= \cos(w\Delta t) \mathbb{1} - i \sin(w\Delta t) \begin{pmatrix} 0 & 1 \\ 1 & 0 \end{pmatrix}. \end{aligned} \quad (3.16)$$

This expansion is important as it allows us to write

$$\begin{cases} \psi_1(t + \Delta t) = \cos(w\Delta t)\psi_1(t) - i \sin(w\Delta t)\psi_N(t) \\ \psi_N(t + \Delta t) = \cos(w\Delta t)\psi_N(t) - i \sin(w\Delta t)\psi_1(t) \end{cases}. \quad (3.17)$$

This method enables us to efficiently diagonalise the relevant operators in momentum space, while having open boundary conditions. As we will see now, this method is easily generalised to the case of our interest.

### 3.2.2 2D lattice model with Twisted Boundary Conditions

We consider now the lattice model introduced in (3.3): the underlying dynamics is schematically represented in Fig.3.3. As for the previous case, we are facing the problem of implementing a condition at the boundary while retaining some sort of periodicity to ensure we can diagonalise in momentum space. As per what found in Sec. (1.5), one can promptly realise that in the Landau gauge we have standard boundary conditions along the  $y$ -direction and twisted boundary conditions along the  $x$ -direction. In particular the twisting phases are

$$\begin{aligned} \Theta_x &= \frac{2\Omega my L_x}{\hbar}, \\ \Theta_y &= 0, \end{aligned} \quad (3.18)$$

and the boundary conditions read

$$\begin{aligned}\psi(x, y) &= e^{-i\Theta_x}\psi(x + L_x, y), \\ \psi(x, y) &= e^{-i\Theta_y}\psi(x, y + L_y).\end{aligned}\tag{3.19}$$

Similarly we can write the expression for the discrete twisted boundary conditions as

$$\begin{aligned}\psi_{n+N_x, l} &= e^{i\Theta_x}\psi_{n, l}, \\ \psi_{n, l+N_y} &= e^{i\Theta_y}\psi_{n, l}.\end{aligned}\tag{3.20}$$

This time we will take into consideration different hopping in the two different directions from the start. Since the interaction term plays no role in the current discussion it will be disregarded and reintroduced when needed. As we will see the twisted boundary conditions can be applied by performing a transformation on the appropriate set of terms. Let us continue for the moment our considerations on the system with PBC.

Let us split the energy functional (3.7) as

$$E_d = E_x + E_y + \sum_{n, l} \frac{\mathcal{U}}{2} |\psi_{n, l}|^4,\tag{3.21}$$

where

$$\begin{aligned}E_x &= -w_x \sum_{n, l} [\psi_{n+1, l}^* \psi_{n, l} + \text{c.c.}] + 2w_x \mathcal{N}, \\ E_y &= -w_y \sum_{n, l} [e^{i\theta_y} \psi_{n, l+1}^* \psi_{n, l} + \text{c.c.}] + 2w_y \mathcal{N}.\end{aligned}\tag{3.22}$$

Since in the Landau gauge the boundary condition along the  $y$ -direction is a simple periodic boundary condition ( $\Theta_y = 0$ ), the terms in  $E_y$  can be promptly diagonalised. Let us then consider the term  $E_x$ . This can be broken

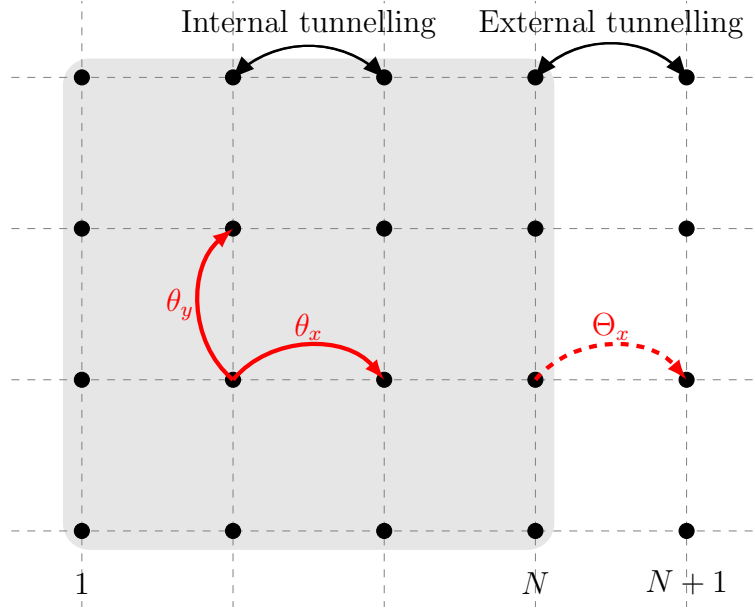


Figure 3.3: Schematic dynamics on the 2D system in the Landau gauge. A particle tunnelling acquires the phases  $\theta_x$  and  $\theta_y$  given in (3.2). For a system respecting periodic boundary conditions one has  $\psi_{N+1} \equiv \psi_1$ . On the other hand, a system respecting twisted boundary conditions has  $\psi_{N+1} \equiv e^{i\Theta_x}\psi_1$ , where the twisting phase is as given in (3.18).

into two parts as it follows:

$$E_x = -w_x \sum_{l=1}^{N_y} \left[ \underbrace{\sum_{n=1}^{N_x-1} (\psi_{n+1,l}^* \psi_{n,l} + \text{c.c.})}_{\text{internal tunnelling}} - \underbrace{(\psi_{N_x,l}^* \psi_{N_x+1,l} + \psi_{N_x+1,l}^* \psi_{N_x,l})}_{\text{external tunnelling}} \right]. \quad (3.23)$$

We can then proceed, as we have done in the preceding Sec. 3.2.1, by adding

and subtracting the term  $w_x(\psi_{N_x,l}^*\psi_{1,l} + \text{c.c.})$ , and find

$$E_x = -w_x \sum_{l=1}^{N_y} \left[ \sum_{n=1}^{N_x} (\psi_{n+1,l}^*\psi_{n,l} + \text{c.c.}) - (\psi_{N_x,l}^*\psi_{N_x+1,l} - \psi_{N_x,l}^*\psi_{1,l} + \text{c.c.}) \right]. \quad (3.24)$$

Once again, the first term in the above expression can now be straightforwardly diagonalised. On the other hand, applying the twisted boundary conditions (3.20) to the second boundary term we find

$$(\psi_{N_x,l}^*\psi_{N_x+1,l} - \psi_{N_x,l}^*\psi_{1,l} + \text{c.c.}) = \begin{pmatrix} \psi_{1,l} \\ \psi_{N_x,l} \end{pmatrix}^\dagger \begin{pmatrix} 0 & e^{-i\Theta_x} - 1 \\ e^{i\Theta_x} - 1 & 0 \end{pmatrix} \begin{pmatrix} \psi_{1,l} \\ \psi_{N_x,l} \end{pmatrix}. \quad (3.25)$$

Therefore, the second term in  $E_x$  leads to the following propagator:

$$\mathcal{P}(1; N_x) = \exp \left[ -iw_x \begin{pmatrix} 0 & (e^{-i\Theta_x} - 1) \\ (e^{i\Theta_x} - 1) & 0 \end{pmatrix} t \right]. \quad (3.26)$$

Notice that, upon the introduction of  $z = e^{i\Theta_x} - 1$ , the previous can be written as

$$\mathcal{P}(1; N_x) = \exp \left[ -iw_x |z| \underbrace{\begin{pmatrix} 0 & z^*/|z| \\ z/|z| & 0 \end{pmatrix}}_{\mathcal{M}} t \right] = \exp[-iw_x |z| \mathcal{M} t]. \quad (3.27)$$

Now matrix  $\mathcal{M}$  has the nice following properties

$$\text{Tr}(\mathcal{M}) = 0, \quad \det(\mathcal{M}) = -1 \quad (3.28)$$

which allow us to infer that its eigenvalues are  $\lambda_{1,2} = \pm 1$ . Moreover,  $\mathcal{M}$  is



Hermitian ( $\mathcal{M}^\dagger = \mathcal{M}$ ): the spectral theorem tells us then that  $\mathcal{M}$  is diagonalised by a unitary operator  $\mathcal{U}$ ; with this information we can proceed as follows:

$$\begin{aligned}
\mathcal{P}(1; N_x) &= \mathcal{U}^\dagger \mathcal{U} \exp[-i w_x |z| \mathcal{M} t] \mathcal{U}^\dagger \mathcal{U} \\
&= \mathcal{U}^\dagger \exp \left[ -i w_x |z| \begin{pmatrix} 1 & 0 \\ 0 & -1 \end{pmatrix} t \right] \mathcal{U} \\
&= \mathcal{U}^\dagger \left[ \cos(w_x |z| t) \mathbb{1} - i \sin(w_x |z| t) \begin{pmatrix} 1 & 0 \\ 0 & -1 \end{pmatrix} \right] \mathcal{U} \\
&= \cos(w_x |z| t) \mathcal{U}^\dagger \mathbb{1} \mathcal{U} - i \sin(w_x |z| t) \mathcal{U}^\dagger \begin{pmatrix} 1 & 0 \\ 0 & -1 \end{pmatrix} \mathcal{U} \\
&= \cos(w_x |z| t) \mathbb{1} - i \sin(w_x |z| t) \begin{pmatrix} 0 & z^*/|z| \\ z/|z| & 0 \end{pmatrix}.
\end{aligned} \tag{3.29}$$

This result allows us to find the following expression for the enforcing of the twisted boundary conditions:

$$\begin{cases} \psi_{1,l}(t + \Delta t) = \cos(w_x \Delta t |z|) \psi_{1,l}(t) - i \sin(w_x \Delta t |z|) \frac{z^*}{|z|} \psi_{N_x,l}(t) \\ \psi_{N_x,l}(t + \Delta t) = \cos(w_x \Delta t |z|) \psi_{N_x,l}(t) - i \sin(w_x \Delta t |z|) \frac{z}{|z|} \psi_{1,l}(t) \end{cases}. \tag{3.30}$$

### 3.3 The Magnetic Fourier Transform

The procedure (3.30) we have just described to enforce the twisted boundary conditions, turns out not to be the most natural way to go, nor a particularly efficient one. We will now show that a more natural approach exists and a more efficient one as well. In order to do that, we will go back to the continuum, and subsequently translate the results back onto the lattice.

The conventional Fourier transform allows us to expand the wave function  $\psi$  in a basis of functions which are eigenstates of the canonical momentum operators and which satisfy periodic boundary conditions. We would like

then to generalise this approach to our system; here we will expand in terms of eigenfunctions of the generators of magnetic translation and require the twisted boundary conditions to be satisfied. Let us consider once again then, the generators (1.117), in the continuum:

$$\begin{aligned}\Pi_x &= p_x - 2\Omega my - \partial_x \lambda, \\ \Pi_y &= p_y - \partial_y \lambda,\end{aligned}\tag{3.31}$$

in a general gauge. It is straightforward to see that these operators have eigenfunctions of the form  $e^{ik_x x} e^{i2\Omega mxy/\hbar} e^{i\lambda/\hbar} f(y)$  and  $e^{ik_y y/\hbar} e^{i\lambda/\hbar} g(x)$  respectively, with eigenvalues  $\hbar k_j$ , for some arbitrary function  $f$  of the  $y$ -coordinate, and  $g$  arbitrary function of the  $x$ -coordinate. Indeed, writing the eigenfunctions as

$$\begin{aligned}\Pi_x |k_x\rangle &= \hbar k_x |k_x\rangle, \\ \Pi_y |k_y\rangle &= \hbar k_y |k_y\rangle,\end{aligned}\tag{3.32}$$

we can proceed by looking at the transformation elements between the coordinate and momentum representations:

$$\begin{aligned}\langle x | \Pi_x | k_x \rangle &= \hbar k_x \langle x | k_x \rangle, \\ \langle x | \Pi_x | k_x \rangle &= (-i\hbar\partial_x - 2\Omega my - \partial_x \lambda) \langle x | k_x \rangle,\end{aligned}\tag{3.33}$$

where we have acted with the operator  $\Pi_x$  first on the right and then on the left. Equating the last two equations we find the ODE

$$-i\hbar\partial_x \langle x | k_x \rangle = (\hbar k_x + 2\Omega my + \partial_x \lambda) \langle x | k_x \rangle,\tag{3.34}$$

with solution

$$\begin{aligned}\langle x | k_x \rangle &= f(y) \exp \left[ \int \left( ik_x + \frac{i}{\hbar} 2\Omega m y + \frac{i}{\hbar} \partial_x \lambda \right) dx \right] \\ &= \exp \left[ ik_x x + \frac{i}{\hbar} 2\Omega m x y + \frac{i}{\hbar} \lambda \right] f(y),\end{aligned}\quad (3.35)$$

leading to the eigenfunction given above. One can proceed similarly to find the eigenfunction of  $\Pi_y$ . Then, one can make use of the identity operators

$$\mathbb{1} = \int_{-\infty}^{\infty} |k_j\rangle \langle k_j| dk_j, \quad (3.36)$$

(since the set  $|k_j\rangle$  is an orthonormal basis of the Hilbert space), to write an expression in the position basis as

$$|x\rangle = \int_{-\infty}^{\infty} |k_j\rangle \langle k_j | x \rangle dk_j. \quad (3.37)$$

This allows for the wavefunctions to be expanded as

$$\begin{aligned}\psi(x, y) &= \frac{1}{\sqrt{2\pi}} \int_{-\infty}^{\infty} e^{i[k_x x + \frac{1}{\hbar} 2\Omega m x y + \frac{1}{\hbar} \lambda]} \tilde{\psi}(k_x, y) dk_x, \\ \psi(x, y) &= \frac{1}{\sqrt{2\pi}} \int_{-\infty}^{\infty} e^{i[k_y y + \frac{1}{\hbar} \lambda]} \tilde{\psi}(x, k_y) dk_y,\end{aligned}\quad (3.38)$$

and consequently, inverting these relations, we have then found a way to generalise the Fourier transform to what we call a *Magnetic Fourier Transforms* (MFT):

$$\begin{aligned}\tilde{\psi}(k_x, y) &= \frac{1}{\sqrt{2\pi}} \int_{-\infty}^{\infty} e^{-i[k_x x + \frac{1}{\hbar} 2\Omega m x y + \frac{1}{\hbar} \lambda]} \psi(x, y) dx, \\ \tilde{\psi}(x, k_y) &= \frac{1}{\sqrt{2\pi}} \int_{-\infty}^{\infty} e^{-i[k_y y + \frac{1}{\hbar} \lambda]} \psi(x, y) dy.\end{aligned}\quad (3.39)$$

The MFT amounts to a standard Fourier transform plus an additional gauge

dependent phase factor  $Q$ : this allows to easily implement the MFT by means of standard *fft* packages. It is also straightforward to check that the normalisation factors of the Fourier Transform and MFT are the same: indeed

$$\begin{aligned}\mathcal{MFT}[\psi(x, y)] &= \mathcal{F}[e^{iQ}\psi(x, y)], \\ e^{-iQ}\mathcal{F}^{-1}[\mathcal{MFT}[\psi(x, y)]] &= \psi(x, y), \\ e^{-iQ}\mathcal{F}^{-1}[\mathcal{F}[e^{iQ}\psi(x, y)]] &= \psi(x, y).\end{aligned}\tag{3.40}$$

For the same reason it is also straightforward to see that Parseval's theorem<sup>1</sup> holds for the MFT.

If we now restrict our discussion, as done in the previous section, on a finite square domain  $L_x \times L_y$ , then the momenta become quantised in multiples of  $2\pi/L_j$ , the MFTs become

$$\begin{aligned}\tilde{\psi}(k_x, y) &= \frac{1}{\sqrt{L_x}} \int_0^{L_x} dx e^{-i[k_x x + \frac{2\Omega m}{\hbar} xy + \frac{1}{\hbar} \lambda(x, y)]} \psi(x, y), \\ \tilde{\psi}(x, k_y) &= \frac{1}{\sqrt{L_y}} \int_0^{L_y} dy e^{-i[k_y y + \frac{1}{\hbar} \lambda(x, y)]} \psi(x, y),\end{aligned}\tag{3.41}$$

and the corresponding inverses

$$\begin{aligned}\psi(x, y) &= \frac{1}{\sqrt{L_x}} \sum_{k_x} e^{i[k_x x + \frac{2\Omega m}{\hbar} xy + \frac{1}{\hbar} \lambda(x, y)]} \tilde{\psi}(k_x, y), \\ \psi(x, y) &= \frac{1}{\sqrt{L_y}} \sum_{k_y} e^{i[k_y y + \frac{1}{\hbar} \lambda(x, y)]} \tilde{\psi}(x, k_y).\end{aligned}\tag{3.42}$$

The MFT we have just described naturally incorporates the twisted boundary conditions which must be satisfied by the system. We will now complete the building up of our model, started in the preceding section, employing the MFT and showing how it diagonalises the relevant terms in the Hamiltonian.

---

<sup>1</sup>  $\int_{-\infty}^{\infty} f(x)g^*(x) dx = \int_{-\infty}^{\infty} \tilde{f}(k)\tilde{g}^*(k) dk.$

### 3.4 The Discrete Model

Let us now go back to the expression for the discrete energy (3.7), which presented in a general gauge reads

$$E_d = E_x + E_y + E_{\text{int}}, \quad (3.43)$$

with

$$\begin{aligned} E_x &= -w_x \sum_{n,l} [e^{-i\theta_x} \psi_{n,l}^* \psi_{n+1,l} + \text{c.c.}] + 2w_x \mathcal{N}, \\ E_y &= -w_y \sum_{n,l} [e^{-i\theta_y} \psi_{n,l}^* \psi_{n,l+1} + \text{c.c.}] + 2w_y \mathcal{N}, \\ E_{\text{int}} &= \sum_{n,l} \frac{\mathcal{U}}{2} |\psi_{n,l}|^4, \end{aligned} \quad (3.44)$$

which is, as we mentioned, accurate to second order in the spatial discretisation:  $E - E_d = \mathcal{O}(a_x^2) + \mathcal{O}(a_y^2)$ . Introducing a discrete expression for the pure gauge as  $\lambda_{n,l} = \lambda(a_x n, a_y l)/\hbar$ , and also, for simplicity, the dimensionless quantity  $\mathcal{B} = 2\Omega m a_x a_y / \hbar$ , one finds from (3.2), that in a general gauge the expression for the tunnelling phases are given by

$$\begin{aligned} \theta_x &= \lambda_{n+1,l} - \lambda_{n,l}, \\ \theta_y &= \mathcal{B}n + \lambda_{n,l+1} - \lambda_{n,l}. \end{aligned} \quad (3.45)$$

We can write the *discrete Magnetic Fourier Transform* (dMFT) as

$$\begin{aligned} \tilde{\psi}_{k_x,l} &= \frac{1}{\sqrt{N_x}} \sum_n e^{-i[k_x n + \mathcal{B}n l + \lambda_{n,l}]} \psi_{n,l}, \\ \tilde{\psi}_{n,k_y} &= \frac{1}{\sqrt{N_y}} \sum_l e^{-i[k_y l + \lambda_{n,l}]} \psi_{n,l}, \end{aligned} \quad (3.46)$$

and the respective inverses as

$$\begin{aligned}\psi_{n,l} &= \frac{1}{\sqrt{N_x}} \sum_{k_x} e^{i[k_x n + \mathcal{B}nl + \lambda_{n,l}]} \tilde{\psi}_{k_x,l}, \\ \psi_{n,l} &= \frac{1}{\sqrt{N_y}} \sum_{k_y} e^{i[k_y l + \lambda_{n,l}]} \tilde{\psi}_{n,k_y}.\end{aligned}\tag{3.47}$$

We are now ready to consider the action of the dmFT on the energy functional (3.43). Consider the term entering  $E_x$ :

$$\begin{aligned}& (e^{-i\theta_x} \psi_{n,l}^* \psi_{n+1,l} + \text{c.c.}) = \\ &= \frac{e^{-i\theta_x}}{N_x} \left[ \left( \sum_{k_x} e^{-i[k_x n + \mathcal{B}nl + \lambda_{n,l}]} \tilde{\psi}_{k_x,l}^* \right) \cdot \left( \sum_{k_x} e^{i[k_x(n+1) + \mathcal{B}(n+1)l + \lambda_{n+1,l}]} \tilde{\psi}_{k_x,l} \right) \right] + \text{c.c.} \\ &= \frac{e^{-i\theta_x} e^{i(\mathcal{B}l + \lambda_{n+1,l} - \lambda_{n,l})}}{N_x} \left[ \sum_{k_x} \sum_{k'_x} e^{-ik'_x n} \tilde{\psi}_{k'_x,l}^* e^{ik_x(n+1)} \tilde{\psi}_{k_x,l} \right] + \text{c.c.} \\ &= \frac{e^{i\mathcal{B}l}}{N_x} \left[ \sum_{k_x} e^{-ik_x} \left| \tilde{\psi}_{k_x,l} \right|^2 \right] + \text{c.c.} \\ &= \frac{1}{N_x} \sum_{k_x} (e^{i(k_x + \mathcal{B}l)} + e^{-i(k_x + \mathcal{B}l)}) \left| \tilde{\psi}_{k_x,l} \right|^2 \\ &= \frac{2}{N_x} \sum_{k_x} \cos(k_x + \mathcal{B}l) \left| \tilde{\psi}_{k_x,l} \right|^2.\end{aligned}\tag{3.48}$$

Similarly, one can consider the term entering  $E_y$ , and find

$$\begin{aligned}
& (e^{-i\theta_y} \psi_{n,l}^* \psi_{n,l+1} + \text{c.c.}) = \\
& = \frac{e^{-i\theta_y}}{N_y} \left[ \left( \sum_{k_y} e^{-i[k_y l + \lambda_{n,l}]} \tilde{\psi}_{n,k_y}^* \right) \cdot \left( \sum_{k_y} e^{i[k_y(l+1) + \lambda_{n,l+1}]} \tilde{\psi}_{n,k_y} \right) \right] + \text{c.c.} \\
& = \frac{e^{-i\theta_y} e^{i(\lambda_{n,l+1} - \lambda_{n,l})}}{N_y} \left[ \sum_{k_y} \sum_{k'_y} e^{-ik'_y l} \tilde{\psi}_{n,k'_y}^* e^{ik_y(l+1)} \tilde{\psi}_{n,k_y} \right] + \text{c.c.} \\
& = \frac{e^{-i\mathcal{B}n}}{N_y} \left[ \sum_{k_y} e^{ik_y} \left| \tilde{\psi}_{n,k_y} \right|^2 \right] + \text{c.c.} \\
& = \frac{1}{N_y} \sum_{k_y} (e^{i(k_y - \mathcal{B}n)} + e^{-i(k_y - \mathcal{B}n)}) \left| \tilde{\psi}_{n,k_y} \right|^2 \\
& = \frac{2}{N_y} \sum_{k_y} \cos(k_y - \mathcal{B}n) \left| \tilde{\psi}_{n,k_y} \right|^2.
\end{aligned} \tag{3.49}$$

We can therefore write for the energy components  $E_x$  and  $E_y$ :

$$\begin{aligned}
E_x &= -2w_x \sum_l \sum_{k_x} \cos(k_x + \mathcal{B}l) \left| \tilde{\psi}_{k_x,l} \right|^2 + 2w_x \mathcal{N}, \\
E_y &= -2w_y \sum_n \sum_{k_y} \cos(k_y - \mathcal{B}n) \left| \tilde{\psi}_{n,k_y} \right|^2 + 2w_y \mathcal{N}.
\end{aligned} \tag{3.50}$$

Finally, recalling the trigonometric relation  $2 \sin^2\left(\frac{x}{2}\right) = 1 - \cos(x)$ , we can incorporate the constant terms in the above expression and obtain

$$\begin{aligned}
E_x &= 4w_x \sum_{k_x,l} \sin^2\left(\frac{k_x + \mathcal{B}l}{2}\right) \left| \tilde{\psi}_{k_x,l} \right|^2, \\
E_y &= 4w_y \sum_{n,k_y} \sin^2\left(\frac{k_y - \mathcal{B}n}{2}\right) \left| \tilde{\psi}_{n,k_y} \right|^2.
\end{aligned} \tag{3.51}$$

Notice the gauge invariance of both expressions in (3.51). This form of the energy functional, in which all the three terms are diagonal in their respective spaces, allows for an easy and efficient implementation of the split-step methods described in Chapter 2.

### 3.4.1 The Split-Step Magnetic Fourier Method

The system described by the energy functional  $E_d = E_x + E_y + E_{\text{int}}$  where each term is diagonal, is particularly suited to be solved by split-step methods. Since we are interested in the ground states of such a system we will make use of the generalised second order method (2.51), consisting in the imaginary time evolution of the equations of motion associated with the energy functional  $E_d$ , once again obtainable through the Wick-rotated variational principle (3.8)  $-\hbar\partial_\tau\psi_{n,l} = \delta E_d/\delta\psi_{n,l}^*$ . The resulting wave function will be the minimiser of the energy functional  $E_d$ . As discussed in Chapter 2, the method of choice for simulations involving the real time dynamic of the system is instead the method described in equation (2.29), as proposed in [71].

Because the energy functional  $E_d$  is composed of three pieces, the splitting method (2.51) needs to be applied twice. The *split-step MFT procedure*, to advance the wave function  $\psi(\tau)$  evolving through the imaginary-time Gross-Pitaevskii equation by a single time step  $\Delta\tau$ , then proceeds with the following computations:

1.  $\psi_1 = e^{-H_{\text{int}}(\rho_a)\frac{\Delta\tau}{2\hbar}}\psi(\tau)$
2.  $\psi_2 = \mathcal{MFT}_x^{-1}\left[e^{-H_x\frac{\Delta\tau}{2\hbar}}\mathcal{MFT}_x[\psi_1]\right]$
3.  $\psi_3 = \mathcal{MFT}_y^{-1}\left[e^{-H_y\frac{\Delta\tau}{\hbar}}\mathcal{MFT}_y[\psi_2]\right]$
4.  $\psi_4 = \mathcal{MFT}_x^{-1}\left[e^{-H_x\frac{\Delta\tau}{2\hbar}}\mathcal{MFT}_x[\psi_3]\right]$
5.  $\psi(\tau + \Delta\tau) = e^{-H_{\text{int}}(\rho_b)\frac{\Delta\tau}{2\hbar}}\psi_4$

where  $\mathcal{MFT}_x$  and  $\mathcal{MFT}_y$  are the operations defined in (3.46). The quantities in the exponents directly follow from (3.44) and (3.51). In particu-



lar,  $H_x = 4w_x \sin^2\left(\frac{k_x + Bl}{2}\right)$ ,  $H_y = 4w_y \sin^2\left(\frac{k_y - Bn}{2}\right)$ , and  $H_{\text{int}}(\rho) = \mathcal{U}\rho$ . As discussed in Chapter 2, for certain choices of the densities  $\rho_a$  and  $\rho_b$  (e.g. putting  $\rho_a = \rho_b = |\psi(\tau)|^2$  or even  $\rho_a = |\psi(\tau)|^2$  and  $\rho_b = |\psi_4|^2$ ), the method will lose its second-order accuracy. Instead, one finds that with the choices

$$\rho_a = |e^{-H_{\text{int}}(|\psi(\tau)|^2) \frac{\Delta\tau}{2\hbar}} \psi(\tau)|^2, \quad \rho_b = |\psi_4|^2, \quad (3.52)$$

the method will be second-order accurate. Additionally, as considered in Chapter 2, at the end of each time-step propagation, the resulting wavefunction should be normalised.

Note that the extension of the split-step method from linear to non-linear equations, as done above, is of small influence on the computational time. For instance, if we put  $g = 0$  making the Gross-Pitaevskii equation linear, the computational cost of the split-step method at leading order will not be affected. The MFT can be implemented in a straightforward way by using existing fast Fourier transform packages as it can be written in terms of direct multiplications and Fourier transforms as:

$$\mathcal{MFT}_x[\psi] = \mathcal{F}_x [e^{-iBnl} e^{-i\lambda_{n,l}} \psi] \quad (3.53)$$

$$\mathcal{MFT}_y[\psi] = \mathcal{F}_y [e^{-i\lambda_{n,l}} \psi] \quad (3.54)$$

where  $\mathcal{F}_x$  and  $\mathcal{F}_y$  denote the standard Fourier transforms. Thus the MFT algorithm is as fast as the conventional fast Fourier transform to leading order. More specifically, for  $N$  discretisation points, the method has  $N \log N$  computational cost.

### 3.4.2 Dynamical variation of the aspect ratio

Thusfar we have neglected the discussion on the anisotropic tunnelling amplitudes  $w_x$  and  $w_y$  introduced in (3.3). As discussed in Chapter 1, the ground state solution of a homogeneous rotating superfluid consists of a triangular

lattice of vortices carrying quantised circulation. The unit cell describing a triangular lattice necessarily has an irrational aspect ratio. Hence, the introduction of the anisotropic tunnelling amplitudes was foresightedly made necessary by the need to account for irrational aspect ratios. In fact, we can relate the anisotropic tunnelling amplitudes to the aspect ratio of the computational unit cell as  $\mathcal{R} = \frac{L_y}{L_x} = \frac{N_y}{N_x} \sqrt{\frac{w_x}{w_y}}$ . In order for the discrete theory to accurately describe the continuum theory, the discretisation lattice constants,  $a_x$  and  $a_y$ , must be the smallest length scales in the problem. Specifically, we require  $a_x, a_y \ll \xi, \ell_\Omega$ . On the other hand, we note that the discrete theory remains well-defined and physically relevant away from this limit.

With this in mind, assuming  $N_x = N_y$ , we can once again re-formulate the energy functional as

$$E_d[\psi_{n,l}, \mathcal{R}] = 4\sqrt{w_x w_y} \left( \mathcal{R} \sum_{k_x, l} \sin^2 \left( \frac{k_x + \mathcal{B}l}{2} \right) \left| \tilde{\psi}_{k_x, l} \right|^2 + \frac{1}{\mathcal{R}} \sum_{n, k_y} \sin^2 \left( \frac{k_y - \mathcal{B}n}{2} \right) \left| \tilde{\psi}_{n, k_y} \right|^2 \right) + \sum_{n, l} \frac{\mathcal{U}}{2} |\psi_{n, l}|^4. \quad (3.55)$$

The energy functional  $E_d$  can be directly minimised with respect to  $\mathcal{R}$  as

$$\frac{d\mathcal{R}}{d\tau} = \frac{dE_d}{d\mathcal{R}} = 0, \quad (3.56)$$

and the minimiser found is

$$\mathcal{R} = \sqrt{\frac{\sum_{n, k_y} \sin^2 \left( \frac{k_y - \mathcal{B}n}{2} \right) \left| \tilde{\psi}_{n, k_y} \right|^2}{\sum_{k_x, l} \sin^2 \left( \frac{k_x + \mathcal{B}l}{2} \right) \left| \tilde{\psi}_{k_x, l} \right|^2}}. \quad (3.57)$$

Notice this implies that the total energy is minimised when  $E_x = E_y$ . Then, at the end of each time-step advancement in the split-step procedure, we

can vary dynamically the aspect ratio of the computational unit cell by enforcing (3.57). In the long imaginary time limit, the wave function and the aspect ratio will both converge to the true minimisers of the energy functional  $E_d[\psi_{n,l}, \mathcal{R}]$ .

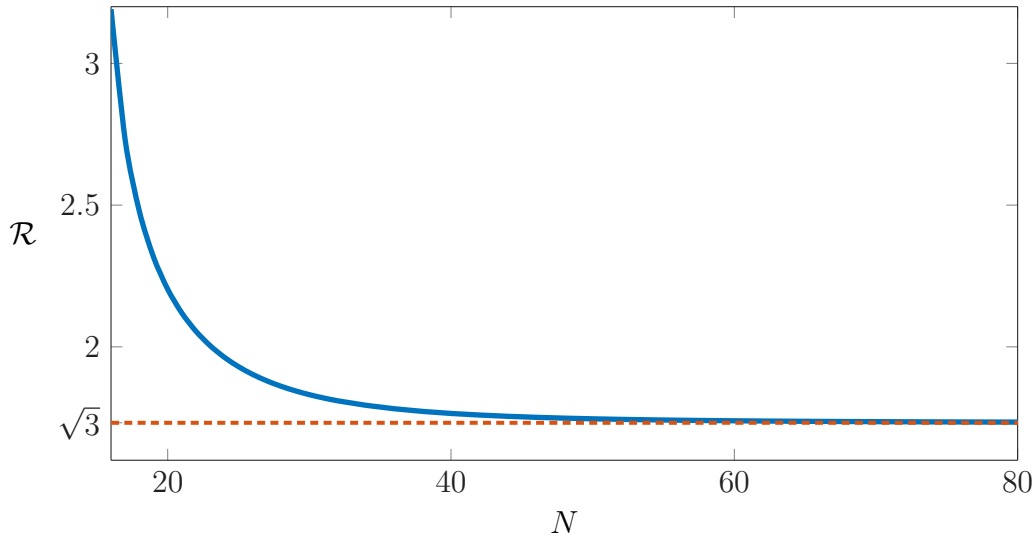


Figure 3.4: Convergence of the lattice model aspect ratio to the continuum value  $\mathcal{R} = \sqrt{3}$  for increasing number of computational points  $N = N_x N_y$ . The simulation considers a periodic unit cell containing two vortices.

The minimiser  $\mathcal{R}$  of the lattice energy functional, is therefore going to be exact for the given wave function. However, this is going to be just an approximation to the true continuum minimiser. More specifically, the accuracy is going to be a function of the number of computational points (or equivalently the size of the lattice discretisation constant). In Fig. 3.4 we considered an infinite triangular lattice with two vortices per unit cell. The true minimiser in the continuum limit is  $\mathcal{R} = \sqrt{3}$ : Fig. 3.4 shows the lattice minimiser quickly converges to this value.

### 3.5 Numerical Tests

In this Section, we will provide some preliminary applications of the split-step magnetic Fourier method, showing how it can reproduce known results in appropriate regimes and also how these results can be extended. We start by considering the lowest lowest-Landau-level regime, since this case has several known results with which we can compare.

To characterise vortex lattices, following [72], it is helpful to introduce the dimensionless *inhomogeneity parameter*

$$\beta = A \frac{\int |\psi|^4 dx dy}{\left(\int |\psi|^2 dx dy\right)^2}, \quad (3.58)$$

where  $A = L_x L_y$  is the area of the computational unit cell. This dimensionless parameter depends only on the geometry of the system, i.e. on the geometry of the vortex lattice. Moreover, it is of particular interest because it can be directly related to the interaction energy of the system as  $\frac{g}{2}\beta\frac{\mathcal{N}^2}{A}$ , with  $\mathcal{N} = \int |\psi|^2 dx dy$ . In the LLL regime the remaining terms in the energy are quenched, thus minimising the energy is equivalent to minimising  $\beta$ . When the number of vortices is restricted to two per computational unit cell, one can compute  $\beta$  analytically as a function of the aspect ratio  $\mathcal{R}$  [36]

$$\beta^A(\mathcal{R}) = \sqrt{\frac{\mathcal{R}}{2}} (f_0^2 + 2f_0 f_1 - f_1^2), \quad (3.59)$$

with

$$f_n = \sum_{m=-\infty}^{\infty} e^{-\pi\mathcal{R}(2m+n)^2/2}, \quad (3.60)$$

where the vortices are placed within the unit cell so as to maximise the separation between neighbouring vortices. A depiction of equation (3.59) can be found in Fig. 3.5. The minima correspond to the aspect ratios

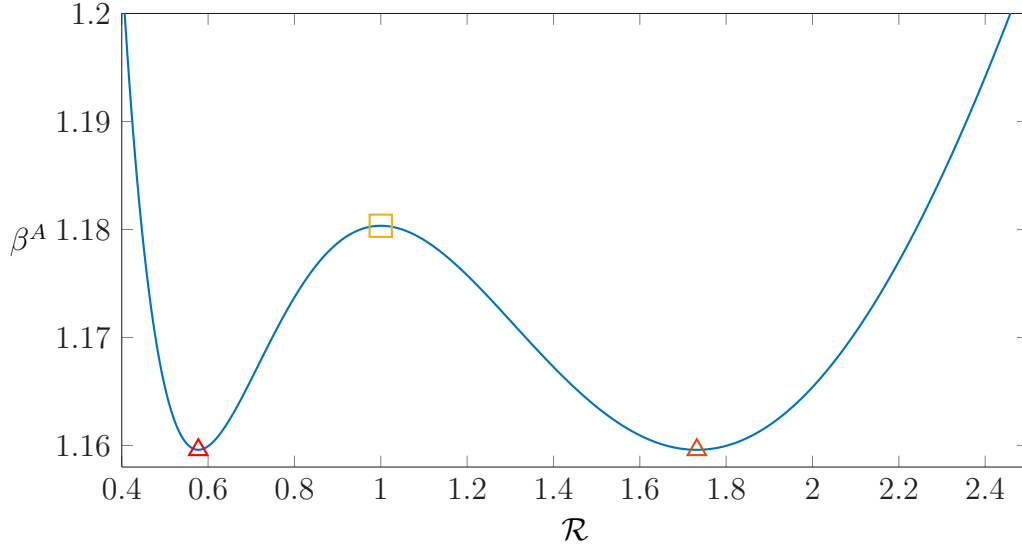


Figure 3.5: Plot of the inhomogeneity parameter defined in equation (3.59). The stationary points corresponding to triangular and square lattices are labelled.

$\mathcal{R}_\Delta = \{3^{\frac{1}{2}}, 3^{-\frac{1}{2}}\}$ , where one finds triangular lattices, while the local maximum has aspect ratio  $\mathcal{R}_\square = 1$  corresponding to a square lattice. The corresponding values of  $\beta^A$  are reported in the following Table 3.1.

$\beta_\Delta^A = 1.159595$
$\beta_\square^A = 1.180341$

Table 3.1: Minimum and local maximum of the inhomogeneity parameter  $\beta^A$  corresponding to triangular and square lattices respectively.

Recall that a unit cell commensurate with that of the ground state vortex lattice of infinite spatial extent must be chosen to obtain the ground state energy. Unit cell sizes differing from this will introduce frustration. Therefore  $\beta$  should be minimised with respect to  $\mathcal{R}$ . One expects minima to occur at aspect ratios which are commensurate with a triangular vortex lattice [36, 115]. Since  $\beta(\mathcal{R}) = \beta(\mathcal{R}^{-1})^2$ , in the following we will restrict our attention

<sup>2</sup>This can be proved by realising that  $f_0(\mathcal{R}) + f_1(\mathcal{R}) = f_0(\mathcal{R}/4)$  and that

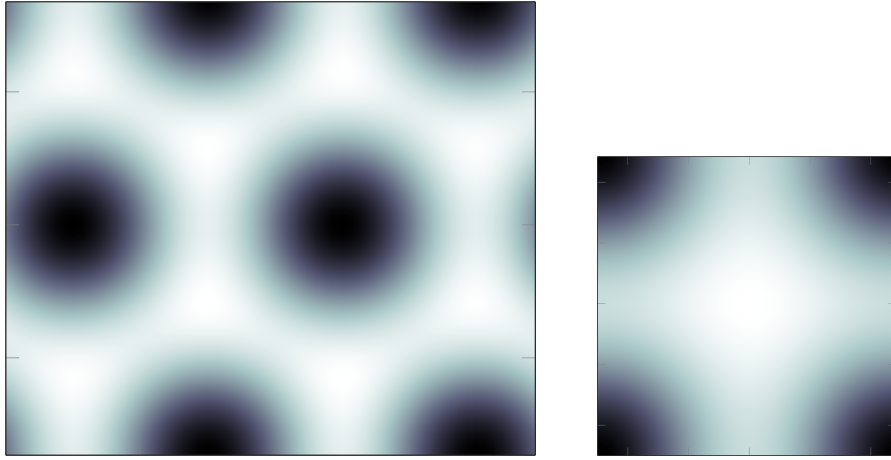


Figure 3.6: Numerical solutions for  $N_v = 4$  and  $N_v = 1$  leading to triangular and square lattices. The aspect ratios are  $R = 2/\sqrt{3}$  and  $R = 1$  respectively.

to  $\mathcal{R} \geq 1$ .

We now turn to numerically computing  $\beta$  using the split-step magnetic Fourier method. For fixed values of  $\mathcal{R}$  and  $\ell_\Omega/\xi$ , starting with an initial randomised state, the imaginary-time GPE is evolved on a  $256 \times 256$  grid until a time-independent state is obtained. Convergence as a function of the time step  $\Delta\tau$  is also checked. In Fig. 3.7, several curves of  $\beta$  versus the aspect ratio  $\mathcal{R}$  are shown for different values of  $\ell_\Omega/\xi$  for systems containing two vortices per computational unit cell. In the limit  $\ell_\Omega \ll \xi$  one finds excellent agreement with the LLL analytical expression  $\beta^A$  as expected. The scheme naturally allows one to extend beyond the LLL regime for which simple analytical expressions for  $\beta$  are not available. As  $\ell_\Omega/\xi$  is increased, one finds that  $\beta$  decreases, reflecting the system's tendency towards a nearly uniform density (apart from the vortex cores) in the large interaction limit. Also, as expected, the minimum for all curves occurs at  $\mathcal{R} = \sqrt{3}$ , which is commensurate with the triangular vortex lattice. A local maximum occurs

---

$f_0(\mathcal{R}) = \sqrt{\frac{1}{2\mathcal{R}}} f_0\left(\frac{1}{4\mathcal{R}}\right)$ . The first expression can be shown by expanding the series telescopically, while the second follows directly from the Poisson summation formula. Plugging these two into (3.59) one obtains that  $\beta(\mathcal{R}) = \beta(\mathcal{R}^{-1})$ .

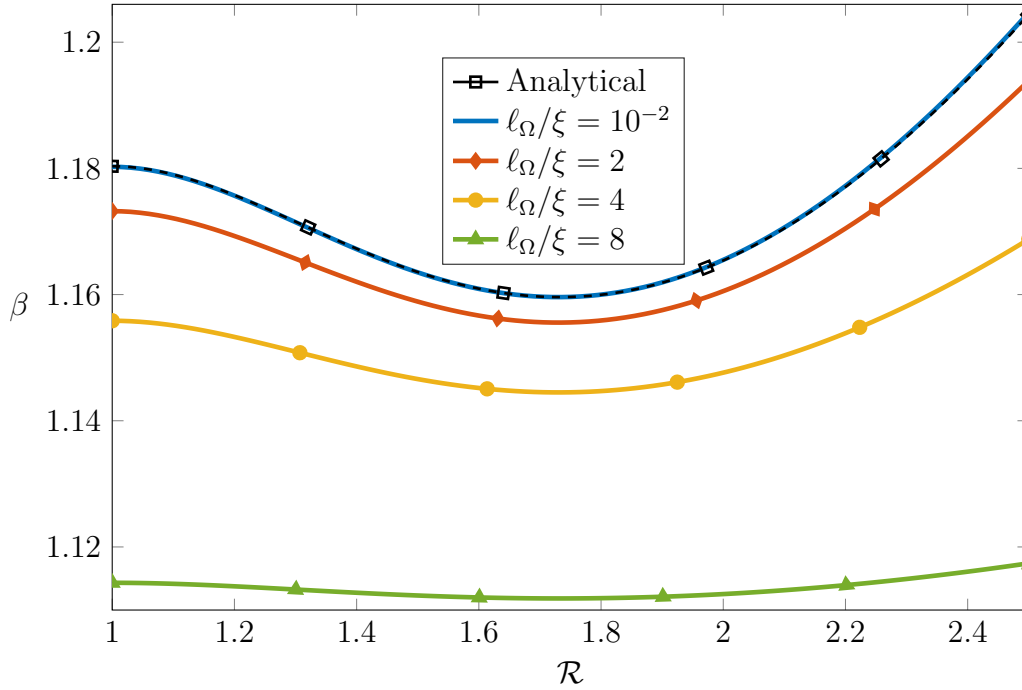


Figure 3.7: Numerical results of the dimensionless inhomogeneity parameter  $\beta$  (3.58) characterising the interaction energy of the system as a function of the aspect ratio of the computational unit cell. Excellent agreement is found between the numerical results and the analytical expression  $\beta^A$  in the lowest Landau level regime.

at  $\mathcal{R} = 1$  which corresponds to the square vortex lattice.

Because the energy of the system is an extensive quantity, one might expect the energy per particle,  $\tilde{E} \equiv \frac{E}{N}$ , to be unchanged when the size of the computational cell is increased *ceteris paribus*. This is only true, however, for computational unit cells commensurate with the ground state vortex configuration as increasing the size of the cell while keeping the vortex density fixed allows the system to have more degrees of freedom. In the following, we consider doubling the spatial dimensions of the computational unit cell from one containing two vortices to one containing eight vortices. From general principles one will have  $\tilde{E}_8 \leq \tilde{E}_2$  where  $\tilde{E}_8$  and  $\tilde{E}_2$  are the

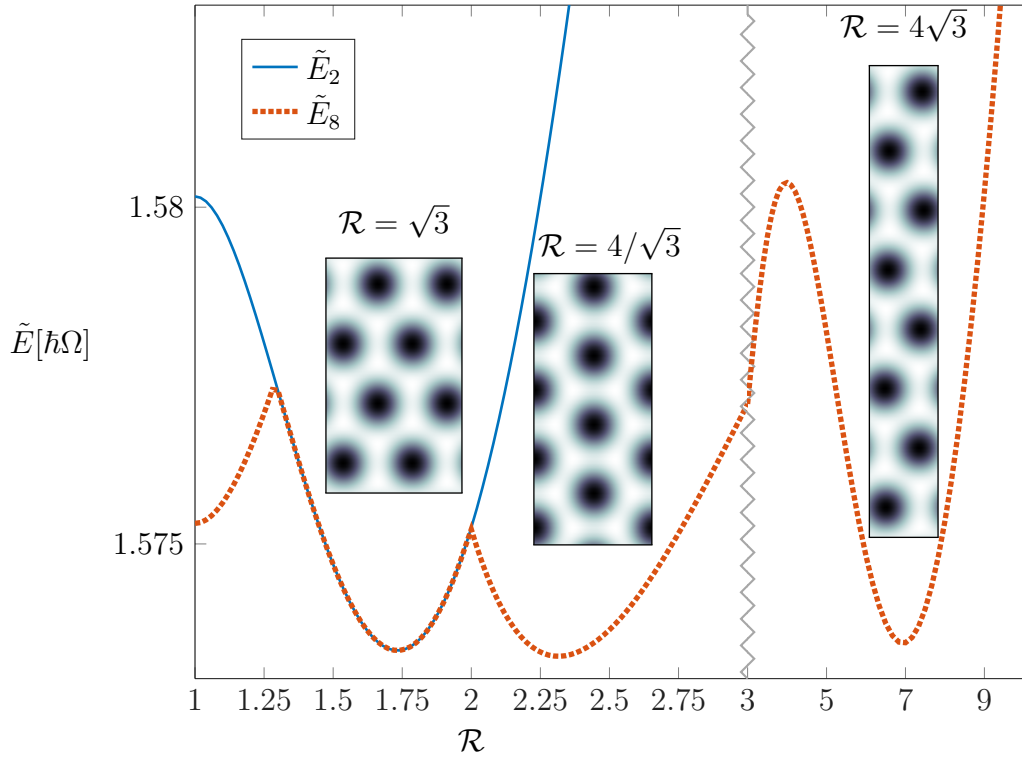


Figure 3.8: The energy per particle of systems with two and eight vortices in the computational unit cell,  $\tilde{E}_2$  and  $\tilde{E}_8$ , as a function of the ratio  $\mathcal{R}$ . The former provides an upper bound for the latter. The triangular lattices corresponding to the ground states are degenerate and the arrangements of the vortices in each of the ground states of the eight-vortex system are shown.

energies per particle of the systems with smaller and larger computational unit cells respectively.

In Fig. 3.8 the energy per particle obtained using the split-step magnetic Fourier method is shown for systems having two and eight vortices per computational unit cell. As expected, we have  $\tilde{E}_8 \leq \tilde{E}_2$  for all curves. The curves coincide near  $\mathcal{R} = \sqrt{3}$  which is commensurate with the triangular vortex lattice in both cases. The system with eight vortices can also achieve a triangular vortex lattice at aspect ratios  $\mathcal{R} = 4/\sqrt{3}, 4\sqrt{3}$  and we note that degenerate minima of  $\tilde{E}_8$  occur at these values. The computation has been



---

carried out for  $\ell_\Omega/\xi = 1$  but the same results—namely  $\tilde{E}_2$  being an upper bound for  $\tilde{E}_8$ , their equivalence close to  $\mathcal{R} = \sqrt{3}$  and the existence of the three degenerate minima for  $\tilde{E}_8$ —hold for any ratio  $\ell_\Omega/\xi$ .

## 3.6 Outlook

In conclusion, we have described a computational method which can efficiently find the minimum energy of an infinite vortex lattice within Gross-Pitaevskii mean field theory. We have shown how to extend the conventional split-step Fourier method to include twisted boundary conditions through use of the magnetic translation group. We have tested the method for particular cases, and showed that it reproduces known results in the lowest Landau level regime.

In the subsequent chapters we will consider multicomponent systems. It turns out the method we have just described requires one additional essential ingredient if one wants to use it to investigate such multicomponent systems. This is however true only in the case of repulsive inter-species interactions. Therefore a natural extension of the method can be used to investigate systems in which the inter-species interaction is attractive. Thus, in the following chapter, we will briefly study a scalar two-component system with attractive inter-species interactions, before discussing how to extend the model and investigate more complicated repulsively interacting systems in the subsequent chapters.



# Chapter 4

## Mixtures of Attractive Superfluids

In this brief Chapter, we are going to briefly consider the case of attractive interspecies interactions  $g_{12} < 0$  in a mixture of two rotating superfluids.

The response of the system under rotation in this attractive regime, is arguably more intuitive, even more so for homogeneous systems. This is possibly the reason why the problem did not receive much attention in the past years. The attractive interaction between the two species translates onto the interaction between vortices of different species, which turns out to be attractive as well. As a consequence, it is for instance simple to conclude that the ground state of such a system when the masses of the constituents of the two components are equal is going to consist of two perfectly overlapping triangular vortex lattices. However, when investigated more thoroughly, these systems can exhibit interesting and unexpected characteristics.

The method used to simulate attractive multicomponent systems is akin to the method presented in the preceding Chapter 3: one can just evolve a set of coupled equations of motions, one for each of the order parameter of each component.

## 4.1 Locking of vortices

In the early works [116, 92], the case of two condensates under rotation and within an harmonic confining potential was considered for small deviation from unity of the constituents' masses ratio  $m_2/m_1$ . Under such conditions, one would expect, from Feynman relation (1.78), to find the two components rotating at the same driving frequency  $\Omega_d$ , and therefore with unequal vortex densities. However, this turns out to be true only on average. One finds

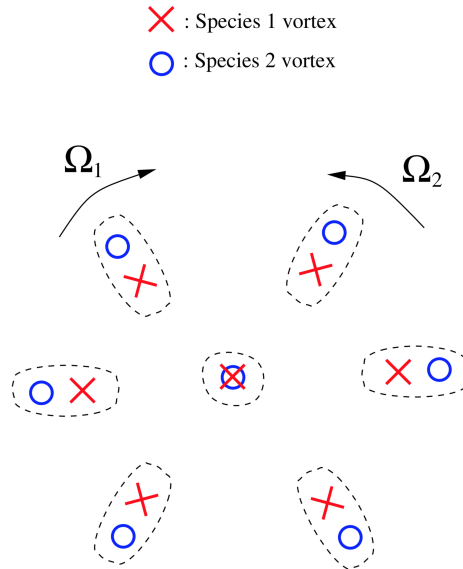


Figure 4.1: Depiction of bound vortex pairs for species with masses  $m_1 > m_2$  [116]. Within a certain locking radius  $r_c$  the vortices of the two species form bound pairs which rotate together at the driving frequency, while the two superfluids adapt their rotational rate so as to allow for equal vortex densities. Outside the disk defined by  $r_c$ , the pairs become unbound, both vortices and the superfluids rotate at the driving frequency and the two vortex densities become unequal.

instead, for large enough attractive interaction, that there exist a *locking radius*  $r_c$  within which the two components do not rotate at the driving frequency, but at angular velocities inversely proportional to their masses, so

that  $m_1\Omega_1 = m_2\Omega_2$ . The vortex densities in turn, are forced to be the same in this region. This implies that within the locking radius, the vortex lattices of the two condensates are perfectly overlapping, locked together, rotating at the driving frequency  $\Omega_d$  lying between  $\Omega_1$  and  $\Omega_2$ . Outside the disk defined by the locking radius, one finds a short healing region where pairs of vortices of the two species are paired, and eventually the two condensates will be found rotating at the same frequency and vortices of different species unbound. In particular, in this outer region, the vortex densities will be found to respect  $\rho_v^{(1)}m_2 = \rho_v^{(2)}m_1$ , as expected on average from Feynman relation (1.78). This counterintuitive result, derives from a purely quantum effect, with no analogue in classical physics.

An explanation to this phenomenon can be found in the competition between the vortices attractive force and the Magnus force<sup>1</sup>. Indeed, equating estimates obtained from gaussian ansatzs for the wave functions, it is possible to find an expression for the locking radius as

$$r_c = |g_{12}| \frac{\bar{\rho}}{4\hbar\Omega_d\sqrt{e}} \frac{m_1 + m_2}{m_1 - m_2} \xi, \quad (4.1)$$

where equal average densities  $\bar{\rho}_1 = \bar{\rho}_2 = \bar{\rho}$  and equal healing lengths  $\xi_1 = \xi_2 = \xi$  (and consequently equal interaction strengths  $g_1 = g_2 = g$ ) were assumed.

The expression for the locking radius, interestingly reveals that very quickly, for large mass ratios, this effect vanishes, exception made for the two vortices sitting at the centre of the trapping paraboloid. The effect is therefore expected to be observable especially in the range  $1 < m_1/m_2 < 2$ . This is indeed the case considered in [116] where, motivated by the experimentally relevant case of a mixture composed of the isotopes  $^{133}\text{Cs}$ - $^{87}\text{Rb}$ , it was taken the mass ratio  $m_1/m_2 = 1.5$  [117]. Lastly, it is important to notice that also for large rotational frequency  $\Omega_d$  the radius is quenched, and no such effect should be expected in the limit of vortices.

---

<sup>1</sup>Lorentz force in the charged particle in a magnetic field analogy.

## 4.2 Vortex lattice configurations

The case of two-species condensates for large rotation rates under attractive interactions was investigated in [118] for components with different constituents masses. In particular, only integer mass ratios were considered. Recalling the Feynman relation (1.78), it is clear that to different masses are going to be associated different vortex densities, if equal rotation is assumed for each components. This is certainly the case for mass ratio much larger than unity, even more so in the limit of large number of vortices and low inter-species interaction, as we have argued in the previous section.

Similarly to the case of unitary mass ratio, one finds that in general the two vortex lattices tend to arrange in a triangular configuration. As we will discuss in further detail in the last Chapter 6, such states can be achieved without frustration only for certain mass ratios: only in these cases are in fact the two lattices commensurate. Deferring the proof to Chapter 6, we now simply state that two triangular lattices with a mass ratio  $m_1/m_2 = 2$  are not commensurate. On the other hand, the mass ratios  $m_1/m_2 = 3$  and  $m_1/m_2 = 4$  do allow the corresponding triangular vortex lattices to be commensurate (deferring again the proof to the last chapter). In Fig. 4.3, a summary of some of the ground state configurations for different integer mass ratios is given. Notice in particular the configuration corresponding to the mass ratio  $m_1/m_2 = 2$ . Because two triangular lattices would not be commensurate, the system can choose in this case, the second best configuration which minimises the total energy, namely the square lattice configuration.

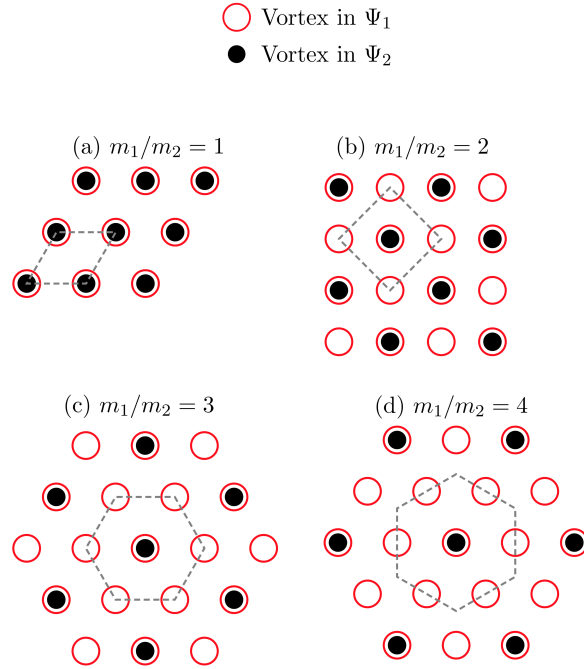


Figure 4.2: Schematic depiction of the regular vortex lattice ground state configurations attainable for a binary system of rotating condensates [118]. When the triangular vortex lattices associated with each mass ratio (and hence vortex density ratios) are commensurate, then the overlapping of these such triangular lattices provides the ground state configuration of the system. The triangular lattices associated with the mass ratio  $m_1/m_2$  are not commensurate. For this reason the configuration minimising the total energy is not a combination of two triangular lattices but a combination of two square lattices instead.

### 4.3 Multiply quantised vortices

For large enough inter-species interaction strength  $g_{12}$ , vortices in the heavier species will start forming bounded  $n$ -tuples, where  $n$  is the integer mass ratio. At the same time the vortices in the lighter species will arrange into a triangular configuration and each  $n$ -tuple will be centred on one of the lighter species vortices. The distance of the  $n$  vortices composing each  $n$ -tuple is controlled by the strength of the inter-species interaction. When  $g_{12}$  approaches

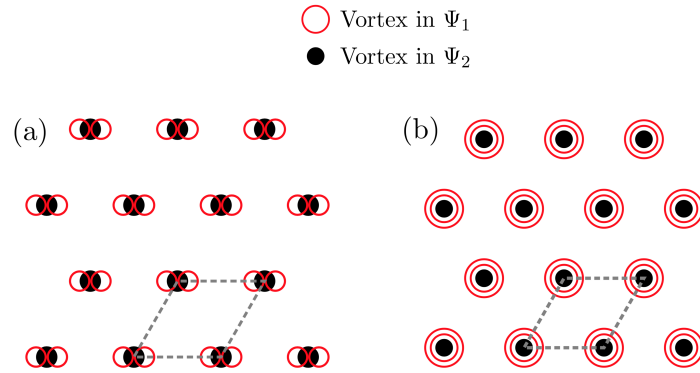


Figure 4.3: Schematic depiction of bounded pairs of vortices (a) and multiply quantised vortices (b), in the heavier species. The configuration of the vortices in the lighter species as well as that of the bounded pairs and of the multiply quantised vortices is triangular.

the miscibility/immiscibility boundary, the numerical calculations [112] seem to suggest that the  $n$ -tuples collapse into a single multiply quantised vortex with  $n$  quanta of circulation. Clearly, for large  $n$  (i.e. for large mass ratios), the existence of such multiply quantised lattices will also depend on the relative intra-species interaction strengths. In fact, for sufficiently large  $n$ , one can expect not to find such states when  $g_1 = g_2$ .



# Chapter 5

## Mixtures of Repulsive Superfluids: Equal Masses

“See how Mathematick rideth as a queen  
cheer’d on her royal progress thru’out nature’s realm;  
see how physical Science, which is Reason’s trade  
and high profession, booketh ever and docketeth  
all things in order and pattern.”

---

Robert Bridges, *Testament of Beauty*, 1929.

In this chapter we will build on the previously introduced non-linear Hofstadter model in order to incorporate more than one component into the system. Although one might naïvely think that the generalisation to two components is as trivial as writing two coupled equations of motion, it turns out that the model developed in Chapter 3 requires two extra degrees of freedom for each extra component added to the system.

We will begin this chapter discussing on the extension of the method presented in the previous Chapter 3 and then proceed to apply the full method to the study of a system composed of two interacting superfluids.

## 5.1 Reconsidering boundary conditions for multicomponent systems

To begin, for simplicity, let us consider again in more detail the case of a single-component Bose-Einstein condensate under uniform rotation in the continuum. The physical quantities describing such a system are the gauge invariant velocity  $\mathbf{v} = \frac{\hbar}{m}\nabla\theta - \frac{1}{m}\mathcal{A}$  and the superfluid density  $\rho$ . Both of these quantities follow from the condensate order parameter  $\psi = \sqrt{\rho}e^{i\theta}$  and the vector potential corresponding to uniform rotation for which we choose the Landau gauge:  $\mathcal{A} = 2m\Omega(0, x)$ .

Now let us consider an infinite periodic vortex lattice. Without loss of generality, we may choose an  $L_x \times L_y$  rectangular unit cell that tiles the system. The superfluid velocity and density must have the periodicity of this unit cell, namely

$$\begin{aligned} \mathbf{v}(x + L_x, y) &= \mathbf{v}(x, y + L_y) = \mathbf{v}(x, y), \\ \rho(x + L_x, y) &= \rho(x, y + L_y) = \rho(x, y). \end{aligned} \tag{5.1}$$

From the first equality, the  $x$ -periodicity requirement reads

$$\begin{aligned} \partial_x\theta(x + L_x, y) &= \partial_x\theta(x, y), \\ \partial_y\theta(x + L_x, y) - 2m\Omega L_x &= \partial_y\theta(x, y), \end{aligned} \tag{5.2}$$

so that upon integration one gets

$$\begin{aligned} \theta(x + L_x, y) &= \theta(x, y) + f(y), \\ \theta(x + L_x, y) - 2m\Omega L_x y &= \theta(x, y) + g(x), \end{aligned} \tag{5.3}$$

with  $f(y)$  and  $g(x)$  general functions of the  $y$  and  $x$  coordinates only, which clearly have to satisfy  $f(y) = 2m\Omega L_x y + g(x)$ . Thus we find that  $g(x) = \kappa_x$  is a constant, and  $f(y) = 2m\Omega L_x y + \kappa_x$ . Thus one finds that the phase must

satisfy

$$\begin{aligned}\theta(x + L_x, y) &= \theta(x, y) + \frac{2\Omega m}{\hbar} L_x y + \kappa_x \\ \theta(x, y + L_y) &= \theta(x, y) + \kappa_y\end{aligned}\tag{5.4}$$

where the constant  $\kappa_y$  is obtained from the integration of the  $y$ -periodicity condition. For the sake of convenience and clarity, let us introduce a rescaled version of these constants, namely the phases  $\tau_j = \kappa_j/L_j$  appearing above in (5.18) and (5.19). Next we introduce the magnetic translation operator defined in Chapter 1,  $T(\mathbf{r}) = e^{\frac{i}{\hbar}\mathbf{\Pi}\cdot\mathbf{r}}$ , where  $\Pi_x = p_x - 2m\Omega y$  and  $\Pi_y = p_y$  are the generators of magnetic translation in the Landau gauge (1.117) [1]. Then one can verify that the periodicity condition for the superfluid density,  $\rho(x, y) = \rho(x + L_x, y) = \rho(x, y + L_y)$  and velocity, Eq. (5.4), can be written succinctly as

$$\begin{aligned}e^{\frac{i}{\hbar}\Pi_x L_x}\psi(x, y) &= e^{i\kappa_x}\psi(x, y) = e^{i\tau_x L_x}\psi(x, y), \\ e^{\frac{i}{\hbar}\Pi_y L_y}\psi(x, y) &= e^{i\kappa_y}\psi(x, y) = e^{i\tau_y L_y}\psi(x, y).\end{aligned}\tag{5.5}$$

Now let us consider magnetically translating this wave function by  $-\mathbf{r} = -(r_x, r_y)$ :  $\tilde{\psi}(x, y) \equiv T(-\mathbf{r})\psi(x, y)$ . Due to the symmetries of the problem (namely that the generators of magnetic translation commute with the kinetic momenta), the energy per unit area corresponding to  $\psi(x, y)$  is the same as that of  $\tilde{\psi}(x, y)$ . Moreover the densities of these two wave functions are identical apart from translation:  $\tilde{\rho}(x, y) \equiv |\tilde{\psi}(x, y)|^2 = \rho(x - r_x, y - r_y)$ . Therefore the vortex lattice given by  $\psi$  is related to that given by  $\tilde{\psi}$  by a simple translation. By choosing  $\mathbf{r}$  to satisfy

$$\begin{aligned}2m\Omega r_y &= -\hbar\tau_x, \\ 2m\Omega r_x &= \hbar\tau_y\end{aligned}\tag{5.6}$$

we have the simplified boundary condition

$$e^{\frac{i}{\hbar}\Pi_x L_x} \tilde{\psi}(x, y) = \tilde{\psi}(x, y) \quad (5.7)$$

$$e^{\frac{i}{\hbar}\Pi_y L_y} \tilde{\psi}(x, y) = \tilde{\psi}(x, y) \quad (5.8)$$

which was the condition taken by us previously in [1] (see Appendix A). A closer look at (5.5) reveals that one can alternatively consider the following transformation of the operators of the magnetic translation group

$$\Pi_j \rightarrow \Pi_j - \hbar\tau_j. \quad (5.9)$$

This corresponds to a gauge transformation  $\psi \rightarrow e^{i\lambda}\psi$  with  $\lambda = \tau_x x + \tau_y y$ . As can be readily verified from (5.5), the transformed wave function is invariant under magnetic translation across a unit cell.

Through the above considerations, one sees that by specifying  $\tau_x$  and  $\tau_y$ , a particular unit cell of the vortex lattice is specified. Changing  $\tau_x$  and  $\tau_y$  will translate this unit cell, but will not affect the energy per unit cell or the vortex geometry of the periodic system. Thus, without loss of generality, we can set  $\tau_x = \tau_y = 0$  for the single component system. However, for the two-component system, such a freedom does not exist. In the method described in Chapter 3, we have set the  $\tau$ -parameters for the first component to zero, while keeping those of the second component as degrees of freedom to be minimised over.

### 5.1.0.1 An example

Consider for example the case of two overlapping triangular lattices. In order to obtain two interlaced triangular lattices, as those depicted in Fig. 5.1(a), one of the two lattices needs to be shifted with respect to the other by a vector  $\mathbf{r} = (0, \pm \frac{L_y}{3}) = (\frac{\hbar\kappa_y}{2m\Omega L_y}, -\frac{\hbar\kappa_x}{2m\Omega L_x})$ . Recalling the Feynman relation (1.78), and realising that in Fig. 5.1  $\rho_v = \frac{2}{L_x L_y}$  for each component, it is

straightforward to see that

$$\begin{aligned}\kappa_x &= \mp 2m\Omega L_x \frac{L_y}{3\hbar} = \mp 2\pi\rho_v \frac{L_x L_y}{3} = \mp \frac{4\pi}{3}, \\ \kappa_y &= 0.\end{aligned}\tag{5.10}$$

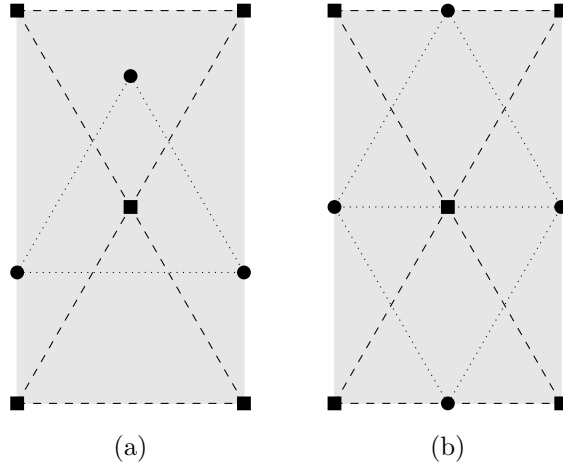


Figure 5.1: Two possible ways of overlapping two triangular lattices with equal lattice constant. The square and circle marks refer to points (vortices) corresponding to different lattices. In (a) is what we refer to as *interlaced triangular lattices*, while in (b) are shown two *interlaced oblique lattices*.

On the other hand in order to obtain two interlaced oblique lattices with aspect ratio  $R = \sqrt{3}$ , as in Fig. 5.1(b), the shift required is given by the vector  $\mathbf{r} = (\pm \frac{L_x}{2}, 0)$ , which gives the following phase factors:

$$\begin{aligned}\kappa_x &= 0, \\ \kappa_y &= \pm 2m\Omega L_y \frac{L_x}{2\hbar} = \pm 2\pi\rho_v \frac{L_x L_y}{2} = \pm 2\pi.\end{aligned}\tag{5.11}$$

Thus, it is clear that in this case the same geometrical arrangement can be equivalently achieved with  $\kappa_x = \kappa_y = 0$ . Moreover, a similar result can be found for the case of two interlaced triangular lattices in Fig. 5.1(a): all that is necessary is to take a number of vortices  $N_v = 6$  per unit cell. Then, in

this case, we can also take  $\kappa_x = \kappa_y = 0$ .

This example shows that the extra phases  $\kappa_j$ s, are not needed provided one takes the right unit cell. However, there is a catch. First of all, larger unit cells are both less accurate (because the density of computational points is lower) and take longer to converge (because the space of possible configurations is larger). Moreover, the  $\kappa_j$  parameters provide a simple mean to probe the state of the system and its phase transitions. To be more specific, it allows for instance to distinguish between configurations (a) and (b) in Fig. 5.1, while there is no parameter allowing to directly distinguish such configurations in a unit cell with  $N_v = 6$ . Thus, although not strictly necessary, it is more efficient to take the  $\tau_j$  parameters into consideration.

## 5.2 Computational framework for multicomponent systems

The computational framework introduced in Chapter. 3 can now be generalised to multicomponent systems, provided we bear in mind the arguments given at the beginning of this chapter.

The two-dimensional energy functional associated with a system of  $N_s$  coupled species in a rotating frame of reference is given, within Gross-Pitaevskii mean field theory, by

$$E = \int \mathcal{E}[\psi_1, \dots, \psi_{N_s}] dx dy, \quad (5.12)$$

where the energy density is

$$\begin{aligned} \mathcal{E}[\psi_1, \dots, \psi_{N_s}] = & \sum_{j=1}^{N_s} \left[ \frac{\hbar}{2m_j} |\nabla \psi_j|^2 + \frac{1}{2} m_j \omega_j^2 r^2 |\psi_j|^2 \right. \\ & \left. - \psi_j^\dagger \Omega L_z \psi_j - \mu_j |\psi_j|^2 \right] + \frac{1}{2} \boldsymbol{\rho}^T \mathcal{G} \boldsymbol{\rho}. \end{aligned} \quad (5.13)$$

Here,  $L_z = -i\hbar(x\partial_y - y\partial_x)$  is the angular momentum operator along the  $z$ -axes,  $\Omega$  is the rotational frequency, and  $m_j, \mu_j, \omega_j$  are respectively the mass, the chemical potential, and the trapping frequency of the  $j$ th species. The matrix

$$\mathcal{G} = \begin{pmatrix} g_1 & \cdots & g_{1N_s} \\ \vdots & \ddots & \vdots \\ g_{1N_s} & \cdots & g_{N_s} \end{pmatrix} \quad (5.14)$$

accounts for intra and inter-species interactions which are related to the  $s$ -wave scattering lengths  $a_{jk}$ :  $g_j = 4\pi\hbar^2 a_{jj}/m_j$ ,  $g_{jk} = 2\pi\hbar^2 a_{jk}(m_j+m_k)/m_j m_k$ . Finally  $\boldsymbol{\rho}^T = (|\psi_1|^2, \dots, |\psi_{N_s}|^2)$ . The miscibility condition which ensures the two species do not phase separate is for  $\mathcal{G}$  to be positive semi-definite; this can be analogously expressed in terms of the dimensionless parameter previously introduced as  $\alpha \leq 1$ .

The energy density functional (5.12) can be rearranged in a convenient way: introducing the symmetric gauges  $\mathcal{A}_j = \Omega m_j(-y, x)$  and setting the effective frequencies  $\omega_j^{\text{eff}} = \sqrt{\omega_j^2 - \Omega^2} = 0$ , we can write (5.12) as

$$\begin{aligned} \mathcal{E}[\psi_1, \dots, \psi_{N_s}] &= \sum_{j=1}^{N_s} \left[ \frac{1}{2m_j} |(-i\hbar\nabla - \mathcal{A}_j)\psi_j|^2 - \mu_j |\psi_j|^2 \right] \\ &+ \frac{1}{2} \boldsymbol{\rho}^T \mathcal{G} \boldsymbol{\rho}, \end{aligned} \quad (5.15)$$

where we have retained the chemical potentials  $\mu_j$  for later convenience. Notice that this term can be removed at any time, as it does not contribute to the dynamics of the system, and because the total energy can be consistently obtained by the appropriate normalisation of the wave functions. The preceding energy functional, leads to  $N_s$  corresponding coupled Gross-Pitaevskii equations  $i\hbar\partial_t\psi_j = \delta E/\delta\psi_j^*$  describing the dynamics of the system. The above form of the energy density functional is particularly appealing as it makes the gauge invariance of the system explicit. This property allows us

to switch to the Landau gauge  $\mathcal{A}_j^{\mathbf{L}} = 2\Omega m_j x \hat{y}$  without affecting the energy functional (5.12). Such a perspective will prove useful later.

We now approach the problem of the discretisation of the energy (5.15) following the arguments put forward in Chapter 3 and in [1]. More specifically, upon defining  $\Psi = (\psi_1, \dots, \psi_{N_s})^T$ , we consider the coupled generalised Hofstadter model

$$\begin{aligned}
 E_d = & - \sum_{n,l} \left[ \Psi_{n,l}^\dagger \mathbf{W}^{(x)} \Phi_l^{(x)} \Psi_{n+1,l} \right. \\
 & \left. + \Psi_{n,l}^\dagger \mathbf{W}^{(y)} \Phi_n^{(y)} \Psi_{n,l+1} + \text{h.c.} \right] \\
 & + \sum_{n,l} \left[ \frac{1}{2} \rho_{n,l}^\dagger \mathcal{U} \rho_{n,l} - \Psi_{n,l}^\dagger \bar{\mu} \Psi_{n,l} \right],
 \end{aligned} \tag{5.16}$$

defined on a grid of  $N_x \times N_y$  points taking values  $\mathbf{r} = a_x n \hat{x} + a_y l \hat{y}$ , with  $n, l \in \mathbb{Z}^+$ ,  $n \leq N_x$ ,  $l \leq N_y$ , with lattice constants  $a_k = L_k/N_k$ , and with  $L_x, L_y$  being the lengths of the computational unit cell. In the above,  $\mathbf{W}^{(x)}$ ,  $\mathbf{W}^{(y)}$  account for the anisotropic tunnelling for each component while the  $\Phi_n^{(k)}$  arise from the Peierls substitution needed to incorporate the gauge fields:

$$\begin{aligned}
 \mathbf{W}^{(k)} &= \frac{\hbar^2}{2a_k^2} \text{diag} \left[ \frac{1}{m_1}, \dots, \frac{1}{m_{N_s}} \right], \\
 \Phi_n^{(k)} &= \text{diag} \left[ e^{-i\delta_{yk} \mathcal{B}_1 n}, \dots, e^{-i\delta_{yk} \mathcal{B}_{N_s} n} \right].
 \end{aligned} \tag{5.17}$$

As we have discussed in the preceding chapter, the energy (5.16) reduces to the energy functional (5.12) provided that the lattice constant is the smallest length scale in the problem. In doing so, provided one considers the Landau gauge, it is possible to verify the following identifications:  $\mathcal{B}_j = 2\Omega m_j a_x a_y / \hbar$ ,  $\mathcal{U} = \mathcal{G} / a_x a_y$  and  $\bar{\mu} = \text{diag}[\mu_1, \dots, \mu_{N_s}] - 2(\mathbf{W}^{(x)} + \mathbf{W}^{(y)})$ . As we have mentioned, an alternative to fixing the chemical potential is to fix the total particle numbers per unit cell as  $\int |\psi_j|^2 dx dy = \mathcal{N}_j$ .



We next perform  $N_s - 1$  local gauge transformations on the wave functions of the additional components:

$$\Psi_{n,l} \rightarrow \text{diag} \left[ 1, e^{-i\lambda_{n,l}^{(2)}}, \dots, e^{-i\lambda_{n,l}^{(N_s)}} \right] \cdot \Psi_{n,l}, \quad (5.18)$$

where the pure gauges are  $\lambda^{(j)} = \tau_x^{(j)} a_x n + \tau_y^{(j)} a_y l$ . Clearly here we have taken  $\tau_x^{(1)} = \tau_y^{(1)} = 0$ , which can be done without any loss of generality, as discussed. Inserting (5.18) into (5.16), one finds that

$$\Phi_n^{(k)} \rightarrow \text{diag} \left[ 1, e^{-i\tau_k^{(2)} a_k}, \dots, e^{-i\tau_k^{(N_s)} a_k} \right] \cdot \Phi_n^{(k)}, \quad (5.19)$$

The terms  $a_k$  entering the phase factors in the above equation (5.19) arise from the Peierls integrals calculated over the Hofstadter computational lattice vectors. A comment on the need for this gauge transformation will be given below. We further assume that  $\Psi_{n,l}$  can be expanded in the basis of states

$$\begin{aligned} \tilde{\Psi}_{k_x,l} &= \left( \tilde{\psi}_{1;k_x l}, \tilde{\psi}_{2;k_x l}, \dots, \tilde{\psi}_{N_s;k_x l} \right)^T \\ \tilde{\Psi}_{n,k_y} &= \left( \tilde{\psi}_{1;n k_y}, \tilde{\psi}_{2;n k_y}, \dots, \tilde{\psi}_{N_s;n k_y} \right)^T \end{aligned} \quad (5.20)$$

as

$$\begin{aligned} \psi_{j;nl} &= \frac{1}{\sqrt{N_x}} \sum_{k_x} e^{i(k_x n + B_j n l)} \tilde{\psi}_{j;k_x l}, \\ \psi_{j;nl} &= \frac{1}{\sqrt{N_y}} \sum_{k_y} e^{i k_y l} \tilde{\psi}_{j;n k_y}. \end{aligned} \quad (5.21)$$

This is equivalent to demanding  $\Psi_{n,l}$  to be an eigenfunction of the magnetic translation operators with eigenvalue equal to one. In doing so, we also automatically satisfy the required twisted boundary conditions [1, 106]. Inverting the relation in (5.21), we can then define the discrete magnetic

Fourier transform (dMFT) of the  $j$ th component as

$$\begin{aligned}\tilde{\psi}_{j;k_x l} &= \frac{1}{\sqrt{N_x}} \sum_n e^{-i(k_x n + \mathcal{B}_j n l)} \psi_{j;n l}, \\ \tilde{\psi}_{j;n k_y} &= \frac{1}{\sqrt{N_y}} \sum_l e^{-i k_y l} \psi_{j;n l},\end{aligned}\tag{5.22}$$

which will be fundamental for the diagonalisation of the problem at hand.

A comment is needed concerning the gauge transformation given above and the boundary conditions of the system. The gauge transformation (5.18) has the effect of introducing two new degrees of freedom contributing to an overall phase of the second component's wavefunction. In Chapter 3, the wave functions were taken to be invariant when magnetically translated along a vortex lattice vector. While this constraint is appropriate for the single-component case, it must be relaxed for the multi-component system. For the present case, we must consider the whole set of possible states obtainable by translating one component with respect to the other. Clearly one needs to translate only one of the two components to obtain such a set. Such a translation is accounted for by the parameters  $(\tau_x^{(j)}, \tau_y^{(j)})$  introduced in (5.18) and (5.19).

As discussed in the previous chapter, the employment of the magnetic Fourier transform (MFT) diagonalises the kinetic part of the model. The expansion (5.21) is of great importance as it allows, through its inverse (5.22), for the diagonalisation of the linear (kinetic) part of the model (5.16). The discrete energy (5.16) can now be written compactly as

$$\begin{aligned}E_d &= 4\mathcal{R} \sum_{k_x, l} \tilde{\Psi}_{k_x, l}^\dagger \overline{\mathbf{W}} \mathbf{K}_{k_x, l}^{(x)} \tilde{\Psi}_{k_x, l} \\ &\quad + \frac{4}{\mathcal{R}} \sum_{n, k_y} \tilde{\Psi}_{n, k_y}^\dagger \overline{\mathbf{W}} \mathbf{K}_{n, k_y}^{(y)} \tilde{\Psi}_{n, k_y} \\ &\quad + \sum_{n, l} \frac{1}{2} \rho_{n, l}^\dagger \mathcal{U} \rho_{n, l},\end{aligned}\tag{5.23}$$

where we have defined the matrices accounting for the kinetic terms

$$\begin{aligned} \mathbf{K}_{k_x, l}^{(x)} &= \text{diag} \left[ \sin^2 \left( \frac{k_x + \mathcal{B}_1 l}{2} \right), \dots, \sin^2 \left( \frac{k_x + \mathcal{B}_{N_s} l + \tau_x^{(N_s)}}{2} \right) \right], \\ \mathbf{K}_{n, k_y}^{(y)} &= \text{diag} \left[ \sin^2 \left( \frac{k_y - \mathcal{B}_1 n}{2} \right), \dots, \sin^2 \left( \frac{k_y - \mathcal{B}_{N_s} n + \tau_y^{(N_s)}}{2} \right) \right], \end{aligned} \quad (5.24)$$

and introduced  $\overline{\mathbf{W}} = (\mathbf{W}^{(x)} \mathbf{W}^{(y)})^{\circ \frac{1}{2}}$ , denoting by ‘ $\circ$ ’ element-wise exponentiation. We have also introduced the aspect ratio  $\mathcal{R} = \frac{L_y}{L_x} = \frac{a_y}{a_x}$ , which explicitly accounts for anisotropic tunnelling.

Each term in (5.23) is now diagonal and the minimisation of the energy functional with respect to  $\Psi$  can thus be achieved by solving the associated equations of motion in imaginary time in conjunction with a split-step method; a further minimisation is then required with respect to  $\tau_x$ ,  $\tau_y$  and  $\mathcal{R}$ . Holding  $\tilde{\Psi}$ ,  $\tau_x^{(j)}$  and  $\tau_y^{(j)}$  fixed, it is straightforward to show that (5.23) is minimised by requiring

$$\mathcal{R} = \sqrt{\frac{\sum_{n, k_y} \tilde{\Psi}_{n, k_y}^\dagger \overline{\mathbf{W}} \mathbf{K}_{n, k_y}^{(y)} \tilde{\Psi}_{n, k_y}}{\sum_{k_x, l} \tilde{\Psi}_{k_x, l}^\dagger \overline{\mathbf{W}} \mathbf{K}_{k_x, l}^{(x)} \tilde{\Psi}_{k_x, l}}}. \quad (5.25)$$

Similarly one can find that holding  $\tilde{\Psi}$  and  $\mathcal{R}$  fixed, the discrete energy (5.23) is minimised with respect to  $\tau_x^{(j)}$  and  $\tau_y^{(j)}$  by choosing

$$\begin{aligned} \tau_x^{(j)} &= -\arctan \left[ \frac{\sum_{k_x, l} \sin(k_x + \mathcal{B}_j l) |\tilde{\psi}_{j; k_x, l}|^2}{\sum_{k_x, l} \cos(k_x + \mathcal{B}_j l) |\tilde{\psi}_{j; k_x, l}|^2} \right] + \pi \Theta \left( -\sum_{k_x, l} \cos(k_x + \mathcal{B}_j l) |\tilde{\psi}_{j; k_x, l}|^2 \right), \\ \tau_y^{(j)} &= -\arctan \left[ \frac{\sum_{n, k_y} \sin(k_y - \mathcal{B}_j n) |\tilde{\psi}_{j; n, k_y}|^2}{\sum_{n, k_y} \cos(k_y - \mathcal{B}_j n) |\tilde{\psi}_{j; n, k_y}|^2} \right] + \pi \Theta \left( -\sum_{n, k_y} \cos(k_y - \mathcal{B}_j n) |\tilde{\psi}_{j; n, k_y}|^2 \right), \end{aligned} \quad (5.26)$$

where  $\Theta(x)$  is the Heaviside function.

The minimisation of (5.23) can then be performed numerically by repeatedly alternating the minimisation with respect to  $\Psi$ ,  $\mathcal{R}$  and the  $\tau_x^{(j)}$ ,  $\tau_y^{(j)}$ . As before, the minimisation over  $\Psi$  can be performed by solving the imaginary-time Gross-Pitaevskii equations using a split-step method. In practice, we find that it is most efficient to perform more steps to evolve  $\Psi$  and less for the remaining parameters. A schematic description of this algorithmic procedure is given in the following Fig. 5.2. Finally, one must check for convergence in

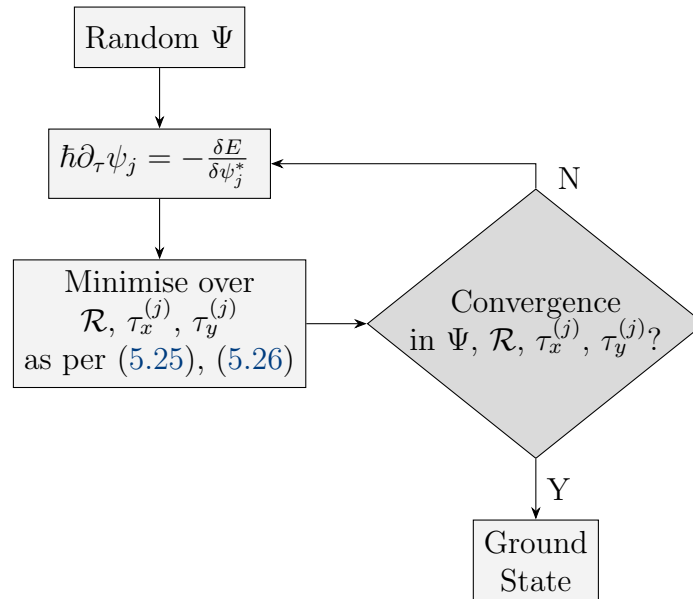


Figure 5.2: Schematic description of the algorithmic procedure. The equations of motion in the top left of the figure are obtained by Wick-rotating the Gross-Pitaevskii equations to imaginary time  $\tau = it$ .

the time step and the discretisation lattice constants.

### 5.2.1 The relation between model and physical parameters

The parameters entering the model described so far do not necessarily relate directly with the physical parameters needed to characterise each vortex

lattice configuration. For this reason, we will devote this section to the description of the relation between this two sets of parameters.

Consider the diagram presented in Fig. 5.3 for a system of two components made of constituents of equal masses. The black circles represent locations of vortices in the lattice of one species, while the grey squares represent vortices in the second species lattice. The relevant parameters needed to describe such a configuration, are the aspect ratio  $R = \frac{|\mathbf{v}_2|}{|\mathbf{v}_1|}$ , the angle  $\eta = \arccos(\hat{\mathbf{v}}_1 \cdot \hat{\mathbf{v}}_2)$  and the vector  $\mathbf{r} = r_1\mathbf{v}_1 + r_2\mathbf{v}_2$  defining the relative translation between the two lattices.

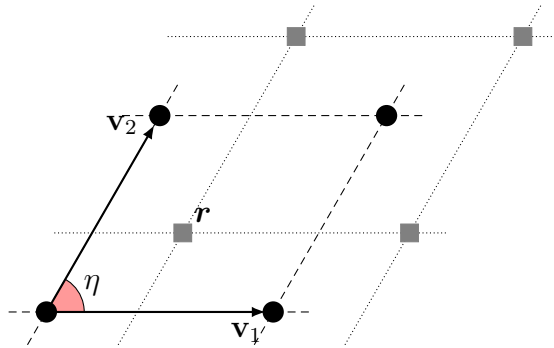


Figure 5.3: The diagram defines the parameters  $R = |\mathbf{v}_2|/|\mathbf{v}_1|$ ,  $\eta$  and  $\mathbf{r}$ .

As we have discussed, the  $\tau_j$  parameters are directly related to the relative translation of lattices as mandated by equation (5.6). However it is not clear yet what relation there exist between  $R$  and  $\eta$  and the parameters of the model. In order to understand the nature of such a relation we need to consider carefully what possibilities we have in the computational unit cell.

More specifically, it is particularly interesting to look at the interlaced square lattices case: in fact here it is possible to find two completely equivalent unit cells, both shown in Fig. 5.4. The first unit cell has aspect ratio  $\mathcal{R}_a = 1$  while the second one  $\mathcal{R}_b = 2$ . Consider now the first unit cell: when the aspect ratio  $\mathcal{R}$  is varied this has the effect of changing the angle of the interlaced square lattices which continuously transform into interlaced oblique lattice. It is now straightforward to find that the angle characterising such

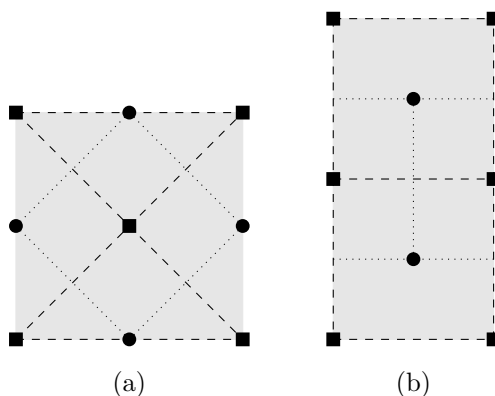


Figure 5.4: Two equivalent unit cells tiling a system made of two interlaced square lattices.

an oblique lattice is given by  $\eta = \min(2 \arctan \mathcal{R}_a, \pi - 2 \arctan \mathcal{R}_a)$ . On the other hand, the lattice aspect ratio is untouched so that  $R = 1$ . Consider now instead the second unit cell: at the variation of its aspect ratio  $\mathcal{R}_b$  something different happens. This time the effect is a change in the aspect ratio of the lattice  $R$ . In particular it is easy to see that the relation linking these two aspect ratios is simply  $R = \mathcal{R}_b/2$ . This time what remains untouched is the angle characterising the lattice which stays constant:  $\eta = \pi/2$ .

### 5.3 Components with equal masses: the phase transitions

For simplicity, we will consider here the case of a mixture of two superfluids with constituents of equal masses  $m_1 = m_2$ , which in turn implies equal vortex densities. Furthermore we will also take the particle densities to be the same. An early important result for equal masses in the repulsive regime  $g_{12} \geq 0$  was obtained semi-analytically in the LLL [66], assuming equal scattering lengths for the two coupled systems  $a_{11} = a_{22}$ , and consequently equal intra-species interactions for this equal masses case:  $g_1 = g_2 \equiv g$ . This as-

sumption in particular allows for the achievement of an  $SU(2)$  symmetric system. One consequence for such a system is, for example, that the system becomes invariant under the exchange of the two superfluids, as it was discussed in Chapter 1.

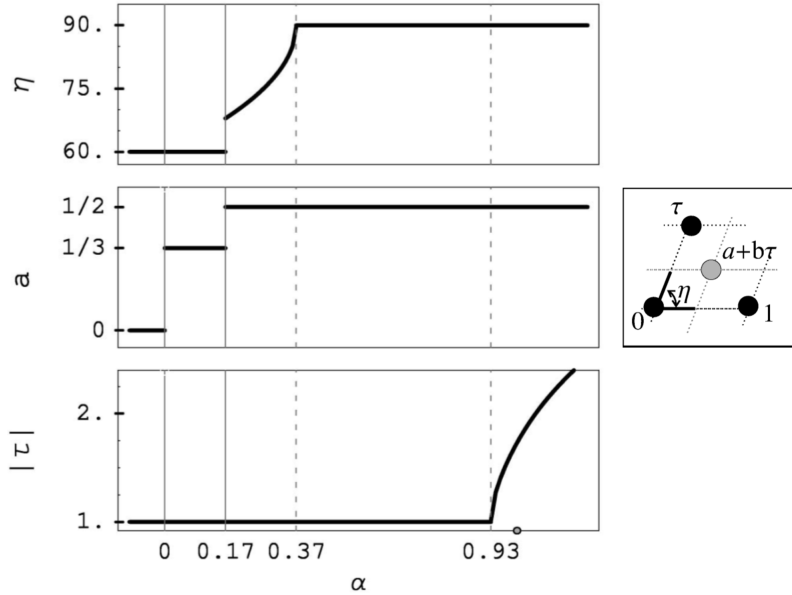


Figure 5.5: Results from the early work of Mueller and Ho [66]. The relation of the parameters used in these plots with those used in our treatment can be understood by comparing with Fig. 5.6.

In [66], the two superfluids were found to transition, at the variation of the parameter  $\alpha = g_{12}/\sqrt{g_1 g_2}$ , between four different states. This results are summed up in the plots presented in Fig. 5.5 below; we will perform a reparameterization of the problem which are more suitable for our treatment (see also Fig. 5.6), as it will become apparent later. The attractive regime is simple and consists of two perfectly overlapping triangular lattices. At low positive interacting strengths ( $0 < \alpha < T_1 = 0.172$ ) the ground state consists of two interlaced triangular lattices with a vortex of the first species centered between three vortices of the second species. At  $T_1$  the first transition occurs: for  $T_1 < \alpha < T_2 = 0.373$  the system is found to be made of two interlaced

oblique lattices with varying angle  $\eta$ ; the vortices of the first species are now sitting centered between four vortices of the second species. The second transition occurs when  $\eta = 90^\circ$  giving place to two interlaced square lattices. The system remains stable in this state for  $T_2 < \alpha < T_3 = 0.926$  until the third and last transition takes place. For  $\alpha > T_3$  the square lattices, following a spontaneous breaking of symmetry, continuously stretches into interlaced rectangular lattices of aspect ratio  $R$ . We recall that above the boundary  $\alpha = 1$  the two superfluids become immiscible and the so-called stripe phase is obtained [70]. In this region the density of each superfluid concentrates in the central area perpendicular to the long side of the rectangle. Because these results were obtained in the LLL, the connection to experiments is not immediate as most experiments on vortex lattices are away from this regime. The method outlined in the previous sections allows for the extension of these results to regimes of larger intra-species interaction or slower rotation rates. In Fig. 5.6 we present a detailed characterisation of the transitions undergone by the system as reflected by the behaviour of the two parameters  $\eta$  and  $R$ . In particular,  $\eta$  experiences a discontinuous jump at  $T_1$ ; this transition is also marked by a discontinuous jump in the parameter  $r_1 = r_2$ . The second transition  $T_2$  is characterised instead by a discontinuity in the derivative of  $\eta$ . Finally, the last transition  $T_3$  is marked by a discontinuity in the derivative of  $R$ . This result can be directly compared with that of [66]. It is also possible to notice that, at the  $SU(2)$  symmetric point, the lattice configuration is independent of the strength of the interactions. Here we find a lattice configuration consisting of two interlaced rectangular lattices of aspect ratio  $R = \sqrt{3}$ , such that the combination of the two lattices gives rise to a triangular lattice.

Let us finally comment a bit further on the phase transitions. It is in fact worth noticing that the order parameter critical exponent is given by  $\beta = 1/2$ , as it is after all expected for mean field theories. In the spirit of the Ginzburg-Landau treatment of phase transitions [79], we can exploit one of



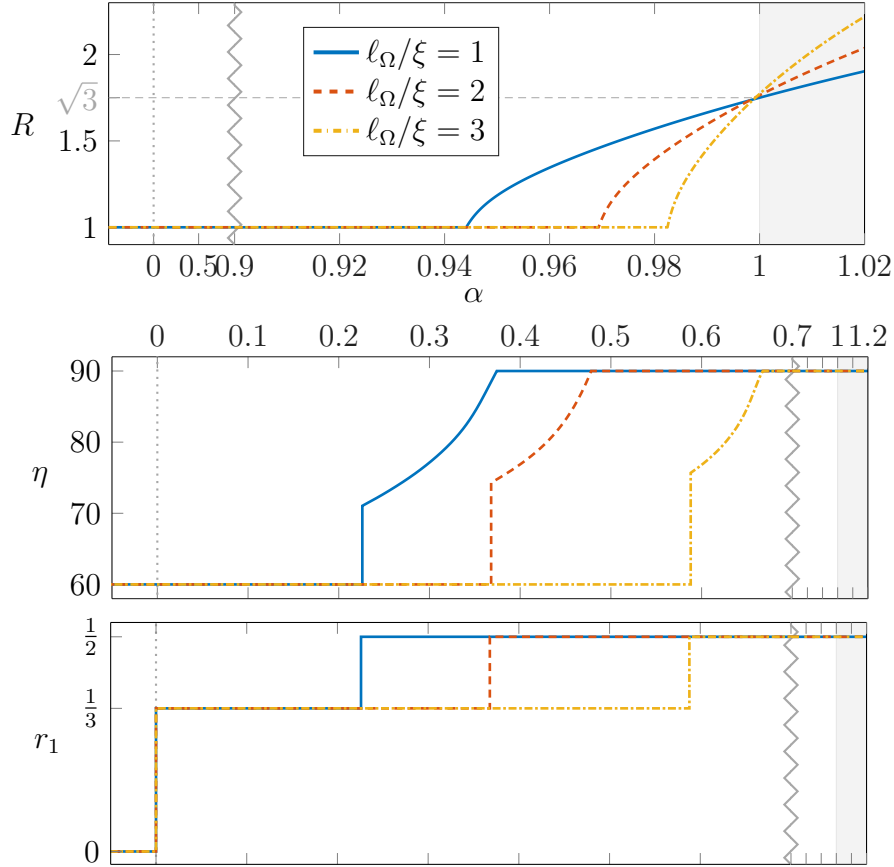


Figure 5.6: Extension of the results from [66]. When varying  $\alpha$ , the parameter  $R$  describes the second order transition transforming a square lattice into a rectangular lattice; the parameter  $\eta$  instead, experiences at first a jump, signalling a first order transition responsible for the transformation of the triangular lattice into the oblique lattice. Further observing the behaviour of  $\eta$ , it is possible to spot where another second order transition occurs, continuously transforming the oblique lattice into the square lattice. For components of equal masses one always obtains minimisers satisfying  $r_1 = r_2$ . At the occurrence of the first order transition  $r_1$  experiences a discontinuity as well: this permits the transition from the triangular to the square configurations. The beginning of the immiscible regime area is highlighted in grey.

the symmetries of the system to study the phase transitions. In particular, recall that  $E(\mathcal{R}) = E(1/\mathcal{R})$ , so that  $E(\mathcal{R} + 1)$  is approximately even at the origin<sup>1</sup> (see for example Fig. 3.5). Let us now introduce  $\phi = \mathcal{R} - \frac{1}{\mathcal{R}}$ . We can then write the symmetry associated with the energy functional as<sup>2</sup>  $E(\phi) = E(-\phi)$ , and  $\phi \xrightarrow{\mathcal{R} \rightarrow 1} 0$ . This is the familiar condition for  $\phi^4$  Landau theory. The symmetry allows for an expansion in terms of even powers only as:

$$E(\phi) = c_0(\alpha) + c_2(\alpha)\phi^2 + c_4(\alpha)\phi^4 + \mathcal{O}(\phi^6). \quad (5.27)$$

The smooth expansion coefficients  $c_j$  entering the expression above, really are functions of all the parameters  $c_j \equiv c_j(g, \alpha, \tau_x, \tau_y)$ . Here it will suffice to consider the dependence of such coefficients on  $\alpha = g_{12}/g$  only. Truncating at the fourth order, we must assume  $c_4$  to be positive in order to have the energy bounded from below. For  $c_2(\alpha) > 0$ , the free energy as a function of  $\mathcal{R}$ , has a minimum at  $\mathcal{R} = 1$  (i.e. at  $\phi = 0$ ). On the other hand, when  $c_2(\alpha)$  becomes negative the symmetry breaks: the transition therefore occurs at  $c_2 = 0$ . We can thus expand the coefficient  $c_2$  around the critical point  $\alpha^*$ :

$$c_2(\alpha) = \bar{c}_2(\alpha^* - \alpha), \quad (5.28)$$

for some constant  $\bar{c}_2$ . Notice that when  $\mathcal{R} = 1$ , all the non-zeroth order terms vanish: consequently  $c_0(\alpha)$  is interpreted as the energy associated with the interlaced square lattices. Now, setting  $\partial E/\partial\phi = 0$ , one finds the minimiser

---

<sup>1</sup>More rigorously, one can show that the requirement  $f(x) = f(\frac{1}{x})$ , imposes a constraint on the expansion coefficients  $c_j(\alpha)$ s. In particular, expanding  $f(1+x) - f(\frac{1}{1+x})$ , one finds that  $f'(1) = 0$ ,  $f'''(1) = -3f''(1)$ ,  $f^{(5)}(1) = 60f''(1) - 10f^{(4)}(1)$ , etc. As a consequence, it must be that the coefficients of the expansion of  $E(\mathcal{R})$ , respect the conditions  $c_1 = 0$ ,  $c_2 = -c_3$ ,  $c_5 = c_2 - 2c_4$ , etc. Minimising the free energy with these coefficient constraints, still leads to the result for the critical exponent  $\mathcal{R}(\alpha) \sim |\alpha - \alpha^*|^{\frac{1}{2}}$ .

<sup>2</sup>Notice in fact that  $R = \frac{\phi}{2} \pm \frac{1}{2}\sqrt{\phi^2 + 4}$ , and  $\left(\frac{\phi}{2} \pm \frac{1}{2}\sqrt{\phi^2 + 4}\right)^{-1} = -\frac{\phi}{2} \pm \frac{1}{2}\sqrt{\phi^2 + 4}$ .

of  $E(\phi)$  to be

$$\phi = \sqrt{\frac{\bar{c}_2}{2c_4}} (\alpha^* - \alpha)^{\frac{1}{2}}. \quad (5.29)$$

Consequently, the minimiser of  $E(\mathcal{R})$  is given by

$$\mathcal{R}(\alpha) = \sqrt{\frac{\bar{c}_2}{8c_4}} (\alpha - \alpha^*)^{\frac{1}{2}} \pm \sqrt{\frac{\bar{c}_2}{8c_4} (\alpha - \alpha^*) + 4}. \quad (5.30)$$

Furthermore, since from symmetry considerations (cf. Section 1.2.1) we know that  $\mathcal{R}(\alpha = 1) = \sqrt{3}$ , we can write an expression for the critical point:

$$\alpha^* = 1 - \frac{2c_4}{3\bar{c}_2}. \quad (5.31)$$

The behaviour of  $\mathcal{R}(\alpha)$  can be made clearer by considering small variations around the transition point. Let us then expand around  $\phi = 0$ , as

$$\mathcal{R} = \frac{\phi}{2} + \frac{1}{2}\sqrt{\phi^2 + 4} = \frac{\phi}{2} + \left(1 + \frac{\phi^2}{8} + \mathcal{O}(\phi^4)\right), \quad (5.32)$$

so that to first order in  $\phi$ , we can write

$$\mathcal{R}(\alpha) = 1 + \sqrt{\frac{\bar{c}_2}{8c_4}} (\alpha - \alpha^*)^{\frac{1}{2}}. \quad (5.33)$$

The critical exponent is then  $\beta = 1/2$ , as it was mentioned before. The same argument holds for  $\mathcal{R}(g)$  when we consider a fixed  $\alpha$ .

When considering the transition from interlaced triangular to interlaced oblique lattices instead, there is no symmetry principle we can invoke which allows to expand the free energy in even powers only. The other relevant order parameter here are the  $\tau_j$ s which are periodic with period  $2\pi/L_j$ . The presence of a non-zero cubic term in particular, gives rise to a different kind of transition (a first order transition) in which the global minimum suddenly

jumps from one local minimum to another. This results in a discontinuity in the order parameter, as shown in the second and bottom panels in Fig. 5.6.

## 5.4 Components with equal masses: the phase diagram

It is now possible to go even further and explore the phase diagram going towards the Coulomb limit: Fig. 5.7 shows the complete phase diagram for the ground states of two interacting superfluids. As can be intuitively expected, for  $\alpha < 0$  a configuration consisting of two overlapping triangular lattices is found. In the particular case of  $\alpha = 0$ , a configuration consisting of two non-interacting triangular lattices is found instead and the ground state is degenerate with respect to translations of the two lattices. The red lines in Fig. 5.7 mark the three phase boundaries  $T_1$ ,  $T_2$  and  $T_3$  corresponding to each phase transition occurring for  $\alpha > 0$ ; the colours encode the value of either  $\phi$  or  $R$ . For states below  $T_2$  the only varying parameter is  $\phi$ . The colour coding the highest value of  $\phi$  is the same as the colour coding the lowest value of  $R$ : this appears in the region between  $T_3$  and  $T_2$ , where neither of these two parameters varies. Above  $T_3$  the varying parameter is  $R$  and the colour code changes accordingly. Although in the LLL the square configuration is predominant, our results demonstrate that in the Coulomb limit the triangular lattice configuration takes over while the other configurations are suppressed.

### 5.4.1 Linearity of the phase boundaries

While it is convenient to study the phase space in Fig. 5.7 as a function of the parameters  $\alpha$  and  $\ell_\Omega/\xi$ , this approach conceals some very simple properties of the phase boundaries  $T_1$ ,  $T_2$  and  $T_3$ . In Fig. 5.8 the phase diagram is plotted in terms of the alternative parameters  $g$  and  $g_{12}$ . One sees that the phase

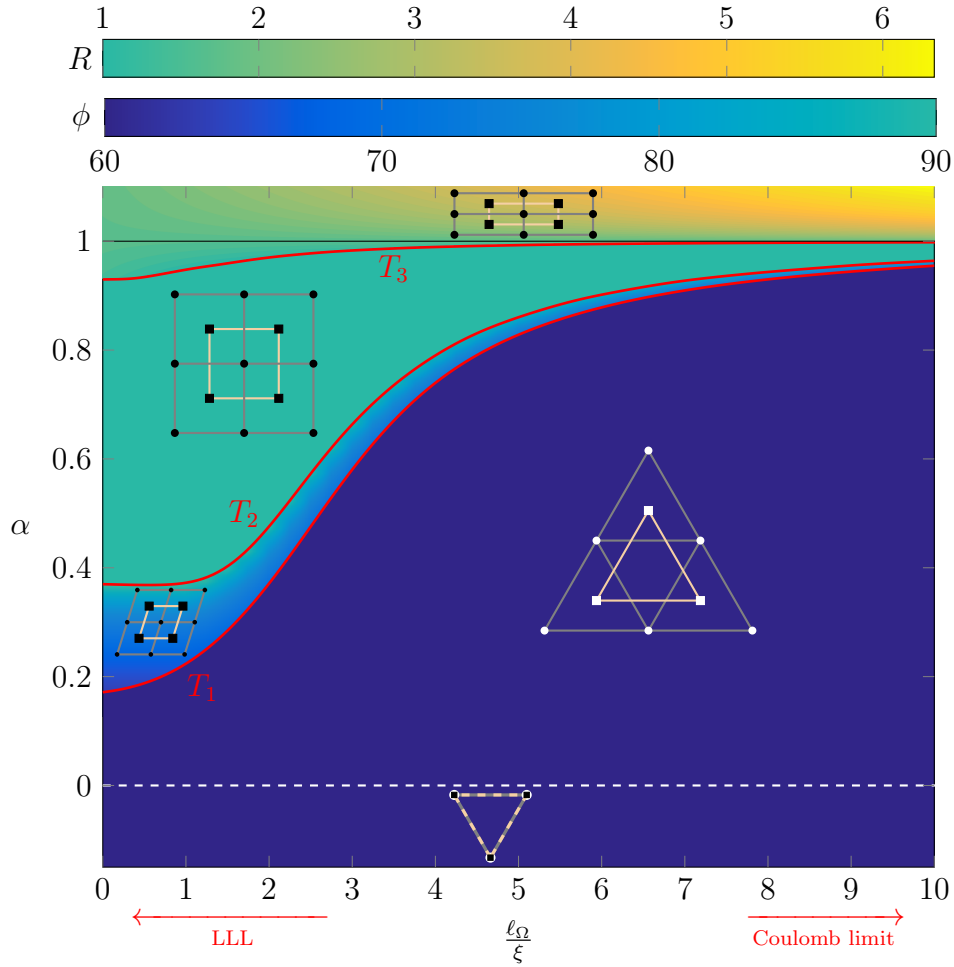


Figure 5.7: Phase diagram describing the ground states of two interacting superfluids of equal masses and same particle number per unit cell  $\mathcal{N}_1 = \mathcal{N}_2$ . The abscissa represents the intraspecies interaction strength (which is assumed to be the same for both species) while the ordinate the interaction strength amongst the two different species. The area of the phase space below  $T_2$  is characterised by the parameter  $\phi$ , while that above is characterised by  $R$ . Transition  $T_1$  is of first order, while  $T_2$  and  $T_3$  are second order transitions. For completeness the trivial attractive regime ( $\alpha < 0$ ) is included as well, showing a ground state consisting of two overlapping triangular lattices.

boundaries asymptotically become linear in the Coulomb regime. An argument explaining this behaviour goes as follows. Deep in the Coulomb regime, the energy of the system is dominated by terms representing interactions. In this limit, one can write the energy density as

$$\mathcal{E}(g, g_{12}) \sim \frac{g}{2}(\rho_1^2 + \rho_2^2) + g_{12}\rho_1\rho_2 = \frac{1}{2}g\rho^2 + (g_{12} - g)\rho_1\rho_2, \quad (5.34)$$

where  $\rho = \rho_1 + \rho_2$  is the total density. Since a phase boundary  $\bar{T}(g)$  between a phase configuration  $A$  and a configuration  $B$  can be defined as the value

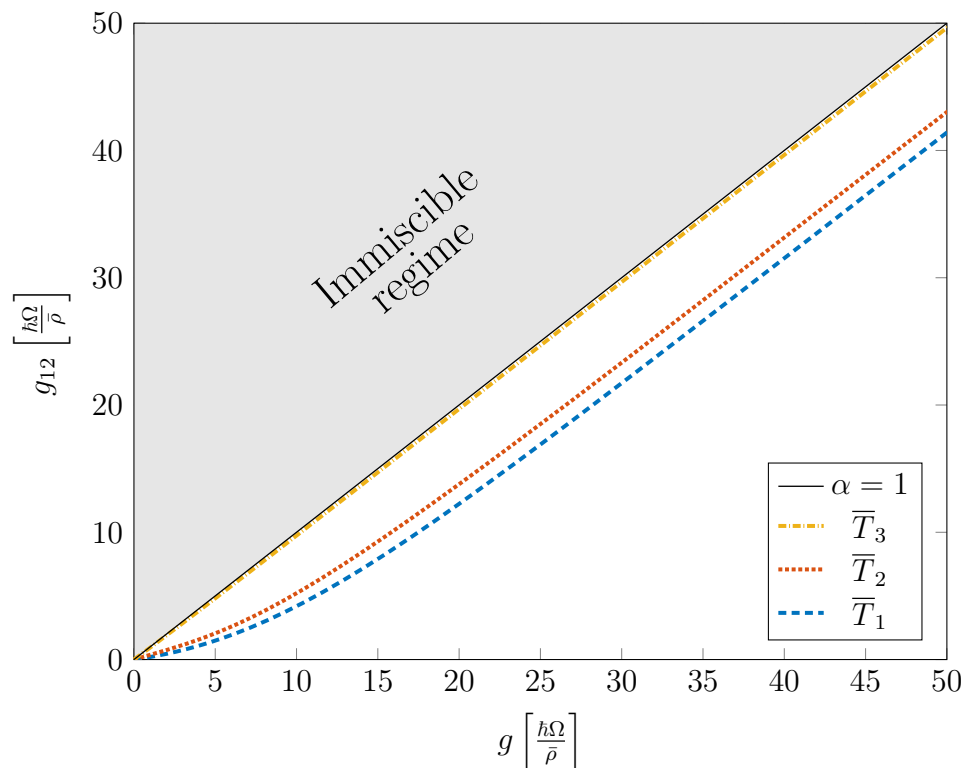


Figure 5.8: Linear phase boundaries in the miscible regime.  $\bar{T}_1$  marks the boundary between the triangular phase and the oblique phase,  $\bar{T}_2$  divides the oblique and the square phases and  $\bar{T}_3$  is the last phase boundary leading to the rectangular phase.

of the interspecies strength such that  $E^A(g, g_{12} = \bar{T}) = E^B(g, g_{12} = \bar{T})$ , it is possible to write an expression for  $\bar{T}(g)$ . In particular, one finds that

$$\frac{\bar{T}(g)}{g} = \frac{1}{2} \frac{\langle \rho_{A,1}^2 \rangle + \langle \rho_{A,2}^2 \rangle - \langle \rho_{B,1}^2 \rangle - \langle \rho_{B,2}^2 \rangle}{\langle \rho_{B,1} \rho_{B,2} \rangle - \langle \rho_{A,1} \rho_{A,2} \rangle}, \quad (5.35)$$

where brackets denote spatial average. Next, we note that deep in the Coulomb regime, variations in the *total* density are energetically prohibitive and so the total density, at this level of approximation, is constant. For instance, while  $\rho_1$  will approach zero near a vortex in  $\psi_1$ ,  $\rho_2$  will have a local maximum there, making the total density nearly constant. Writing density with respect to its average as  $\delta\rho_{A,1} = \rho_{A,1} - \langle \rho_{A,1} \rangle$  (with similar notation for the other components) we then have

$$\frac{\bar{T}(g)}{g} = \frac{\langle \delta\rho_A^2 \rangle - 2\langle \delta\rho_{A,1} \delta\rho_{A,2} \rangle - \langle \delta\rho_B^2 \rangle + 2\langle \delta\rho_{B,1} \delta\rho_{B,2} \rangle}{2(\langle \delta\rho_{B,1} \delta\rho_{B,2} \rangle - \langle \delta\rho_{A,1} \delta\rho_{A,2} \rangle)}. \quad (5.36)$$

In the Coulomb limit, the variances in the total densities become negligible and the leading order behaviour of the phase boundaries can be found to be

$$\lim_{g \rightarrow \infty} \frac{\bar{T}(g)}{g} = 1. \quad (5.37)$$

Therefore, the phase boundaries have the form  $\bar{T}_j = g + a_j$ <sup>3</sup> where the intercepts  $a_j$ , are determined by the kinetic energy difference between the two configurations and likely cannot be determined from such simple arguments. Operating the appropriate transformations to the phase boundaries in Fig. 5.7, we obtain the linear phase boundaries  $\bar{T}_j$  presented in Fig. 5.8. The numerical solution for the phase diagram indeed verifies these simple arguments.

For computational convenience, the phase space in Fig. 5.7 was calcu-

<sup>3</sup>In the next Chapter 6 a generalisation of this expression to general particle numbers  $\mathcal{N}_1 \neq \mathcal{N}_2$ , masses  $m_1 \neq m_2$  and intra-species interaction strength  $g_1 \neq g_2$  will be given. The derivation is presented in Appendix B.

---

lated with two vortices per species per unit cell. Considering a unit cell containing only one vortex per species, as done for instance in the early work by Abrikosov [72], does not allow for configurations other than the square and rectangular lattices. The smallest unit cell needed to obtain the correct ground states contains a minimum of two vortices (per species). The results obtained in this setting can be found to be consistent with those obtained in larger unit cells, as long as the size of the cell is appropriate (namely if the unit cell contains an even number of vortices). For other unit cells (e.g. a unit cell containing an odd number of vortices per species) one will in general observe frustrated lattices. However, such configurations of the system have higher energy densities and are therefore disregarded.



## Mixture of Repulsive Superfluids: the General Case

We will now move on to study systems of two superfluids with different components' atomic masses. While the extension of the method developed in the previous sections is fairly straightforward, it is important to devote some attention to a problem which we have so far ignored, namely that of commensurability. In this chapter we will start by discussing the implications of non unitary mass ratios on the possibility to achieve a consistent and periodic infinite vortex lattice. Recall that given two superfluids with different atomic masses, the Feynman relation (1.78) clearly indicates that the ratio of vortex densities will be proportional to the mass ratio:

$$\frac{m_2}{m_1} = \frac{\rho_v^{(2)}}{\rho_v^{(1)}}. \quad (6.1)$$

This allows the system to explore new exotic phases and configurations. However, as we will show, this also constitutes a constraint for some simple configurations that will not be allowed in the system because of lack of commensurability. More specifically, we will show that even for simple mass ratios (e.g.  $m_2/m_1 = 2$ ) it will not be possible to find regular triangular

ground states. In this scenario, the lack of commensurability implies, for large enough systems, the rise of frustration.

With this in mind we will present a phase diagram, analogous to that presented in Fig. 1.6 in the previous section, for the case  $m_2/m_1 = 2$ , showing that although the state consisting of two interlaced triangular lattices is not allowed, the system can still achieve novel unexpected configurations.

At last we will discuss in generality the results for higher mass ratios giving a summary of a few results in Table 6.1.

## 6.1 General considerations regarding commensurability

Until now we have ignored an issue that presents itself when considering infinite vortex lattices, namely that of commensurability. We could do so because we were considering the case of two species with equal atomic masses. If we are to investigate the nature of such systems in more generality we ought to first discuss the topic of lattice commensurability. The simplest scenario in which such issues arise is that occurring close to the zero intraspecies interaction point  $\alpha \approx 0$ : here, from fundamental considerations, one expects each component to be found in a triangular lattice configurations. Because of the lack of interaction between the two atomic species there is not a preferred position of one lattice with respect to the other. However, as soon as we consider an infinitesimal positive interaction  $\alpha = \epsilon$  we would expect the two lattices to arrange as to maximise the distance between each other, in order to minimise the energy arising from their interaction. The  $i$ th lattice associated with a species made of constituents of mass  $m_i$ , with magnetic length  $\ell_\Omega^{(i)} = \sqrt{\frac{\hbar}{2\Omega m_i}}$ , built on the basis vectors  $b_j$ s can be written in generality as  $\Lambda_i = \left\{ \ell_\Omega^{(i)} (j_i b_1 + \kappa_i b_2 + \dots) \mid j_i, \kappa_i, \dots \in \mathbb{Z} \right\}$ , and given two lattices  $\Lambda_1$  and  $\Lambda_2$ , a sufficient condition for commensurability is that the diophantine

equation  $|\Lambda_1| = |\Lambda_2|$  has a countably infinite number of solution. Considering triangular lattice simplifies things as only two basis vectors are necessary:

$$\Lambda_i = \left\{ \ell_{\Omega}^{(i)} (j_i b_1 + \kappa_i b_2) \mid j_i, \kappa_i \in \mathbb{Z} \right\}. \quad (6.2)$$

More specifically the two basis vectors are given by  $b_1 = [1, 0]$  and  $b_2 = [1/2, \sqrt{3}/2]$ , so that the commensurability condition then reads

$$\frac{m_2}{m_1} (j_1^2 + j_1 \kappa_1 + \kappa_1^2) = j_2^2 + j_2 \kappa_2 + \kappa_2^2. \quad (6.3)$$

As one would expect, the condition for commensurability is clearly satisfied for the trivial case of  $m_1/m_2 = 1$ . Let's consider then the next simplest case of  $m_1/m_2 = 2$ : the condition above (6.3) becomes

$$2 (j_1^2 + j_1 \kappa_1 + \kappa_1^2) = (j_2^2 + j_2 \kappa_2 + \kappa_2^2). \quad (6.4)$$

Assume that there exist a set of nonzero integers  $j_1, \kappa_1, j_2, \kappa_2 \in \mathbb{Z} \setminus \{0\}$  satisfying the above equation. The left hand side in (6.4) is even, so even must be the term on the right hand side. In turn, for this to be the case both  $j_2$  and  $\kappa_2$  are to be even. If that's the case, we can introduce two new scaled integer variables  $\bar{j}_2 = j_2/2, \bar{\kappa}_2 = \kappa_2/2$  so that

$$2 (j_1^2 + j_1 \kappa_1 + \kappa_1^2) = 4(\bar{j}_2^2 + \bar{j}_2 \bar{\kappa}_2 + \bar{\kappa}_2^2). \quad (6.5)$$

Thus, by the same argument, also  $j_1$  and  $\kappa_1$  both must be even. Now, it is possible to write any even integer  $j$  as  $2^J \mathfrak{o}_j$  for some integer  $J$  and odd integer  $\mathfrak{o}_j$ . Therefore

$$\begin{aligned} 2(2^{2J_1} \mathfrak{o}_{j_1}^2 + 2^{J_1+K_1} \mathfrak{o}_{j_1} \mathfrak{o}_{\kappa_1} + 2^{2K_1} \mathfrak{o}_{\kappa_1}^2) &= (2^{2J_2} \mathfrak{o}_{j_2}^2 + 2^{J_2+K_2} \mathfrak{o}_{j_2} \mathfrak{o}_{\kappa_2} + 2^{2K_2} \mathfrak{o}_{\kappa_2}^2) \\ 2^{2J_1+1} (\mathfrak{o}_{j_1}^2 + 2^{K_1-J_1} \mathfrak{o}_{j_1} \mathfrak{o}_{\kappa_1} + 2^{2(K_1-J_1)} \mathfrak{o}_{\kappa_1}^2) &= 2^{2J_2} (\mathfrak{o}_{j_2}^2 + 2^{K_2-J_2} \mathfrak{o}_{j_2} \mathfrak{o}_{\kappa_2} + 2^{2(K_2-J_2)} \mathfrak{o}_{\kappa_2}^2). \end{aligned} \quad (6.6)$$

If  $2J_1 + 1 > 2J_2$  then we can write

$$2^{2(J_1-J_2)+1}(\mathfrak{o}_{j_1}^2 + 2^{K_1-J_1}\mathfrak{o}_{j_1}\mathfrak{o}_{\kappa_1} + 2^{2(K_1-J_1)}\mathfrak{o}_{\kappa_1}^2) = (\mathfrak{o}_{j_2}^2 + 2^{K_2-J_2}\mathfrak{o}_{j_2}\mathfrak{o}_{\kappa_2} + 2^{2(K_2-J_2)}\mathfrak{o}_{\kappa_2}^2). \quad (6.7)$$

Clearly, (6.7) is a contradiction as the left hand side is even and the right hand side is odd. Mutatis mutandis, the same holds for  $2J_1 + 1 < 2J_2$ . Thus we have proved by contradiction that two triangular lattices, one twice as dense as the other, are not commensurate as (6.4) holds only when  $j_1 = \kappa_1 = j_2 = \kappa_2 = 0$ .

With more generality it is possible to find that (6.3) has more than one solution (the trivial one) if and only if the mass ratio is a Lösschian numbers [119], namely if it can be expressed as

$$\frac{m_2}{m_1} = \mu^2 + \mu\nu + \nu^2 = 1, 3, 4, 7, 9, 12, 13, \dots \quad (6.8)$$

for any  $\mu \geq \nu$  with  $\mu, \nu \in \mathbb{Z}$ . This result can be proved by realising that the following factorisation

$$(\mu^2 + \mu\nu + \nu^2)(j_1^2 + j_1\kappa_1 + \kappa_1^2) = (j_2^2 + j_2\kappa_2 + \kappa_2^2), \quad (6.9)$$

always holds with  $j_2 = \mu j_1 - \nu \kappa_1$ ,  $\kappa_2 = \nu(j_1 + \kappa_1) + \mu \kappa_1$ . For a given Lösschian mass ratio it is possible to find that one vortex lattice will be rotated with respect to the other by an angle  $\theta = \arctan\left(\frac{\sqrt{3}\nu}{2\mu+1}\right)$ . Thus we find  $\theta = 0$  if and only if the mass ratio is a perfect square. This result (6.8) has a clear geometrical interpretation: in a triangular lattice, the distance from the origin of the elements of every set of points equidistant from the origin is given by the square root of a Lösschian number. This is clearly depicted in Fig. 6.1. Looking at the figure it is also possible to better understand where the above expression for  $\theta$  comes from: the integers  $\mu > \nu$  composing the Lösschian number  $(\mu^2 + \mu\nu + \nu^2)$ , exactly give the closest point to the  $x$ -axis at a distance  $(\mu^2 + \mu\nu + \nu^2)$  from the origin as  $\mu b_1 + \nu b_2$ . The simplest

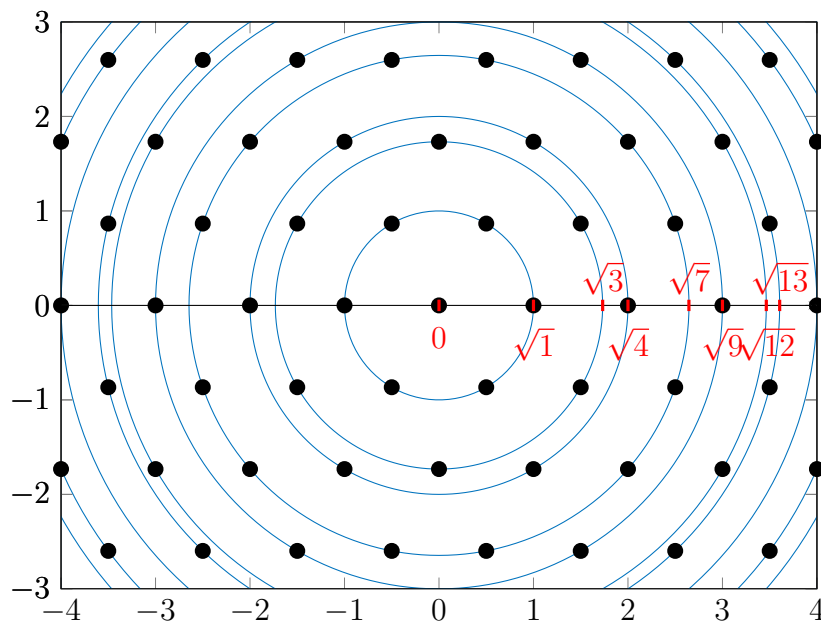


Figure 6.1: Geometrical significance of Lösschian numbers. In a triangular lattice, the distance from the origin of the elements of every set of points equidistant from the origin, is given by the square root of a Lösschian number.

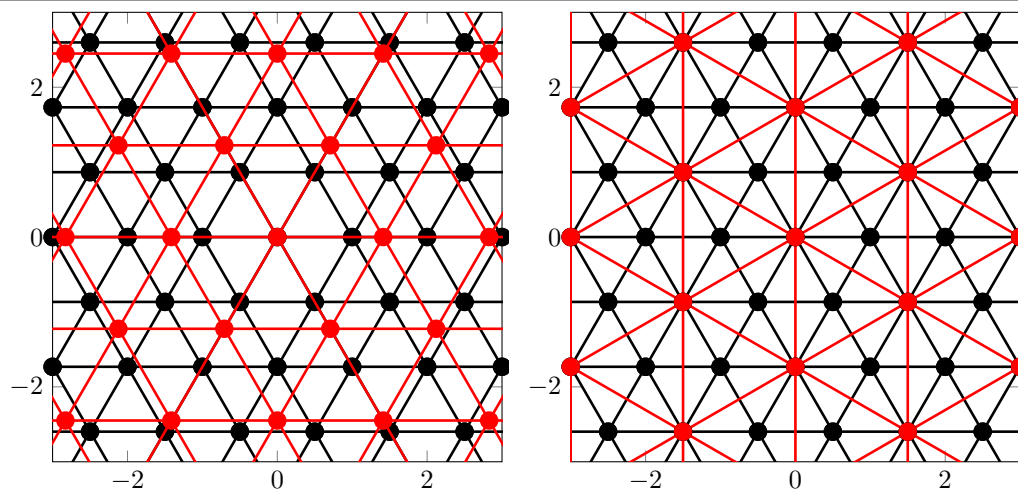


Figure 6.2: On the left: two non-commensurate triangular lattices with corresponding mass ratio  $m_2/m_1 = 2$ . In the presence of non-commensurability one would in practice observe geometrical frustration. On the right: two commensurate triangular lattices with  $m_2/m_1 = 3$ .

case of two such nontrivial commensurate triangular lattices occur for a mass ratio of 3 and is depicted in Fig 6.2: the two lattices are rotated at an angle  $\theta = \pi/6$  as expected.

To sum up, we have shown that for the case of mass ratio 2, the two associated triangular vortex lattices are not commensurate as 2 is not L\"oschian. However we might still be able to find commensurate states for stronger interactions between components. Let's consider then another lattice: the square lattice. In this case we have the basis vectors  $b_1 = [1, 0]$  and  $b_2 = [0, 1]$ , thus the commensurability condition reads

$$\frac{m_2}{m_1}(J_1^2 + \kappa_1^2) = (J_2^2 + \kappa_2^2). \quad (6.10)$$

Similarly to what was done before, one can easily realise that the following

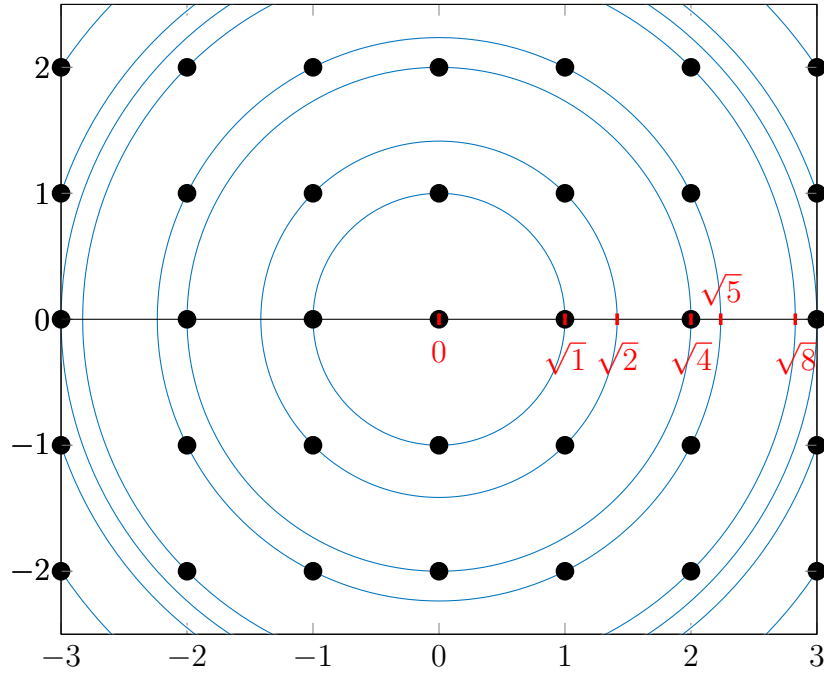


Figure 6.3: Geometrical significance of (6.12). In a square lattice, the distance from the origin of the elements of every set of points equidistant from the origin, is given by the square root of the sum of squares (6.12).

equality holds

$$(\mu^2 + \nu^2)(j_1^2 + \kappa_1^2) = (j_2^2 + \kappa_2^2), \quad (6.11)$$

provided that  $j_2 = \mu j_1 + \nu \kappa_1$  and  $\kappa_2 = \mu \kappa_1 - \nu j_1$ . Therefore, given two integers  $\mu \geq \nu \in \mathbb{Z}$ , the diophantine equation (6.10) is satisfied by requiring

$$\frac{m_2}{m_1} = \mu^2 + \nu^2 = 1, 2, 4, 5, 8, 9, 10, \dots \quad (6.12)$$

This time the lattices will be found tilted with respect to each other at an angle  $\theta = \arctan\left(\frac{\nu}{\mu}\right)$ . The geometrical interpretation of such a result is analogous to that of the triangular lattice and is depicted in Fig. 6.3.

## 6.2 The mass ratio $m_2/m_1 = 2$

As we have just discussed, since the ratio  $m_2/m_1 = 2$  is not L\"oschian, and thus being it impossible to find a regular arrangement for the two triangular vortex lattices, we will find a non-commensurate configuration close to the non-interacting limit  $\alpha \approx 0$ . Nonetheless we might still be able to find other states which are commensurate for higher interspecies interactions. This mass ratio is of particular relevance, as in experiments one can achieve it with good approximation with the mixture of isotopes  $^{41}\text{K}$ – $^{87}\text{Rb}$  (with mass ratio  $m_2/m_1 \approx 2.1$ ) [120, 121], but also  $^{87}\text{Rb}$ – $^{174}\text{Yb}$  ( $m_2/m_1 \approx 2.0014$ ) and  $^{84}\text{Sr}$ – $^{168}\text{Er}$  ( $m_2/m_1 \approx 2.0013$ ).

Again as before we restrict our analysis to equal  $\ell_\Omega/\xi$  for both components. Fig. 6.4 presents the ground states' phase diagram associated with the mass ratio  $m_2/m_1 = 2$ . As it is possible to observe, in this scenario we encounter two new commensurate ground states. For  $\alpha = 0$ , as expected from arguments made earlier, we find a region of non-commensurate ground states. The first transition we find when increasing  $\alpha$  is of second order and transforms the lighter species ground state into a square lattice, while the lattice associated with the heavier one is transformed into a *snub-square lattice*. Such configuration has lattice parameter  $(\sqrt{3} - 1)\ell_\Omega^{(1)}$ , where we can take  $\ell_\Omega^{(1)}$  to be the lattice constant of the first component due to its simpler lattice geometry.

Increasing  $\alpha$  further, we encounter a second transition, again of second order: the lighter species' vortex configuration is transformed into a triangular lattice while the heavier is transformed into a *honeycomb lattice* as shown in Fig. 6.6. For the honeycomb case one easily finds the lattice parameter to be  $\ell_\Omega^{(1)}/\sqrt{3}$ .

Fig. 6.5 shows instead the phase diagram obtained under the condition of equal healing lengths  $\xi^{(1)} = \xi^{(2)} \equiv \xi$ . In this regime one finds different intra-species interaction strengths, in particular  $g_1 = 2g_2$ . It is interesting here to notice the important role that strong interactions play for the existence of



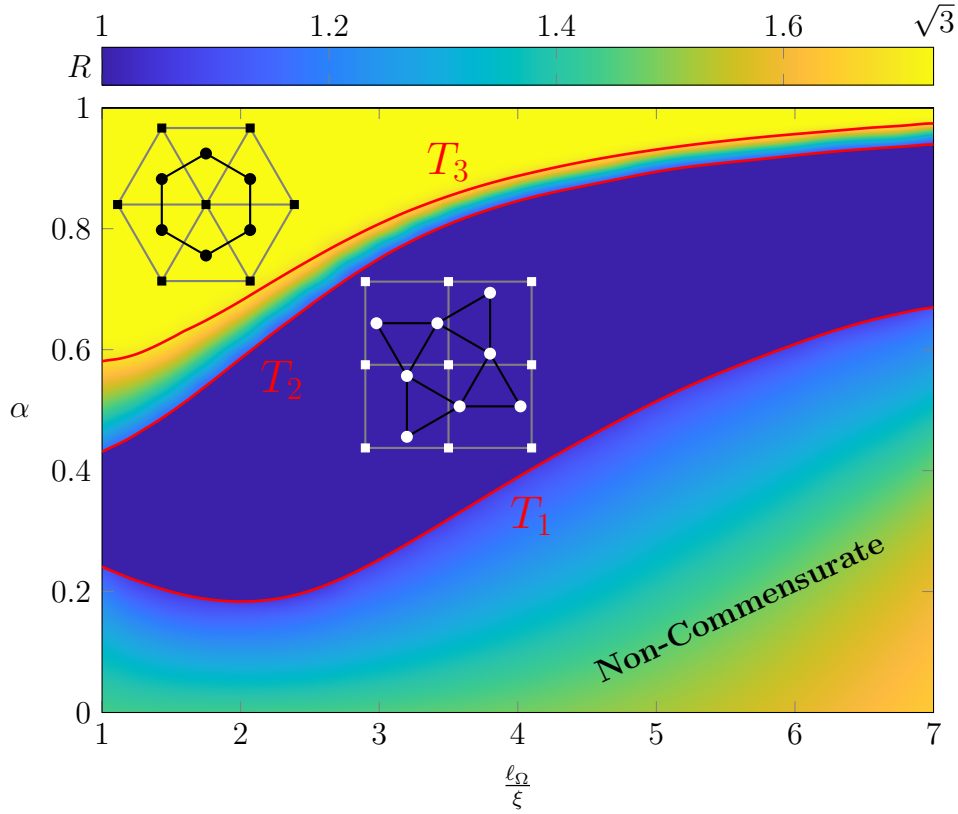


Figure 6.4: Phase diagram for two rotating superfluids with atomic mass ratio  $m_2/m_1 = 2$ . The intra-species interaction strengths are taken so as to satisfy  $\ell_\Omega^{(1)}/\xi^{(1)} = \ell_\Omega^{(2)}/\xi^{(2)} \equiv \ell_\Omega/\xi$ . As discussed in the text, this system does not have a commensurate ground state for small inter-species interactions. One should hence expect to observe frustration in this regime. For stronger interactions one finds instead two novel vortex configurations: the snub-square lattice and the honeycomb lattice.

certain configurations. In fact, close to the LLL, we cannot find a snub-square configuration and the system evolves from a non-commensurate configuration to the honeycomb-triangular state.

At last, let us mention that the result (5.37) given in the previous chapter describing the phase boundaries as affine functions of the intra-species interaction strength, can be generalised to the case of different intra-species

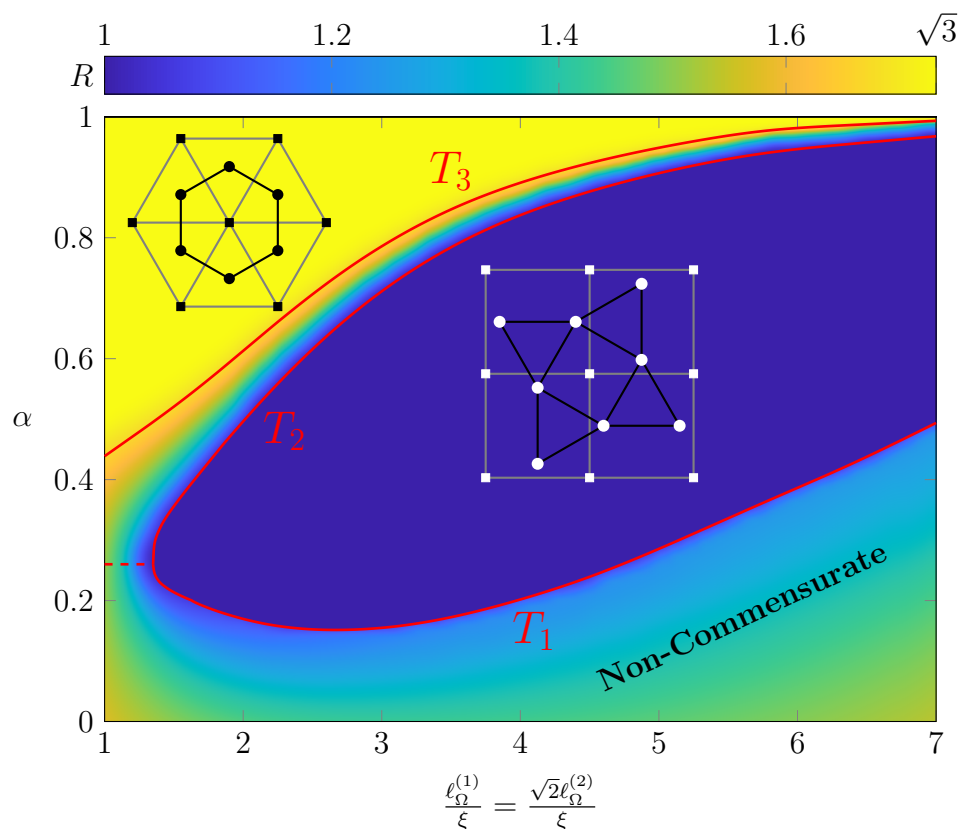


Figure 6.5: Phase diagram for two rotating superfluids with atomic mass ratio  $m_2/m_1 = 2$ . Here the intraspecies interactions are taken so as to have equal healing lengths in each component  $\xi^{(1)} = \xi^{(2)} \equiv \xi$ .

interaction strengths  $g_1 \neq g_2$ <sup>1</sup>. More specifically, in the Coulomb limit, one can write:

$$\bar{T} = \sqrt{g_1 g_2} + a. \quad (6.13)$$

for some intercept  $a$ . It is straightforward to see that the above equation (6.13) reduces to the linear relation in (5.37) for  $g_1 = g_2$ . This result is particularly interesting, as it allows for a the characterisation of a vaster

<sup>1</sup>See Appendix B.

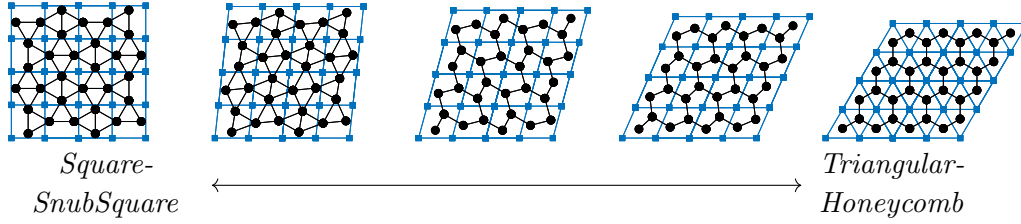


Figure 6.6: The continuous transformation of the Square-SnubSquare lattices into the Triangular-Hexagonal lattices, occurring between the transition boundaries  $T_2$  and  $T_3$ .

phase diagram in the Coulomb limit. Once the intercept is obtained from the simplest linear case  $g_1 = g_2$ , equation (6.13) allows us to infer, at least under the approximation of strong inter-species interactions, the behaviour of the phase boundaries for arbitrary interaction strengths  $g_1 \neq g_2$ . Notice however, that the same argument cannot be extended to the mass ratio, as at its variation different configurations are expected. The intercept should thus be thought of as depending on the mass ratio.

### 6.3 Higher mass ratios

We now turn our attention to the case of higher integer mass ratios. Table 6.1 provides a summary of the commensurate lowest energy configurations we find for the first integer mass ratios. The next integer case, namely that of mass ratio  $m_2/m_1 = 3$ , might be of interest for the experimental realisation with isotopes  $^{41}\text{K}-^{133}\text{Cs}$  ( $m_2/m_1 \approx 3.2$ ) [122], for  $^7\text{Li}-^{23}\text{Na}$  ( $m_2/m_1 \approx 3.3$ ), or for  $^{52}\text{Cr}-^{164}\text{Dy}$  ( $m_2/m_1 \approx 3.1561$ ). In this case we can find again a complete commensurate phase space. For  $\alpha \approx 0$  we find two commensurate triangular lattices, one tilted with respect to the other by an angle  $\theta = \pi/6$ . When the interactions are stronger we find at first that the lighter component's vortices form a triangular lattice, while the heavier component arranges its vortices into a *kagome lattice* with parameter  $\ell_\Omega^{(1)}/2$ . For higher interspecies interac-

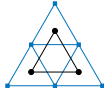
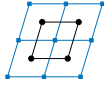
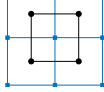
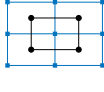
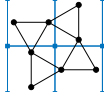
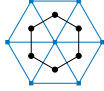
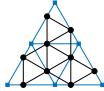
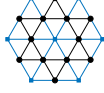
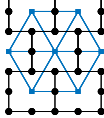
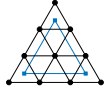
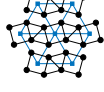
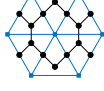
$\frac{m_2}{m_1}$	Ground State	Species Type	Symmetry Group
1		<b>1:</b> Triangular <b>2:</b> Triangular	p6m p6m
		<b>1:</b> Oblique <b>2:</b> Oblique	p2 p2
		<b>1:</b> Square <b>2:</b> Square	p4m p4m
		<b>1:</b> Rectangular <b>2:</b> Rectangular	pmm pmm
2		<b>1:</b> Square <b>2:</b> Snub Square	p4m p4g
		<b>1:</b> Triangular <b>2:</b> Honeycomb	p6m p6m
3		<b>1:</b> Triangular <b>2:</b> $\frac{1}{3}$ Triangular	p6m p6m
		<b>1:</b> Triangular <b>2:</b> Kagome	p6m p6m
		<b>1:</b> Triangular <b>2:</b> Shifted-Rectangular	p6m p2
4		<b>1:</b> Triangular <b>2:</b> $\frac{1}{4}$ Triangular	p6m p6m
		<b>1:</b> Triangular <b>2:</b> Fishbone Square	p6m pgg
		<b>1:</b> Triangular <b>2:</b> Non-Regular Hexagonal	p6m cmm

Table 6.1: Commensurate ground states for different mass ratios. For each lattice it is given its symmetry classification in IUC notation. We denoted by ‘ $\frac{1}{n}$  Triangular’ the triangular lattice with unit cell an  $n$ th of the unit cell area of the lattice denoted as ‘Triangular’.

tion, closer to the miscibility-immiscibility boundary  $\alpha = 1$ , the latter turns into a *shifted-rectangular lattice* (with lattice parameter  $\ell_{\Omega}^{(1)}/2$ ) while the lighter component retains its triangular arrangement. Notice that throughout the whole phase diagram, the lightest species remains stable in its triangular configuration. This is a feature that seems to persist at higher mass ratios.

Finally, the last mass ratio we consider is  $m_2/m_1 = 4$  which could be implemented with the isotopes  $^{23}\text{Na}$ – $^{87}\text{Rb}$  which have mass ratio  $m_2/m_1 \approx 3.8$  [123] or even more accurately with  $^{41}\text{K}$ – $^{164}\text{Dy}$  ( $m_2/m_1 \approx 4.0021$ ). As mentioned at the beginning of this section, because this mass ratio is a perfect square, at  $\alpha \approx 0$  we can obtain two commensurate triangular lattices tilted with respect to each other by an angle  $\theta = 0$ .

When  $\alpha$  is increased, the symmetry is broken along one direction and we observe the formation of a new state made of squares with diagonal  $D = \sqrt{3} - 1$ , centered on the points belonging to the triangular lattice formed by the lighter species. The squares are arranged as on a fishbone, tilted at an angle  $\theta = \pm\pi/12$ . For higher inter-species interactions, this state smoothly transitions to a state made of rectangles hinged in a fishbone shape overlapping the lighter species' triangular lattice. The rectangles are found centred on the vortices of the lighter species, characterised by a diagonal of length  $D = (1 + \sqrt{7})/3$ , aspect ratio  $(1 + 2\sqrt{7})/3\sqrt{3}$  and tilted at an angle  $\theta = \mp \arccos\left(\sqrt{\frac{1}{2} + \frac{1}{\sqrt{7}}}\right)$ . At last, yet a further increase of the interaction parameter  $\alpha$  leads to a lattice made of non-regular hexagons centered on the triangular lattice of the lighter species.

Notice again that the vortex lattices corresponding to the lighter component tend to retain their triangular arrangement for higher mass ratios. This occurs because of the requirement for  $\ell_{\Omega}/\xi$  to be the same in both components. For the case of unequal masses in fact, although this requirement implies equal interaction strength between particles of the same species in both components  $g_1 = g_2$ , the same does not translate to the force between

vortices of the same species. Recalling (1.92), it is simple to conclude that the force between two vortices of the same species scales as  $|\mathbf{F}_j| \sim g_j \xi_j^2 \sim 1/m_j$ , i.e. it is inversely proportional to the constituents' masses. Moreover, a similar calculation [116], suggests the force between two vortices of two different species scales as

$$|\mathbf{F}_{12}| \sim |g_{12}| \frac{\xi_1^2 \xi_2^2}{\xi_1^2 + \xi_2^2} \sim \frac{1}{m_1 + m_2}. \quad (6.14)$$

Therefore, for  $m_2 > m_1$ , we have that  $|\mathbf{F}_1| > |\mathbf{F}_2| > |\mathbf{F}_{12}|$ . As a consequence, it is reasonable, for sufficiently large mass ratios, to consider the influence of the vortex configurations in the heavier components, as a mere perturbation to the configuration of the vortex lattice in the lightest component (this is of course true only as long as we consider  $g_1 \approx g_2$ ). With this simple logic, we can then infer that for higher mass ratios, the lighter component will always have the strongest interaction within the system and will, ipso facto, be stable in the triangular lattice configuration, while the heavier component will arrange its vortices around it so as to minimise the total energy, as it is after all observed in the results from the numerical simulations.

# Conclusion

“The path comes into existence only when we observe it.”

---

Werner Heisenberg, *The physical content of quantum kinematics and mechanics*, 1927  
(contained in Quantum Theory and Measurement by J.A. Wheeler and W.H. Zurek)

In this thesis, a novel scheme to investigate systems respecting quasi-periodic boundary conditions was presented, allowing for the study of binary mixtures of superfluids, and leading to a characterisation of the whole phase diagram and prediction of novel exotic ground state configurations.

The scheme relies on the introduction of the *Magnetic Fourier Transform* (MFT) (3.39), which generalises the action of the Fourier transform to system symmetric under the operations of elements of the Magnetic Translation Group (MTG). The MFT allows for the expansion of the wavefunction in a basis of eigenstates of the generators of the MTG (3.38), and the resulting integral transform, satisfies the required *twisted boundary conditions* (1.133). Furthermore, the MFT diagonalises the linear kinetic energy terms in the Hamiltonian.

The MFT is then applied in conjunction with a non-linear *generalised*

*Hofstadter model*, which is proved to describe the system under consideration in the continuum limit, while preserving the exact gauge symmetries of the continuum model. The gauge fields are introduced through the (gauge-dependent) Peierls substitution, but we arrive at a diagonalised form of the model which does not depend on the choice of the gauge (3.51). The resulting equations of motion are used to evolve the system in imaginary time, through a split-step method. The evolution in imaginary time is proved to lead to the lowest energy state even in the case of non-linear systems, but it is also shown that the standard split-step methods loose in accuracy when propagating in imaginary time rather than in real time. A novel splitting is then introduced (3.52), which attains second order accuracy in time when propagating in imaginary time.

This approach overcomes a number of complications present in the previously employed methods. On one hand, it allows to attain a much higher efficiency: in the standard computational approach, the system is simulated within an harmonic trap with periodic boundary conditions, thus requiring large computational cells in order to allow the wavefunction to decay to zero at the boundaries, and consequently wasting many computational points on regions of limited interest. Moreover, the approach presented here permits to study periodic unit cells, thus allowing the investigation of the perfect infinite vortex lattice arising naturally, without the disturbance of the confinement which acts to distort it. The employment of a fundamental periodic unit cell also greatly reduces the number of effective degrees of freedom as less vortices are taken into consideration: when considering the system within the confining potential, aside to the previously mentioned side effects, one would also need to consider a large number of vortices in order to be able to infer the structure of the resulting vortex lattice, resulting in a much more complicated energy landscape to minimise over. Finally, another major advantage brought forth by our approach, is the possibility to classifying the resulting states in terms of parameters directly entering the model, thus al-



lowing for a more quantitative characterisation of the system. To sum up, with the method presented in Chapter 3, one can attain solutions both more efficiently and much more accurately.

We have then employed this scheme to study binary superfluid systems, first where components' constituents have equal masses, and then in the more general case. In the first case, a characterisation of the full phase diagram was provided in Fig. 5.7. This result extends the previous characterisation of such systems due to Mueller and Ho [66], which was however restricted to the *lowest Landau level regime*. Further, a discussion on the commensurability of periodic lattices has been given: in particular we have shown that two triangular lattices are commensurate if and only if the ratio of their densities – which in the case of superfluid vortex lattices equals to the ratio of the components' constituents masses – is Lösschian (6.8) (or its reciprocal). A characterisation of the full phase diagram has been given for the mass ratio  $m_2/m_1 = 2$  as well (Fig. 6.4). A summary of the different ground states found for different mass ratio is provided in Table 6.1. Finally, a relation has been derived (6.13) which accurately describes the phase boundaries, marking the point of transition from one configuration to another, as a function of different coupling strengths, in the Coulomb limit.

Although we have here restricted our attention to binary scalar mixtures of superfluids, the scheme we have presented warrants further investigation in more complex systems such as spinor condensates, and systems under more general gauge fields. The effectiveness of this scheme has already encouraged others [124] to choose this approach into the investigation of vortex lattices, and we hope it will foster even more research in the future.



# Bibliography

- [1] Luca Mingarelli, Eric E. Keaveny, and Ryan Barnett. Simulating infinite vortex lattices in superfluids. *Journal of Physics: Condensed Matter*, 28(28):285201, 2016. URL [Link](#).
- [2] Luca Mingarelli, Eric E. Keaveny, and Ryan Barnett. Vortex lattices in binary mixtures of repulsive superfluids. *Phys. Rev. A*, 97:043622, 2018. URL [Link](#).
- [3] Luca Mingarelli and Ryan Barnett. Exotic vortex lattices in binary repulsive superfluids with unequal masses. Working paper, 2018.
- [4] A. Einstein. *Quantentheorie des einatomigen idealen Gases*. Wiley VCH Verlag GmbH and Co. KGaA, 2006. ISBN 9783527608959. doi: 10.1002/3527608958.ch27. URL [Link](#).
- [5] F. London. On the bose-einstein condensation. *Phys. Rev.*, 54:947–954, Dec 1938. doi: 10.1103/PhysRev.54.947. URL [Link](#).
- [6] A. J. Leggett. Superfluidity. *Rev. Mod. Phys.*, 71:S318–S323, Mar 1999. doi: 10.1103/RevModPhys.71.S318. URL [Link](#).
- [7] L. Landau. Theory of the superfluidity of helium ii. *Phys. Rev.*, 60: 356–358, Aug 1941. doi: 10.1103/PhysRev.60.356. URL [Link](#).

- 
- [8] Google ngram viewer, 2018. URL [Link](#).
- [9] J. M. Vogels, C. C. Tsai, R. S. Freeland, S. J. J. M. F. Kokkelmans, B. J. Verhaar, and D. J. Heinzen. Prediction of feshbach resonances in collisions of ultracold rubidium atoms. *Phys. Rev. A*, 56:R1067–R1070, Aug 1997. doi: 10.1103/PhysRevA.56.R1067. URL [Link](#).
- [10] Oliver Morsch and Markus Oberthaler. Dynamics of bose-einstein condensates in optical lattices. *Rev. Mod. Phys.*, 78:179–215, Feb 2006. doi: 10.1103/RevModPhys.78.179. URL [Link](#).
- [11] O. Boada, A. Celi, J. I. Latorre, and M. Lewenstein. Quantum simulation of an extra dimension. *Phys. Rev. Lett.*, 108:133001, Mar 2012. doi: 10.1103/PhysRevLett.108.133001. URL [Link](#).
- [12] Janne Ruostekoski, Gerald V. Dunne, and Juha Javanainen. Particle number fractionalization of an atomic fermi-dirac gas in an optical lattice. *Phys. Rev. Lett.*, 88:180401, Apr 2002. doi: 10.1103/PhysRevLett.88.180401. URL [Link](#).
- [13] D Jaksch and P Zoller. Creation of effective magnetic fields in optical lattices: the hofstadter butterfly for cold neutral atoms. *New Journal of Physics*, 5(1):56, 2003. URL [Link](#).
- [14] C. C. Bradley, C. A. Sackett, J. J. Tollett, and R. G. Hulet. Evidence of bose-einstein condensation in an atomic gas with attractive interactions. *Phys. Rev. Lett.*, 75:1687–1690, Aug 1995. doi: 10.1103/PhysRevLett.75.1687. URL [Link](#).
- [15] Dale G. Fried, Thomas C. Killian, Lorenz Willmann, David Landhuis, Stephen C. Moss, Daniel Kleppner, and Thomas J. Greytak. Bose-einstein condensation of atomic hydrogen. *Phys. Rev. Lett.*, 81:3811–3814, Nov 1998. doi: 10.1103/PhysRevLett.81.3811. URL [Link](#).

- 
- [16] S. L. Cornish, N. R. Claussen, J. L. Roberts, E. A. Cornell, and C. E. Wieman. Stable  $^{85}\text{Rb}$  bose-einstein condensates with widely tunable interactions. *Phys. Rev. Lett.*, 85:1795–1798, Aug 2000. doi: 10.1103/PhysRevLett.85.1795. URL [Link](#).
- [17] Giovanni Modugno, Gabriele Ferrari, Giacomo Roati, Robert J Brecha, A Simoni, and Massimo Inguscio. Bose-einstein condensation of potassium atoms by sympathetic cooling. *Science*, 294(5545):1320–1322, 2001. URL [Link](#).
- [18] Tino Weber, Jens Herbig, Michael Mark, Hanns-Christoph Nägerl, and Rudolf Grimm. Bose-einstein condensation of cesium. *Science*, 299(5604):232–235, 2003. URL [Link](#).
- [19] Yosuke Takasu, Kenichi Maki, Kaduki Komori, Tetsushi Takano, Kazuhito Honda, Mitsutaka Kumakura, Tsutomu Yabuzaki, Yoshiro Takahashi, et al. General physics. *Phys. Rev. Lett*, 91:040404, 2003. URL [Link](#).
- [20] Axel Griesmaier, Jörg Werner, Sven Hensler, Jürgen Stuhler, and Tilman Pfau. Bose-einstein condensation of chromium. *Physical Review Letters*, 94(16):160401, 2005. URL [Link](#).
- [21] Giacomo Roati, Matteo Zaccanti, C D’Errico, Jacopo Catani, Michele Modugno, Andrea Simoni, Massimo Inguscio, and G Modugno. K 39 bose-einstein condensate with tunable interactions. *Physical review letters*, 99(1):010403, 2007. URL [Link](#).
- [22] Chen Sun, Thomas Nattermann, and Valery L Pokrovsky. Bose-Einstein condensation and superfluidity of magnons in yttrium iron garnet films. *Journal of Physics D: Applied Physics*, 50(14):143002, apr 2017. ISSN 0022-3727. doi: 10.1088/1361-6463/aa5cfc. URL [Link](#).

- [23] Kosuke Yoshioka, Eunmi Chae, and Makoto Kuwata-Gonokami. Transition to a Bose-Einstein condensate and relaxation explosion of excitons at sub-Kelvin temperatures. *Nature Communications*, 2:328, may 2011. URL [Link](#).
- [24] A. Imamoglu, R. J. Ram, S. Pau, and Y. Yamamoto. Nonequilibrium condensates and lasers without inversion: Exciton-polariton lasers. *Phys. Rev. A*, 53:4250–4253, Jun 1996. doi: 10.1103/PhysRevA.53.4250. URL [Link](#).
- [25] P. Kapitza. Viscosity of liquid helium below the  $\lambda$ -point. *Nature*, 141: 74 EP, 01 1938. URL [Link](#).
- [26] J.F. Allen and A.D. Misener. Flow of Liquid Helium II. *Nature*, 141: 75, Jan 1938. URL [Link](#).
- [27] D. D. Osheroff, W. J. Gully, R. C. Richardson, and D. M. Lee. New magnetic phenomena in liquid  $\text{he}^3$  below 3 mk. *Phys. Rev. Lett.*, 29: 920–923, Oct 1972. doi: 10.1103/PhysRevLett.29.920. URL [Link](#).
- [28] D. D. Osheroff, R. C. Richardson, and D. M. Lee. Evidence for a new phase of solid  $\text{he}^3$ . *Phys. Rev. Lett.*, 28:885–888, Apr 1972. doi: 10.1103/PhysRevLett.28.885. URL [Link](#).
- [29] C. Raman, M. Köhl, R. Onofrio, D. S. Durfee, C. E. Kuklewicz, Z. Hadzibabic, and W. Ketterle. Evidence for a critical velocity in a bose-einstein condensed gas. *Phys. Rev. Lett.*, 83:2502–2505, Sep 1999. doi: 10.1103/PhysRevLett.83.2502. URL [Link](#).
- [30] V. I. Yukalov and R. Graham. Bose-einstein-condensed systems in random potentials. *Phys. Rev. A*, 75:023619, Feb 2007. doi: 10.1103/PhysRevA.75.023619. URL [Link](#).
- [31] M. R. Andrews, D. M. Kurn, H.-J. Miesner, D. S. Durfee, C. G. Townsend, S. Inouye, and W. Ketterle. Propagation of sound in a

- bose-einstein condensate. *Phys. Rev. Lett.*, 79:553–556, Jul 1997. doi: 10.1103/PhysRevLett.79.553. URL [Link](#).
- [32] I. Bloch, T. W. Hänsch, and T. Esslinger. Measurement of the spatial coherence of a trapped bose gas at the phase transition. *Nature*, 403: 166 EP –, 01 2000. URL [Link](#).
- [33] Wolfgang Ketterle and Hans-Joachim Miesner. Coherence properties of bose-einstein condensates and atom lasers. *Phys. Rev. A*, 56:3291–3293, Oct 1997. doi: 10.1103/PhysRevA.56.3291. URL [Link](#).
- [34] J. R. Abo-Shaeer, C. Raman, J. M. Vogels, and W. Ketterle. Observation of vortex lattices in bose-einstein condensates. 292(5516):476–479, 2001. ISSN 0036-8075. doi: 10.1126/science.1060182. URL [Link](#).
- [35] RP Feynman. Progress in low temperature physics. *Vol. 1 North-Holland, Amsterdam*, page 17, 1955.
- [36] W. H. Kleiner, L. M. Roth, and S. H. Autler. Bulk solution of ginzburg-landau equations for type ii superconductors: Upper critical field region. *Phys. Rev.*, 133:A1226–A1227, Mar 1964. doi: 10.1103/PhysRev.133.A1226. URL [Link](#).
- [37] D. Cribier, B. Jacrot, L. Madhav Rao, and B. Farnoux. Mise en évidence par diffraction de neutrons d’une structure periodique du champ magnetique dans le niobium supraconducteur. *Physics Letters*, 9(2): 106 – 107, 1964. ISSN 0031-9163. doi: [http://dx.doi.org/10.1016/0031-9163\(64\)90096-4](http://dx.doi.org/10.1016/0031-9163(64)90096-4). URL [Link](#).
- [38] U. Essmann and H. Truble. The direct observation of individual flux lines in type ii superconductors. *Physics Letters A*, 24(10):526 – 527, 1967. ISSN 0375-9601. doi: [http://dx.doi.org/10.1016/0375-9601\(67\)90819-5](http://dx.doi.org/10.1016/0375-9601(67)90819-5). URL [Link](#).

- 
- [39] E. J. Yarmchuk, M. J. V. Gordon, and R. E. Packard. Observation of stationary vortex arrays in rotating superfluid helium. *Phys. Rev. Lett.*, 43:214–217, Jul 1979. doi: 10.1103/PhysRevLett.43.214. URL [Link](#).
- [40] H.E. Hall and W.F. Vinen. The rotation of liquid helium ii ii. the theory of mutual friction in uniformly rotating helium ii. *Proceedings of the Royal Society of London A: Mathematical, Physical and Engineering Sciences*, 238(1213):215–234, 1956. ISSN 0080-4630. doi: 10.1098/rspa.1956.0215. URL [Link](#).
- [41] M. R. Matthews, B. P. Anderson, P. C. Haljan, D. S. Hall, C. E. Wieman, and E. A. Cornell. Vortices in a bose-einstein condensate. *Phys. Rev. Lett.*, 83:2498–2501, Sep 1999. doi: 10.1103/PhysRevLett.83.2498. URL [Link](#).
- [42] J. E. Williams and M. J. Holland. Preparing topological states of a bose–einstein condensate. *Nature*, 401:568 EP –, 10 1999. URL [Link](#).
- [43] Alexander L. Fetter. Vortices and dynamics in trapped bose-einstein condensates. *Journal of Low Temperature Physics*, 161(5):445–459, Dec 2010. ISSN 1573-7357. doi: 10.1007/s10909-010-0202-7. URL [Link](#).
- [44] Alexander L. Fetter. Rotating trapped bose-einstein condensates. *Rev. Mod. Phys.*, 81:647–691, May 2009. doi: 10.1103/RevModPhys.81.647. URL [Link](#).
- [45] Quantal phase factors accompanying adiabatic changes. *Proceedings of the Royal Society of London A: Mathematical, Physical and Engineering Sciences*, 392(1802):45–57, 1984. ISSN 0080-4630. doi: 10.1098/rspa.1984.0023. URL [Link](#).
- [46] Tomoya Isoshima, Mikio Nakahara, Tetsuo Ohmi, and Kazushige Machida. Creation of a persistent current and vortex in a bose-einstein



- condensate of alkali-metal atoms. *Phys. Rev. A*, 61:063610, May 2000. doi: 10.1103/PhysRevA.61.063610. URL [Link](#).
- [47] A. E. Leanhardt, A. Görlitz, A. P. Chikkatur, D. Kielpinski, Y. Shin, D. E. Pritchard, and W. Ketterle. Imprinting vortices in a bose-einstein condensate using topological phases. *Phys. Rev. Lett.*, 89:190403, Oct 2002. doi: 10.1103/PhysRevLett.89.190403. URL [Link](#).
- [48] K. W. Madison, F. Chevy, W. Wohlleben, and J. Dalibard. Vortex formation in a stirred bose-einstein condensate. *Phys. Rev. Lett.*, 84:806–809, Jan 2000. doi: 10.1103/PhysRevLett.84.806. URL [Link](#).
- [49] P. C. Haljan, I. Coddington, P. Engels, and E. A. Cornell. Driving bose-einstein-condensate vorticity with a rotating normal cloud. *Phys. Rev. Lett.*, 87:210403, Nov 2001. doi: 10.1103/PhysRevLett.87.210403. URL [Link](#).
- [50] P. Engels, I. Coddington, P. C. Haljan, V. Schweikhard, and E. A. Cornell. Observation of long-lived vortex aggregates in rapidly rotating bose-einstein condensates. *Phys. Rev. Lett.*, 90:170405, May 2003. doi: 10.1103/PhysRevLett.90.170405. URL [Link](#).
- [51] T. W. Neely, E. C. Samson, A. S. Bradley, M. J. Davis, and B. P. Anderson. Observation of vortex dipoles in an oblate bose-einstein condensate. *Phys. Rev. Lett.*, 104:160401, Apr 2010. doi: 10.1103/PhysRevLett.104.160401. URL [Link](#).
- [52] R. Srinivasan. Vortices in bose-einstein condensates: A review of the experimental results. *Pramana*, 66(1):3–30, Jan 2006. ISSN 0973-7111. doi: 10.1007/BF02704934. URL [Link](#).
- [53] VK Tkachenko. Stability of vortex lattices. *Sov. Phys. JETP*, 23(6):1049–1056, 1966.

- 
- [54] C. D. Andereck, J. Chalups, and W. I. Glaberson. Tkachenko waves in rotating superfluid helium. *Phys. Rev. Lett.*, 44:33–36, Jan 1980. doi: 10.1103/PhysRevLett.44.33. URL [Link](#).
- [55] I. Coddington, P. Engels, V. Schweikhard, and E. A. Cornell. Observation of tkachenko oscillations in rapidly rotating bose-einstein condensates. *Phys. Rev. Lett.*, 91:100402, Sep 2003. doi: 10.1103/PhysRevLett.91.100402. URL [Link](#).
- [56] N. R. Cooper, E. H. Rezayi, and S. H. Simon. Vortex lattices in rotating atomic bose gases with dipolar interactions. *Phys. Rev. Lett.*, 95:200402, Nov 2005. doi: 10.1103/PhysRevLett.95.200402. URL [Link](#).
- [57] C. Reichhardt, C. J. Olson, and Franco Nori. Dynamic phases of vortices in superconductors with periodic pinning. *Phys. Rev. Lett.*, 78:2648–2651, Mar 1997. doi: 10.1103/PhysRevLett.78.2648. URL [Link](#).
- [58] W. V. Pogosov, A. L. Rakhmanov, and V. V. Moshchalkov. Vortex lattice in the presence of a tunable periodic pinning potential. *Phys. Rev. B*, 67:014532, Jan 2003. doi: 10.1103/PhysRevB.67.014532. URL [Link](#).
- [59] Hong-Yin Liao, Shi-Ping Zhou, and Hao-Chen Du. Vortex pinning by point defect in superconductors. *Journal of Physics D: Applied Physics*, 36(13):1439, 2003. URL [Link](#).
- [60] C. J. Olson, C. Reichhardt, and Franco Nori. Superconducting vortex avalanches, voltage bursts, and vortex plastic flow: Effect of the microscopic pinning landscape on the macroscopic properties. *Phys. Rev. B*, 56:6175–6194, Sep 1997. doi: 10.1103/PhysRevB.56.6175. URL [Link](#).
- [61] Gabriel Wlazłowski, Kazuyuki Sekizawa, Piotr Magierski, Aurel Bulgac, and Michael McNeil Forbes. Vortex pinning and dynamics in

- the neutron star crust. *Phys. Rev. Lett.*, 117:232701, Nov 2016. doi: 10.1103/PhysRevLett.117.232701. URL [Link](#).
- [62] Fabrizio Grill and Pierre Pizzochero. Vortex-lattice interaction in pulsar glitches. *Journal of Physics: Conference Series*, 342(1):012004, 2012. URL [Link](#).
- [63] Hai-Dan Wu and Tao Zhou. Vortex pinning by the point potential in topological superconductors: A scheme for braiding majorana bound states. *Phys. Rev. B*, 96:184508, Nov 2017. doi: 10.1103/PhysRevB.96.184508. URL [Link](#).
- [64] C. Reichhardt, C. J. Olson, and Franco Nori. Commensurate and incommensurate vortex states in superconductors with periodic pinning arrays. *Phys. Rev. B*, 57:7937–7943, Apr 1998. doi: 10.1103/PhysRevB.57.7937. URL [Link](#).
- [65] H. Pu, L. O. Baksmaty, S. Yi, and N. P. Bigelow. Structural phase transitions of vortex matter in an optical lattice. *Phys. Rev. Lett.*, 94:190401, May 2005. doi: 10.1103/PhysRevLett.94.190401. URL [Link](#).
- [66] Erich J Mueller and Tin-Lun Ho. Two-component bose-einstein condensates with a large number of vortices. *Phys. Rev. Lett.*, 88(18):180403, 2002. URL [Link](#).
- [67] Kean Loon Lee, Nils B. Jørgensen, I-Kang Liu, Lars Wacker, Jan J. Arlt, and Nick P. Proukakis. Phase separation and dynamics of two-component bose-einstein condensates. *Phys. Rev. A*, 94:013602, Jul 2016. doi: 10.1103/PhysRevA.94.013602. URL [Link](#).
- [68] D. M. Stamper-Kurn, M. R. Andrews, A. P. Chikkatur, S. Inouye, H.-J. Miesner, J. Stenger, and W. Ketterle. Optical confinement of a bose-einstein condensate. *Phys. Rev. Lett.*, 80:2027–2030, Mar 1998. doi: 10.1103/PhysRevLett.80.2027. URL [Link](#).

- 
- [69] J. W. Reijnders, F. J. M. van Lankvelt, K. Schoutens, and N. Read. Rotating spin-1 bosons in the lowest landau level. *Phys. Rev. A*, 69:023612, Feb 2004. doi: 10.1103/PhysRevA.69.023612. URL [Link](#).
- [70] N.R. Cooper. Rapidly rotating atomic gases. *Adv. Phys.*, 57(6):539–616, 2008. doi: 10.1080/00018730802564122. URL [Link](#).
- [71] J. Ruostekoski J. Javanainen. Symbolic calculation in development of algorithms: split-step methods for the gross-pitaevskii equation. *J. Phys. A: Math. Gen.*, 39:L179–L184, 2006. URL [Link](#).
- [72] Alexei A Abrikosov. Magnetic properties of superconductors of the second group. *Sov. Phys. JETP*, 5(6), 1957.
- [73] C.J. Pethick and H. Smith. *Bose-Einstein Condensation in Dilute Gases*. Cambridge University Press, 2002.
- [74] Franco Dalfovo, Stefano Giorgini, Lev P. Pitaevskii, and Sandro Stringari. Theory of bose-einstein condensation in trapped gases. *Rev. Mod. Phys.*, 71:463–512, Apr 1999. doi: 10.1103/RevModPhys.71.463. URL [Link](#).
- [75] Elliott H. Lieb and Robert Seiringer. Proof of bose-einstein condensation for dilute trapped gases. *Phys. Rev. Lett.*, 88:170409, Apr 2002. doi: 10.1103/PhysRevLett.88.170409. URL [Link](#).
- [76] Anthony J. Leggett. Bose-einstein condensation in the alkali gases: Some fundamental concepts. *Rev. Mod. Phys.*, 73:307–356, Apr 2001. doi: 10.1103/RevModPhys.73.307. URL [Link](#).
- [77] E. P. Gross. Structure of a quantized vortex in boson systems. *Il Nuovo Cimento (1955-1965)*, 20(3):454–477, May 1961. ISSN 1827-6121. doi: 10.1007/BF02731494. URL [Link](#).

- [78] LP Pitaevskii. Vortex lines in an imperfect bose gas. *Sov. Phys. JETP*, 13(2):451–454, 1961.
- [79] Lev Pitaevskii and Sandro Stringari. *Bose-Einstein condensation and superfluidity*, volume 164. Oxford University Press, 2016.
- [80] G. Modugno, M. Modugno, F. Riboli, G. Roati, and M. Inguscio. Two atomic species superfluid. *Phys. Rev. Lett.*, 89:190404, Oct 2002. doi: 10.1103/PhysRevLett.89.190404. URL [Link](#).
- [81] C. J. Myatt, E. A. Burt, R. W. Ghrist, E. A. Cornell, and C. E. Wieman. Production of two overlapping bose-einstein condensates by sympathetic cooling. *Phys. Rev. Lett.*, 78:586–589, Jan 1997. doi: 10.1103/PhysRevLett.78.586. URL [Link](#).
- [82] P. Ao and S. T. Chui. Binary bose-einstein condensate mixtures in weakly and strongly segregated phases. *Phys. Rev. A*, 58:4836–4840, Dec 1998. doi: 10.1103/PhysRevA.58.4836. URL [Link](#).
- [83] X. P. Liu. Excitation spectrum and phase separation of double bose-einstein condensates in optical lattices. *Phys. Rev. A*, 76:053615, Nov 2007. doi: 10.1103/PhysRevA.76.053615. URL [Link](#).
- [84] Kenichi Kasamatsu, Makoto Tsubota, and Masahito Ueda. Spin textures in rotating two-component bose-einstein condensates. *Phys. Rev. A*, 71:043611, Apr 2005. doi: 10.1103/PhysRevA.71.043611. URL [Link](#).
- [85] D. M. Harber, H. J. Lewandowski, J. M. McGuirk, and E. A. Cornell. Effect of cold collisions on spin coherence and resonance shifts in a magnetically trapped ultracold gas. *Phys. Rev. A*, 66:053616, Nov 2002. doi: 10.1103/PhysRevA.66.053616. URL [Link](#).
- [86] Erwin Madelung. Quantentheorie in hydrodynamischer form. *Zeitschrift für Physik A Hadrons and Nuclei*, 40(3):322–326, 1927.

- [87] Rémi Carles, Raphaël Danchin, and Jean-Claude Saut. Madelung, Gross-Pitaevskii and Korteweg. *IOP Publishing: Nonlinearity*, 25: 2843–2873, 2012.
- [88] Ryan Barnett, Daniel Podolsky, and Gil Refael. Geometrical approach to hydrodynamics and low-energy excitations of spinor condensates. *Physical Review B*, 80(2):024420, 2009. URL [Link](#).
- [89] L. Onsager. *Nuovo Cimento, Suppl.*, 6:249, 1949.
- [90] RP Feynman. Progress in low temperature physics. *Vol. 1 North-Holland, Amsterdam*, page 17, 1955.
- [91] Russell J Donnelly. *Quantized vortices in helium II*, volume 2. Cambridge University Press, 1991.
- [92] Ryan Barnett, Edward Chen, and Gil Refael. Vortex synchronization in bose-einstein condensates: a time-dependent gross-pitaevskii equation approach. *New J. Phys.*, 12(4):043004, 2010. URL [Link](#).
- [93] Daniel E. Sheehy and Leo Radzihovsky. Vortices in spatially inhomogeneous superfluids. *Phys. Rev. A*, 70:063620, Dec 2004. doi: 10.1103/PhysRevA.70.063620. URL [Link](#).
- [94] Emil Lundh. Multiply quantized vortices in trapped bose-einstein condensates. *Phys. Rev. A*, 65:043604, Mar 2002. doi: 10.1103/PhysRevA.65.043604. URL [Link](#).
- [95] G M Kavoulakis and Gordon Baym. Rapidly rotating bose-einstein condensates in anharmonic potentials. *New Journal of Physics*, 5(1): 51, 2003. URL [Link](#).
- [96] Michele Correggi, Florian Pinsky, Nicolas Rougerie, and Jakob Yngvason. Rotating superfluids in anharmonic traps: From vortex lat-

- tices to giant vortices. *Phys. Rev. A*, 84:053614, Nov 2011. doi: 10.1103/PhysRevA.84.053614. URL [Link](#).
- [97] Nicolas Rougerie. The giant vortex state for a boseeinstein condensate in a rotating anharmonic trap: Extreme rotation regimes. *Journal de Mathematiques Pures et Appliques*, 95(3):296 – 347, 2011. ISSN 0021-7824. doi: <https://doi.org/10.1016/j.matpur.2010.11.004>. URL [Link](#).
- [98] M. Correggi, N. Rougerie, and J. Yngvason. The transition to a giant vortex phase in a fast rotating bose-einstein condensate. *Communications in Mathematical Physics*, 303(2):451–508, Apr 2011. ISSN 1432-0916. doi: 10.1007/s00220-011-1202-4. URL [Link](#).
- [99] M. Correggi, F. Pinsker, N. Rougerie, and J. Yngvason. Critical rotational speeds in the gross-pitaevskii theory on a disc with dirichlet boundary conditions. *Journal of Statistical Physics*, 143(2):261–305, Apr 2011. ISSN 1572-9613. doi: 10.1007/s10955-011-0182-2. URL [Link](#).
- [100] Nicolas Rougerie. Vortex rings in fast rotating bose–einstein condensates. *Archive for Rational Mechanics and Analysis*, 203(1):69–135, Jan 2012. ISSN 1432-0673. doi: 10.1007/s00205-011-0447-6. URL [Link](#).
- [101] Kenichi Kasamatsu, Makoto Tsubota, and Masahito Ueda. Vortex phase diagram in rotating two-component bose-einstein condensates. *Phys. Rev. Lett.*, 91:150406, Oct 2003. doi: 10.1103/PhysRevLett.91.150406. URL [Link](#).
- [102] Lev Davidovich Landau, Evgenii M Lifshitz, and LP Pitaevskii. *Statistical physics, part i*, 1980.
- [103] J. Zak. Magnetic translation group. *Phys. Rev.*, 134:A1602–A1606, Jun 1964. doi: 10.1103/PhysRev.134.A1602. URL [Link](#).

- 
- [104] J. Zak. Magnetic translation group. ii. irreducible representations. *Phys. Rev.*, 134:A1607–A1611, Jun 1964. doi: 10.1103/PhysRev.134.A1607. URL [Link](#).
- [105] Alberto Ramos. The gradient flow running coupling with twisted boundary conditions. *Journal of High Energy Physics*, 2014(11):1–28, 2014. URL [Link](#).
- [106] N. Byers and C. N. Yang. Theoretical considerations concerning quantized magnetic flux in superconducting cylinders. *Phys. Rev. Lett.*, 7: 46–49, Jul 1961. doi: 10.1103/PhysRevLett.7.46. URL [Link](#).
- [107] Weizhu Bao, Dieter Jaksch, and Peter A Markowich. Numerical solution of the gross–pitaevskii equation for bose–einstein condensation. *J. Comput. Phys*, 187(1):318–342, 2003. URL [Link](#).
- [108] Gilbert Strang. On the construction and comparison of difference schemes. *SIAM J. Numer. Anal.*, 5(3):506–517, 1968. doi: 10.1137/0705041. URL [Link](#).
- [109] J.A. Fleck M.D. Feit. On the construction and comparison of difference schemes. *J. Comput. Phys.*, 47(412), 1982.
- [110] Tobias Jahnke and Christian Lubich. Error bounds for exponential operator splittings. *BIT Numerical Mathematics*, 40(4):735–744, 2000. URL [Link](#).
- [111] Peter Mason and Amandine Aftalion. Classification of the ground states and topological defects in a rotating two-component bose–einstein condensate. *Phys. Rev. A*, 84:033611, Sep 2011. doi: 10.1103/PhysRevA.84.033611. URL [Link](#).
- [112] Pekko Kuopanportti, Natalia V Orlova, and Milorad V Milošević. Ground-state multiquantum vortices in rotating two-species superfluids. *Physical Review A*, 91(4):043605, 2015. URL [Link](#).



- [113] Douglas R. Hofstadter. Energy levels and wave functions of bloch electrons in rational and irrational magnetic fields. *Phys. Rev. B*, 14:2239–2249, Sep 1976. doi: 10.1103/PhysRevB.14.2239. URL [Link](#).
- [114] R Peierls. *Z. Phys.*, 80:763, 1933.
- [115] VK Tkachenko. On vortex lattices. *Sov. Phys. JETP*, 22:1282–1286, 1966.
- [116] Ryan Barnett, Gil Refael, Mason A Porter, and Hans Peter Bchler. Vortex lattice locking in rotating two-component boseeinstein condensates. *New Journal of Physics*, 10(4):043030, 2008. URL [Link](#).
- [117] M. Anderlini, D. Ciampini, D. Cossart, E. Courtade, M. Cristiani, C. Sias, O. Morsch, and E. Arimondo. Model for collisions in ultracold-atom mixtures. *Phys. Rev. A*, 72:033408, Sep 2005. doi: 10.1103/PhysRevA.72.033408. URL [Link](#).
- [118] Pekko Kuopanportti, Jukka A. M. Huhtamäki, and Mikko Möttönen. Exotic vortex lattices in two-species bose-einstein condensates. *Phys. Rev. A*, 85:043613, Apr 2012. doi: 10.1103/PhysRevA.85.043613. URL [Link](#).
- [119] August Lösch. *The economics of location: Translated from the second rev. German ed. by William H. Woglom with the assistance of Wolfgang F. Stolper*. Yale University Press, 1954.
- [120] G. Modugno, M. Modugno, F. Riboli, G. Roati, and M. Inguscio. Two atomic species superfluid. *Phys. Rev. Lett.*, 89:190404, Oct 2002. doi: 10.1103/PhysRevLett.89.190404. URL [Link](#).
- [121] G. Ferrari, M. Inguscio, W. Jastrzebski, G. Modugno, G. Roati, and A. Simoni. Collisional properties of ultracold k-rb mixtures. *Phys. Rev. Lett.*, 89:053202, Jul 2002. doi: 10.1103/PhysRevLett.89.053202. URL [Link](#).

- 
- [122] Hannah J. Patel, Caroline L. Blackley, Simon L. Cornish, and Jeremy M. Hutson. Feshbach resonances, molecular bound states, and prospects of ultracold-molecule formation in mixtures of ultracold k and cs. *Phys. Rev. A*, 90:032716, Sep 2014. doi: 10.1103/PhysRevA.90.032716. URL [Link](#).
- [123] Fudong Wang, Xiaoke Li, Dezhi Xiong, and Dajun Wang. A double species  $^{23}\text{Na}$  and  $^{87}\text{Rb}$  bose-einstein condensate with tunable miscibility via an interspecies feshbach resonance. *Journal of Physics B: Atomic, Molecular and Optical Physics*, 49(1):015302, 2016. URL [Link](#).
- [124] B. Mencia Uranga and Austen Lamacraft. Infinite lattices of vortex molecules in rabi-coupled condensates. *Phys. Rev. A*, 97:043609, Apr 2018. doi: 10.1103/PhysRevA.97.043609. URL [Link](#).

# Appendix A

## Significance of the phases $\tau_x$ and $\tau_y$

Let us start considering the following expression

$$\Pi_x(t) = e^{-\frac{i}{\hbar}(\mathbf{\Pi} \cdot \mathbf{r})t} \Pi_x e^{\frac{i}{\hbar}(\mathbf{\Pi} \cdot \mathbf{r})t}, \quad (\text{A.1})$$

with  $t$  being a dummy parameter. The expressions for the generators of the magnetic translations are those in given in the general gauge by equation (1.117) in Chapter 1. From Heisenberg's equations of motion we find

$$\begin{aligned} -i\partial_t \Pi_x(t) &= \frac{1}{\hbar} [\mathbf{\Pi} \cdot \mathbf{r}, \Pi_x(t)] = \frac{1}{\hbar} [\Pi_y r_y, \Pi_x(t)] \\ &= \frac{1}{\hbar} e^{-\frac{i}{\hbar}(\mathbf{\Pi} \cdot \mathbf{r})t} [\Pi_y r_y, \Pi_x] e^{\frac{i}{\hbar}(\mathbf{\Pi} \cdot \mathbf{r})t} \\ &= i2m\Omega r_y, \end{aligned} \quad (\text{A.2})$$

where we have used the commutation relation (1.118). Thus, integrating  $-\partial_t \Pi_x(t) = 2m\Omega r_y$ , we find

$$\Pi_x(t) = \Pi_x(t=0) - 2m\Omega r_y t. \quad (\text{A.3})$$

Setting now  $t = 1$ , we obtain

$$\Pi_x(1) = e^{-\frac{i}{\hbar}(\mathbf{\Pi}\cdot\mathbf{r})}\Pi_x e^{\frac{i}{\hbar}(\mathbf{\Pi}\cdot\mathbf{r})} = \Pi_x - 2m\Omega r_y. \quad (\text{A.4})$$

Similarly, from

$$\Pi_y(t) = e^{-\frac{i}{\hbar}(\mathbf{\Pi}\cdot\mathbf{r})t}\Pi_y e^{\frac{i}{\hbar}(\mathbf{\Pi}\cdot\mathbf{r})t}, \quad (\text{A.5})$$

we obtain

$$\partial_t \Pi_y(t) = 2m\Omega r_x, \quad (\text{A.6})$$

and thus

$$\Pi_y(t) = \Pi_y(t=0) + 2m\Omega r_x t. \quad (\text{A.7})$$

To sum up, we have proved that

$$\begin{aligned} e^{-\frac{i}{\hbar}(\mathbf{\Pi}\cdot\mathbf{r})}\Pi_x e^{\frac{i}{\hbar}(\mathbf{\Pi}\cdot\mathbf{r})} &= \Pi_x - 2m\Omega r_y, \\ e^{-\frac{i}{\hbar}(\mathbf{\Pi}\cdot\mathbf{r})}\Pi_y e^{\frac{i}{\hbar}(\mathbf{\Pi}\cdot\mathbf{r})} &= \Pi_y + 2m\Omega r_x. \end{aligned} \quad (\text{A.8})$$

It follows as a consequence that

$$\begin{aligned} e^{-\frac{i}{\hbar}(\mathbf{\Pi}\cdot\mathbf{r})} e^{\frac{i}{\hbar}\Pi_x L_x} e^{\frac{i}{\hbar}(\mathbf{\Pi}\cdot\mathbf{r})} &= e^{\frac{i}{\hbar}(\Pi_x - 2m\Omega r_y)L_x}, \\ e^{-\frac{i}{\hbar}(\mathbf{\Pi}\cdot\mathbf{r})} e^{\frac{i}{\hbar}\Pi_y L_y} e^{\frac{i}{\hbar}(\mathbf{\Pi}\cdot\mathbf{r})} &= e^{\frac{i}{\hbar}(\Pi_y + 2m\Omega r_x)L_y}. \end{aligned} \quad (\text{A.9})$$

Let us now consider equation (5.5)

$$\begin{aligned} e^{\frac{i}{\hbar}\Pi_x L_x} \psi(x, y) &= e^{i\tau_x L_x} \psi(x, y), \\ e^{\frac{i}{\hbar}\Pi_y L_y} \psi(x, y) &= e^{i\tau_y L_y} \psi(x, y), \end{aligned} \quad (\text{A.10})$$

and introduce the magnetically translated wave function  $\tilde{\psi}$  such that  $e^{i\Pi_j L_j} \tilde{\psi} = \tilde{\psi}$ ,

so that the original wave function can be written as  $\psi(x, y) \equiv T(\mathbf{r})\tilde{\psi}(x, y)$ , where  $\mathbf{r} = (r_x, r_y)$ . Then, we can look at how  $e^{i\Pi_x L_x}$  operates on  $\psi$ :

$$\begin{aligned}
 e^{i\Pi_x L_x} \psi &= e^{i\Pi_x L_x} e^{i\mathbf{\Pi} \cdot \mathbf{r}} \tilde{\psi} = e^{i\tau_x L_x} e^{i\mathbf{\Pi} \cdot \mathbf{r}} \tilde{\psi} \\
 e^{-i\mathbf{\Pi} \cdot \mathbf{r}} e^{i\Pi_x L_x} e^{i\mathbf{\Pi} \cdot \mathbf{r}} \tilde{\psi} &= e^{i\tau_x L_x} \tilde{\psi} \\
 e^{\frac{i}{\hbar}(\Pi_x - 2m\Omega r_y)L_x} \tilde{\psi} &= e^{i\tau_x L_x} \tilde{\psi} \\
 e^{-\frac{i}{\hbar}2m\Omega r_y L_x} \tilde{\psi} &= e^{i\tau_x L_x} \tilde{\psi},
 \end{aligned} \tag{A.11}$$

therefore

$$-2m\Omega r_y = \tau_x \hbar. \tag{A.12}$$

Similarly one can find

$$2m\Omega r_x = \tau_y \hbar. \tag{A.13}$$

These are the results presented in (5.6).



# Appendix **B**

## Linearity of the phase boundaries

Consider the energy density

$$\mathcal{E} = \frac{g_1}{2}\rho_1^2 + \frac{g_2}{2}\rho_2^2 + g_{12}\rho_1\rho_2 \quad (\text{B.1})$$

Since a phase boundary  $\bar{T}(g)$  between a phase configuration  $A$  and a configuration  $B$  can be defined as the value of the interspecies strength such that  $E^A(g, g_{12} = \bar{T}) = E^B(g, g_{12} = \bar{T})$ , it is possible to write an expression for  $\bar{T}(g)$ . In particular:

$$\frac{g_1}{2}\langle\rho_{A,1}^2\rangle + \frac{g_2}{2}\langle\rho_{A,2}^2\rangle + \bar{T}\langle\rho_{A,1}\rho_{A,2}\rangle = \frac{g_1}{2}\langle\rho_{B,1}^2\rangle + \frac{g_2}{2}\langle\rho_{B,2}^2\rangle + \bar{T}\langle\rho_{B,1}\rho_{B,2}\rangle \quad (\text{B.2})$$

where brackets denote spatial average. Then we can write an expression for the phase boundary as

$$\bar{T} = \frac{1}{2} \frac{g_1 (\langle\rho_{A,1}^2\rangle - \langle\rho_{B,1}^2\rangle) + g_2 (\langle\rho_{A,2}^2\rangle - \langle\rho_{B,2}^2\rangle)}{\langle\rho_{B,1}\rho_{B,2}\rangle - \langle\rho_{A,1}\rho_{A,2}\rangle}. \quad (\text{B.3})$$

Let us now introduce the density variations

$$\delta\rho_{\bullet,j} = \rho_{\bullet,j} - \langle\rho_{\bullet,j}\rangle = \rho_{\bullet,j} - \mathcal{N}_j. \quad (\text{B.4})$$

Clearly we have  $\langle\delta\rho_{\bullet,j}\rangle = 0$ . We can now start computing the terms in (B.3): the terms in the numerator become

$$\begin{aligned} \langle\rho_{A,j}^2\rangle &= \langle\delta\rho_{A,j}^2\rangle + \mathcal{N}_j^2, \\ \langle\rho_{B,j}^2\rangle &= \langle\delta\rho_{B,j}^2\rangle + \mathcal{N}_j^2, \end{aligned} \quad (\text{B.5})$$

so that

$$\langle\rho_{A,j}^2\rangle - \langle\rho_{B,j}^2\rangle = \langle\delta\rho_{A,j}^2\rangle - \langle\delta\rho_{B,j}^2\rangle. \quad (\text{B.6})$$

In the denominator we find instead

$$\begin{aligned} \langle\rho_{A,1}\rho_{A,2}\rangle &= \langle\delta\rho_{A,1}\delta\rho_{A,2}\rangle + \mathcal{N}_1\mathcal{N}_2, \\ \langle\rho_{B,1}\rho_{B,2}\rangle &= \langle\delta\rho_{B,1}\delta\rho_{B,2}\rangle + \mathcal{N}_1\mathcal{N}_2. \end{aligned} \quad (\text{B.7})$$

Then we can rewrite (B.3) as

$$\bar{T} = \frac{1}{2} \frac{g_1 (\langle\delta\rho_{A,1}^2\rangle - \langle\delta\rho_{B,1}^2\rangle) + g_2 (\langle\delta\rho_{A,2}^2\rangle - \langle\delta\rho_{B,2}^2\rangle)}{\langle\delta\rho_{B,1}\delta\rho_{B,2}\rangle - \langle\delta\rho_{A,1}\delta\rho_{A,2}\rangle}. \quad (\text{B.8})$$

Let us now introduce the total densities corresponding to each configuration  $\rho_{\bullet} = \rho_{\bullet,1} + \rho_{\bullet,2}$ . From this definition it is easy to find that

$$\langle\delta\rho_{\bullet,1}^2\rangle + \langle\delta\rho_{\bullet,2}^2\rangle = \langle\delta\rho_{\bullet}^2\rangle - 2\langle\delta\rho_{\bullet,1}\delta\rho_{\bullet,2}\rangle. \quad (\text{B.9})$$

Using this expression, the first term in the numerator becomes

$$\langle\delta\rho_{A,1}^2\rangle - \langle\delta\rho_{B,1}^2\rangle = \langle\delta\rho_A^2\rangle - \langle\delta\rho_B^2\rangle - 2\langle\delta\rho_{A,1}\delta\rho_{A,2}\rangle + 2\langle\delta\rho_{B,1}\delta\rho_{B,2}\rangle - \langle\delta\rho_{A,2}^2\rangle + \langle\delta\rho_{B,2}^2\rangle, \quad (\text{B.10})$$



and similarly for the second term. Now the expression for  $\bar{T}$  reads

$$\begin{aligned} \bar{T} = g_1 + g_2 + \frac{g_1 + g_2}{2} \frac{\langle \delta \rho_A^2 \rangle - \langle \delta \rho_B^2 \rangle}{\langle \delta \rho_{B,1} \delta \rho_{B,2} \rangle - \langle \delta \rho_{A,1} \delta \rho_{A,2} \rangle} \\ - \frac{g_1}{2} \frac{\langle \delta \rho_{A,2}^2 \rangle - \langle \delta \rho_{B,2}^2 \rangle}{\langle \delta \rho_{B,1} \delta \rho_{B,2} \rangle - \langle \delta \rho_{A,1} \delta \rho_{A,2} \rangle} - \frac{g_2}{2} \frac{\langle \delta \rho_{A,1}^2 \rangle - \langle \delta \rho_{B,1}^2 \rangle}{\langle \delta \rho_{B,1} \delta \rho_{B,2} \rangle - \langle \delta \rho_{A,1} \delta \rho_{A,2} \rangle}. \end{aligned} \quad (\text{B.11})$$

It is convenient here to introduce the following:

$$\begin{aligned} D &= \langle \delta \rho_{B,1} \delta \rho_{B,2} \rangle - \langle \delta \rho_{A,1} \delta \rho_{A,2} \rangle, \\ \alpha &= \frac{\langle \delta \rho_{A,1}^2 \rangle - \langle \delta \rho_{B,1}^2 \rangle}{2D}, \\ \beta &= \frac{\langle \delta \rho_{A,2}^2 \rangle - \langle \delta \rho_{B,2}^2 \rangle}{2D}, \\ \gamma &= \frac{\langle \delta \rho_A^2 \rangle - \langle \delta \rho_B^2 \rangle}{2D}, \end{aligned} \quad (\text{B.12})$$

so that it is possible to write compactly

$$\bar{T} = g_1 + g_2 + (g_1 + g_2)\gamma - g_1\beta - g_2\alpha. \quad (\text{B.13})$$

Before continuing, it is necessary to make a couple of remarks. First of all, it is important to notice that

$$\begin{aligned} \alpha + \beta &= \frac{1}{2D} (\langle \delta \rho_{A,1}^2 \rangle + \langle \delta \rho_{A,2}^2 \rangle - \langle \delta \rho_{B,1}^2 \rangle - \langle \delta \rho_{B,2}^2 \rangle) \\ &= \frac{1}{2D} (\langle \delta \rho_A^2 \rangle - \langle \delta \rho_B^2 \rangle + 2\langle \delta \rho_{B,1} \delta \rho_{B,2} \rangle - 2\langle \delta \rho_{A,1} \delta \rho_{A,2} \rangle) \\ &= \frac{1}{2D} (\langle \delta \rho_A^2 \rangle - \langle \delta \rho_B^2 \rangle + 2D) \\ &= \gamma + 1. \end{aligned} \quad (\text{B.14})$$

So,  $\alpha + \beta = \gamma + 1$ . This already allows to re-write the expression for the phase boundaries as

$$\bar{T} = \alpha g_1 + \beta g_2. \quad (\text{B.15})$$

Now we would like to consider the limit in which both  $g_1$  and  $g_2$  become large, while preserving a constant ratio between the two. To this end, we write the ratio of the two interaction strengths as  $\mu = g_1/g_2$ . Moreover we write each of the interaction strength parameters as  $g_j = g_0 \chi_j$ , with  $\chi_1 = \mu \chi_2$ , in order to be able to write

$$\frac{\bar{T}}{g_0} = \mu \chi_2 \alpha + \chi_2 \beta. \quad (\text{B.16})$$

The Coulomb limit can then be achieved by taking  $g_0 \rightarrow \infty$ . Because in the Coulomb limit the variances in the total densities become negligible, one finds that

$$\lim_{g_0 \rightarrow \infty} \gamma = 0, \quad (\text{B.17})$$

and as a consequence

$$\lim_{g_0 \rightarrow \infty} \alpha + \beta = 1. \quad (\text{B.18})$$

Therefore we can take the limit:

$$\lim_{g_0 \rightarrow \infty} \frac{\bar{T}}{g_0} = \mu \chi_2 \alpha + \chi_2 (1 - \alpha). \quad (\text{B.19})$$

and write, in the Coulomb limit

$$\bar{T} = \alpha g_1 + (1 - \alpha) g_2 + a, \quad (\text{B.20})$$

for some intercept  $a$ . In the limit of equal interaction strengths  $g_1 = g_2 \equiv g$ , recalling the equality (B.18) valid in the Coulomb limit, this further reduces to

$$\bar{T} = g + a_j. \quad (\text{B.21})$$

Let us then proceed, trying to find an expression for  $\alpha$ . In particular let us look at the ratio  $\beta/\alpha$ : going back from the expression in terms of density variations to expressing the parameters  $\alpha$  and  $\beta$  in terms of densities one can find

$$\frac{\beta}{\alpha} = \frac{\langle \rho_{A,2}^2 \rangle - \langle \rho_{B,2}^2 \rangle}{\langle \rho_{A,1}^2 \rangle - \langle \rho_{B,1}^2 \rangle}. \quad (\text{B.22})$$

Let us now assume the following ansatz [73] for the vortex lattice density profile:

$$\begin{aligned} \rho_{A,j} &= \bar{\rho}_j \prod_{m \in \mathfrak{A}_j} \left( \frac{2\xi_j^2}{(\mathbf{r} - \mathbf{r}_m)^2} + 1 \right)^{-1}, \\ \rho_{B,j} &= \bar{\rho}_j \prod_{m \in \mathfrak{B}_j} \left( \frac{2\xi_j^2}{(\mathbf{r} - \mathbf{r}_m)^2} + 1 \right)^{-1}, \end{aligned} \quad (\text{B.23})$$

where we have denoted by  $\mathfrak{A}_j$  and  $\mathfrak{B}_j$  the sets of vortex positions in the  $j$ th component, with configurations  $A$  and  $B$  respectively. With these expressions, the integrals in (B.22) can be computed exactly. One finds that the numerator and denominator in (B.22) are written, to leading order in  $\xi$ , as

$$\langle \rho_{A,j}^2 \rangle - \langle \rho_{B,j}^2 \rangle = \frac{3\pi^2}{\sqrt{2}} \bar{\rho}_j^2 \xi_j \sum_{l \in \mathfrak{A}_j} \sum_{m \in \mathfrak{B}_j} |\mathbf{r}_l| - |\mathbf{r}_m|. \quad (\text{B.24})$$

where we have dropped terms that do not depend on the vortex positions,

and where we have assumed, as it is legit for small  $\xi$ s, that

$$\int \prod_m \left( \frac{2\xi^2}{(\mathbf{r} - \mathbf{r}_m)^2} + 1 \right)^{-2} d\mathbf{r} \approx \sum_m \int \left( \frac{2\xi^2}{(\mathbf{r} - \mathbf{r}_m)^2} + 1 \right)^{-2} d\mathbf{r}. \quad (\text{B.25})$$

The ratio of the sums factors of each component entering (B.24), assuming  $m_1 = m_2$ , can be written as:

$$\frac{\sum_{l \in \mathfrak{A}_2} \sum_{m \in \mathfrak{B}_2} |\mathbf{r}_l| - |\mathbf{r}_m|}{\sum_{l \in \mathfrak{A}_1} \sum_{m \in \mathfrak{B}_1} |\mathbf{r}_l| - |\mathbf{r}_m|} = 1. \quad (\text{B.26})$$

Thus, we have found that in the Coulomb limit we can write an expression for the ratio in equation (B.22) as

$$\frac{\beta}{\alpha} = \sqrt{\frac{g_1}{g_2}}. \quad (\text{B.27})$$

Recalling that in the Coulomb limit we have  $\beta = 1 - \alpha$ , we consequently find an expression for the two parameters:

$$\begin{aligned} \alpha &= \left( \sqrt{\frac{g_1}{g_2}} + 1 \right)^{-1}, \\ \beta &= \left( \sqrt{\frac{g_2}{g_1}} + 1 \right)^{-1}, \end{aligned} \quad (\text{B.28})$$

Finally, we can write the general expression (B.20) for the phase boundaries as

$$\bar{T} = \sqrt{g_1 g_2} + a. \quad (\text{B.29})$$